A&A 517, A73 (2010)
DOI: 10.1051/0004-6361/201014153

Astronomy & Astrophysics

A snapshot on galaxy evolution occurring in the Great Wall: the role of Nurture at $z = 0$

G. Gavazzi[1], M. Fumagalli[1], O. Cucciati[2], and A. Boselli[2]

[1] Dipartimento di Fisica G. Occhialini, Università di Milano-Bicocca, Milano, Italy
e-mail: [giuseppe.gavazzi;mattia.fumagalli]@mib.infn.it
[2] Laboratoire d'Astrophysique de Marseille, Marseille, France
e-mail: [olga.cucciati;alessandro.boselli]@oamp.fr

Received 28 January 2010 / Accepted 19 March 2010

ABSTRACT

With the aim of quantifying the contribution of the environment on the evolution of galaxies at $z = 0$ we have used the DR7 catalogue of the Sloan Digital Sky Survey (SDSS) to reconstruct the 3-D distribution of 4132 galaxies in 420 square degrees of the Coma supercluster, containing two rich clusters (Coma and A1367), several groups, and many filamentary structures belonging to the "Great Wall", at the approximate distance of 100 Mpc. At this distance the galaxy census is complete to $M_i = -17.5$ mag, i.e. ∼4 mag fainter than M^*. The morphological classification of galaxies into early- (ellipticals) and late-types (spirals) was carried out by inspection of individual SDSS images and spectra. The density around each galaxy was determined in cylinders of 1 Mpc radius and 1000 km s^{-1} half length. The color-luminosity relation was derived for galaxies in bins morphological type and in four thresholds of galaxy density-contrast, ranging from $\delta_{1,1000} \leq 0$ (UL = the cosmic web); $0 < \delta_{1,1000} \leq 4$ (L = the loose groups); $4 < \delta_{1,1000} \leq 20$ (H = the large groups and the cluster's outskirts) and $\delta_{1,1000} > 20$ (UH = the cluster's cores). The fraction of early-type galaxies increases with the log of the over-density. A well defined "red sequence" composed of early-type galaxies exists in all environments at high luminosity, but it lacks of low luminosity (dwarf) galaxies in the lowest density environment. Conversely low luminosity isolated galaxies are predominantly of late-type. In other words the low luminosity end of the distribution is dominated by red dE galaxies in clusters and groups and by dwarf blue amorphous systems in the lowest density regions. At $z = 0$ we find evidence for strong evolution induced by the environment (Nurture). Transformations take place mostly at low luminosity when star forming dwarf galaxies inhabiting low density environments migrate into amorphous passive dwarf ellipticals in their infall into denser regions. The mechanism involves suppression of the star formation due to gas stripping, without significant mass growth, as proposed by Boselli et al. (2008a, ApJ, 674, 742). This process is more efficient and fast in ambients of increasing density. In the highest density environments (around clusters) the truncation of the star formation happens fast enough (few 100 Myr) to produce the signature of post-star-burst in galaxy spectra. PSB galaxies, that are in fact found significantly clustered around the largest dynamical units, represent the remnants of star forming isolated galaxies that had their star formation violently suppressed during their infall in clusters in the last 0.5–1.5 Gyrs, and the progenitors of future dEs.

Key words. galaxies: evolution – galaxies: fundamental parameters – galaxies clusters: general – galaxies: clusters: individual: Coma – galaxies: clusters: individual: A1367

1. Introduction

In 1986 Valerie de Lapparent, Margaret Geller and John Huchra announced their "Slice of the Universe", a strip of 1100 galaxy optical redshifts from the CFA redshift survey, going through the Coma cluster (de Lapparent et al. 1986). A spectacular connected filament of galaxies popped out from their data, later nicknamed the "Great Wall" by Ramella et al. (1992, who more than doubled the number of redshift measurements) running through the spring sky at an approximate distance of 100 Mpc (adopting the modern value of $H_0 = 73$ km s^{-1} Mpc^{-1}, as in the remaining of this paper), and spanning a similar length. Its narrowness in the redshift space, bracketing large voids, was shocking for the epoch, for an universe supposedly "homogeneous and isotropic" on that scale.

Hundreds individual galaxies in the region $11.5^h < \mathrm{RA} < 13.5^h$; $+18° < \mathrm{Dec} < 32°$ that covers the majority of the the Coma Supercluster (CS) were in the mean time being surveyed at 21 cm (e.g. Chincarini et al. 1983; Gavazzi 1987, 1989; Scodeggio & Gavazzi 1993, and references therein) providing additional radio redshifts. Gavazzi et al. (1999), following the pioneering work of Gregory & Thompson (1978), highlighted the 3-D structure of the CS, containing 2 rich clusters: Coma (A1656) and A1367, several minor dynamical units (groups) and a multitude of galaxies belonging to the filaments with a small velocity dispersion. Being at constant distance from us, the CS region offered a unique opportunity for comparing directly the properties of galaxies in very different environmental conditions. As the spread in redshift is minimal in the CS (let alone the fingers of God of the two clusters) the high density contrast with foreground and background structures (large volumes in the foreground of the CS are completely devoid of galaxies) makes it quite straightforward to identify a huge slab of galaxies at approximately constant distance ($D = 96$ Mpc, $\mu = -34.9$ mag corresponding to $cz \sim 7000$ km s^{-1}), making it possible to compare galaxies in extreme environments free from distance biases.

By 2003, when the data from the Coma region were providing the skeleton for the web-based Goldmine database (Gavazzi et al. 2003), the 1127 CS galaxies included in the CGCG catalogue (Zwicky et al. 1961–1968) had all a measured redshift. Due to the shallowness of the CGCG catalogue, however, only

giant galaxies ($m_p \leq 15.7$ mag corresponds to $M_p \leq -19.3$ at the distance of CS) were represented, while dwarfs, that meanwhile were discovered to dominate the galaxy luminosity function, were neglected.

The idea of undertaking a deeper photometric survey of the CS region surpassing by at least 2 mag the CGCG was considered and soon abandoned because it would have been prohibitive for medium size telescopes equipped with CCDs not larger than 10 arcmin on each side, as available in the late '90s, to cover such a large stretch of the sky. Let alone the spectroscopy: for $r < 18$ mag there are about 150 galaxies per square deg (Heidt et al. 2003; Yasuda et al. 2007), so that in 420 deg^2 it would have been necessary to take 65 000 spectra for sorting out the objects in the velocity range $4000 < cz < 9500$ km s^{-1} appropriate for the CS (that a posteriori we know to sum only to approximately 4000).

With the DR7 data release of SDSS (2009) this dream became a reality: not only can we rely on a five color (u, g, r, i, z) photometric survey (with limiting sensitivity of 22.2 mag in the g and r bands and limiting surface brightness of $\mu_g \sim 25.5$ mag arcsec^{-2}), but also on the spectroscopy of (nominally) all galaxies brighter than $r < 17.77$ mag[1] (with effective surface brightness $\mu_e < 24.5$ mag arcsec^{-2}).

The present "near-field cosmology" project makes use of the photometry and the spectroscopy provided by SDSS much in the way astronomers use telescopes in "service observing" mode, but counting on an almost unlimited amount of observing time. By saying so we wish to emphasize that, opposite to most SDSS statistical analyzes that are based on such large number of objects that cannot be inspected individually, the number of galaxies (~4000) in the present study is large enough to ensure statistical significance, but not too large to prevent individual inspection of all images and spectra. The Coma supercluster constitutes the ideal bridge between the near-field and the high-z cosmology.

Several modern studies based on hundreds of thousands galaxies from the SDSS in the local universe (usually $0.05 < z < 0.2$) address environmental issues by quantifying the dependence of galaxy structural and photometric parameters from the local galaxy density. The density around each galaxy is computed counting galaxies in cylinders of given projected radius and depth in the redshift space. Most studies adopt 2 Mpc and 500 km s^{-1} (e.g. Kauffmann et al. 2004) or 1 Mpc and 1000 km s^{-1} (e.g. Hogg et al. 2004), as a compromise for detecting structures intermediate between large groups and small clusters. It is not easy however to visualize what type of structures are found by these automatic algorithms. The present study gives the opportunity to reciprocally calibrate structures that are seen individually in the CS with those that are detected by statistical means.

It is well know that the SDSS pipelines have not been designed for extracting parameters of extended nearby galaxies, which results in problems in creating reliable low-redshift catalogs, due to: 1) "shredding" of large galaxies in multiple pieces leading to wrong magnitude determinations; 2) slight (20%) underestimate of the brightness of galaxies larger than $r_{50} \sim 20''$ due to the way the photometric pipeline determines the median sky, biasing the sky brightness near large extended galaxies, as reported by Mandelbaum et al. (2005), Lauer et al. (2007), Bernardi et al. (2007), and Lisker et al. (2007); 3) the SDSS spectroscopy is meant to be complete down to $r < 17.77$ mag (Strauss et al. 2002). However several sources of incompleteness affect it, primarily due to conflicts in the fiber placement (they cannot be placed more closely than 55″) and because the correlation between galaxy surface brightness and luminosity biases against faint objects. All these sources of incompleteness have been considered by Blanton et al. (2005a,b).

In the Coma supercluster the problems connected with the incompleteness of SDSS are less severe than elsewhere. Even the largest of its galaxies have diameters <2–3 arcmin, making the "shredding" problem much less serious than in nearer surveys (e.g. Virgo). The brightest galaxies are well cataloged and their photometric parameters can be re-determined manually using the SDSS navigator. In principle the spectroscopy of several bright galaxies in the CS can be obtained from the literature beside the SDSS. Moreover even the smallest galaxies belonging to the CS have sizes in excess of 10 arcsec. This allows their classification by visual inspection on SDSS plates, independent from, but consistent with the method of visual morphology undertaken by the the Galaxy Zoo project (Lintott et al. 2008).

In conclusion the SDSS offers a magnificent tool to study a sizable stretch of the local universe, providing a representative census of galaxies at $z = 0$, their color, morphology, luminosity and spectral classification and allowing us to compare these quantities free from distance biases in a variety of environmental conditions, from the center of two rich clusters to the sparse filamentary regions where the local galaxy density is ~100 times lower.

The Coma supercluster offers a unique photographic snapshot of the evolutionary status of galaxies at $z = 0$ in a variety of environmental conditions that can be used to constrain the mechanisms that drive the evolution of galaxies at the present cosmological epoch (see a review in Boselli & Gavazzi 2006). It provides a complementary view to the many statistical determinations that are currently obtained using the unique data-set provided by SDSS (e.g. Kauffmann et al. 2004; Balogh et al. 2004a,b; Blanton et al. 2005a,b,c; Martinez & Muriel 2006; Blanton & Berlind 2007; Haines et al. 2007; just to mention a few, culminating with the review of the physical properties of nearby galaxies and their environment by Blanton & Moustakas 2009). Combined with studies of galaxy evolution at higher redshift (e.g. Scarlata et al. 2007; and Cassata et al. 2007, for $0 < z < 1$; Faber et al. 2007, for $1 < z < 2$; Fontana et al. 2006, for $1 < z < 4$) it will shed light on the mechanisms and processes that contribute to the evolution of galaxies in the cosmological context.

2. Data

2.1. Photometry

The SDSS DR7 spectroscopic database was searched in the window $11.5^h <$ RA (J2000) $< 13.5^h$; $+18° <$ Dec (J2000) $< 32°$ (~420 deg^2) for all galaxies with a measured redshift in the interval $4000 < cz < 9500$ km s^{-1}[2]. We obtained ~4000 targets. For each one we took coordinates, u, g, r, i, z Petrosian magnitudes (AB system) and the redshift.

To fill-in the incompleteness for luminous galaxies (Blanton et al. 2005a,b) we added 101 CGCG galaxies with redshift known from Goldmine that were not included in the SDSS spectral database. Also for these objects we took the u, g, r, i, z

[1] The success rate of redshift determinations from SDSS spectra is reported to be >99% by Stoughton et al. (2002).

[2] The interval $4000 < cz < 9500$ km s^{-1} was quite arbitrarily selected in order to include the whole "finger of God" associated to the Coma cluster.

Petrosian magnitudes using the SDSS DR7 navigation tool, that provides reliable magnitudes.

Additional galaxies that might have been missed in SDSS spectroscopic catalogue mainly due to fiber conflict were searched in NED within the limits of the CS window ($\Delta\alpha$; $\Delta\delta$; Δcz). We obtained only 160 of these serendipitous targets. Also for them we took the u, g, r, i, z magnitudes using the SDSS navigator tool and among them we selected those meeting the condition $r \leq 17.77$ (that matches the selection criterion of the SDSS spectral catalogue). Only 76 such objects were left, emphasizing the high completeness of the SDSS spectroscopic set. As expected from the highest degree of crowding, a significant fraction (50%) of the NED data concentrates on the two clusters, with the remaining 50% objects spread around the whole supercluster.

Some galaxies in the SDSS list have their spectrum taken in a off-nuclear position. Their given magnitudes are often not representative of the whole galaxy. For these we re-measured the u, g, r, i, z magnitudes at the central position using the SDSS navigator, and we assigned this set of magnitudes to the original SDSS redshift, discarding the spectral information. Furthermore we cleaned the SDSS list from double entries: e.g. galaxies with multiple spectra. We remained with 4132 galaxies (3955 from SDSS; 101 from CGCG; 76 from NED) with redshift and photometric parameters.

We did not apply corrections for surface brightness because they are negligible at the present sensitivity limit (Blanton et al. 2005b). Even so, with the contribution of faint objects from NED the catalogue should be nearly (94%) complete down to $r = 17.77$ ($i \sim 17.5$) according to Strauss et al. (2002).

A visual morphological classification aimed at disentangling early (dE, dS0, E, S0, S0a) from late-type (Sa to Sd, dIrr, BCD and S...) galaxies was carryed out using the SDSS online explorer. Since the present analysis is based solely on a two bin classification scheme (early vs. late) we considered sufficient that only one of us (GG) carried out the inspection of all 4132 galaxies.

Giant galaxies (E, S0, S0a, Sa, Sab, Sb, Sbc, Sc, Sd) with mild inclination were classified in steps of half Hubble class on a purely morphological basis, irrespective of their spectral classification. For 224 of them we can rely on the independent classification from Goldmine. The agreement is within $\sigma_{\rm type} = 0.7$ Hubble class. Instead, for high inclination objects, whose possible spiral structure could be hidden and whose color is reddened by internal absorption, our classification relied also on the inspection to the spectra: we separated S... from S0s according to the presence/absence of emission lines. Eventually, the fraction of emission line objects turned out to be negligible (5%) among E and S0 galaxies, it increased to 30% among S0a, and to 70% among S... objects. S0a are dubious transitional objects, as they are separated from S0s only for having a slighltly more evident disk component. They were grouped among early type galaxies.

Among dwarf galaxies, blue compact objects (BCD) were classified according to their amorphous compact morphology, blue color and strong emission lines. dIrr are blue, low surface brightness, emission line objects. Amorphous early-type dwarfs are red, absorption line systems and were classified as dE or dS0 according to the existence of lenticular components. It should be stressed that BCDs, dEs and S..., often have similar structureless morphology. Their difference is mainly dictated by their color and by the presence/absence of strong emission lines in their spectra (see also Fig. 12).

2.2. Spectroscopy

All 4132 galaxies in the present sample have a redshift measurement, but only for 3955 a spectrum was taken in the SDSS (in the central 3″ of the nucleus). For the remaining 177 we searched NED and Goldmine for available spectra and found only 11 (taken in the drift-scan mode, including the nucleus).

For the 3955 galaxies with a nuclear spectrum we obtained from the SDSS spectroscopic database the intensity and the equivalent width of the principal emission and absorption lines (from Hϵ λ 3970 to [SII] λ 6731) along with their signal-to-noise ratios.

Among spectra whose Balmer lines have signal-to-noise ratio >5 we identify 53 galaxies with Post-Star-Burst signature (PSB or k+a) adopting the criterion of Poggianti et al. (2004, inherited from Dressler et al. 1999; see however Quintero et al. 2004) that no emission lines should be present in the spectra and:

$$EW(H\delta) > 3 \text{ Å} \quad (1)$$

(adopting the convention that lines in absorption have positive EW). The PSB galaxies are analyzed in Sect. 7.1.

3. Analysis

3.1. Quantifying the local density

Figure 1 shows the modern version of the "Slice in the Universe" obtained with the SDSS data. The celestial distribution and the wedge diagram are given for the 4132 galaxies in the present study, coded according to their morphological classification (red: early-type; blue: late-type). The two rich clusters, Coma and Abell 1367 and some minor concentrations dominated by early-type galaxies are apparent, clearly indicating the well known correlation between the morphology of galaxies and their surrounding environment (e.g. Dressler 1980; Blanton & Berlind 2007).

Various approaches have been used to characterize the environment of galaxies. One possibility is to recognize groups and clusters, compute their virial mass from the velocity dispersion and assign a density to all the member galaxies. Another possibility consists in evaluating a local density parameter for each galaxy, by counting the number of galaxies in cylinders of given radius and half-length centered on each galaxy. This is the typical strategy of large surveys, for example followed by Kauffmann et al. (2004) (2 Mpc, 500 km s^{-1}), and Hogg et al. (2004) (1 h^{-1} Mpc, 8 h^{-1} Mpc $\sim$ 1000 km s^{-1}).

The typical half-lengths and radii used in the literature appear immediately inadequate to describe a region as the one under study, featuring two rich clusters with a velocity dispersion as large as ~1000 km s^{-1}. For instance, if we chose a cylinder of 500 or 1000 km s^{-1} depth, we would introduce a severe bias because galaxies with the largest velocity dispersion (i.e. the ones belonging to the extremities of the "Fingers of God" of the two clusters) would come out with a much lower density than the real density of the cluster they belong to, as noted by Lee et al. (2010). Conversely, if we used cylinders of 2000–3000 km s^{-1} length to evaluate the density around a relatively isolated object located far away from the two clusters, its density would came out overestimated because background and foreground galaxies not physically associated with it would wrongly contribute to the density.

In order to comply with criteria that are generally adopted in the literature (namely 1 Mpc, 1000 km s^{-1}), so that the results from this work could be easily compared with other reference papers, but also keeping an eye on the physical structures

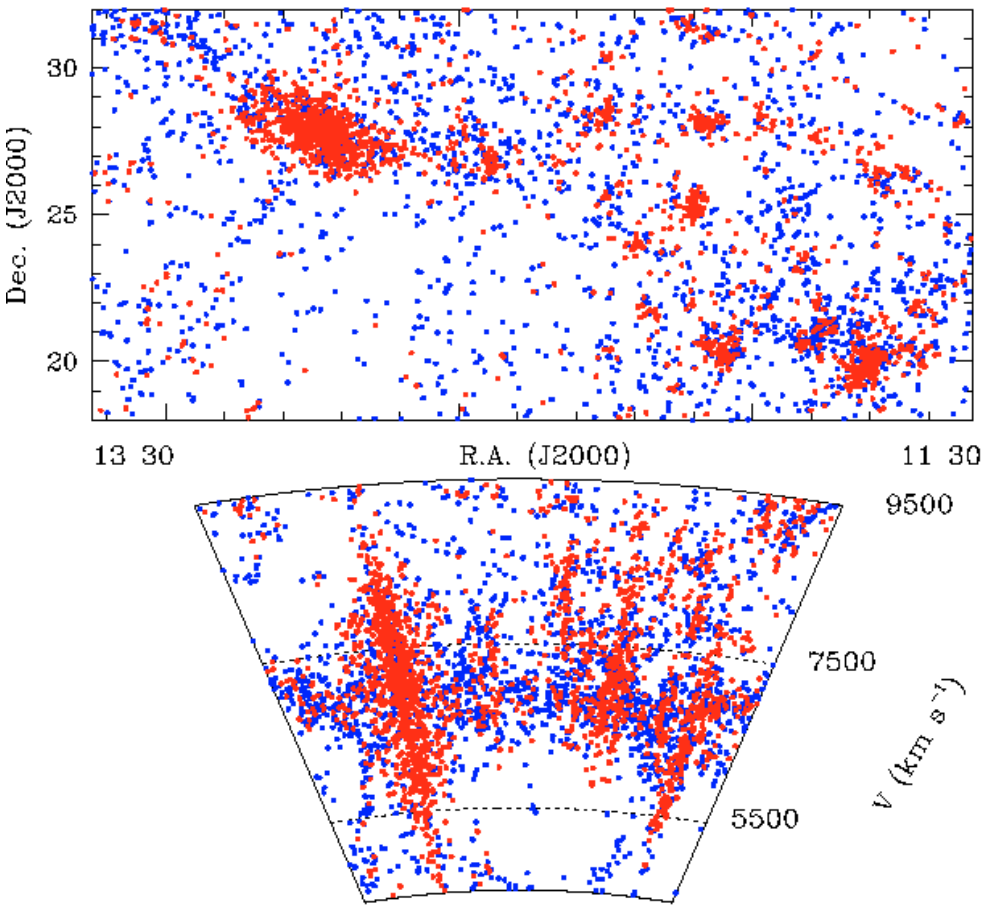

Fig. 1. Celestial distribution of 4132 galaxies from SDSS in the Coma supercluster 11.5^h < RA < 13.5^h; 18° < Dec < 32°; 4000 < zc < 9500 km s^{-1} (*top panel*) and their wedge diagram (*bottom panel*). Objects are color coded according to their morphological type (E+S0+S0a are red; Spirals, BCD, Pec, S... are blue). (This figure is available in color in electronic form.)

that constitute the CS, we decided to evaluate the density adopting the following compromise strategy. First we compress the "Fingers of God" of Coma and Abell 1367 in the redshift space by assigning to galaxies belonging to the "Fingers of God" a velocity equal to the average velocity of the cluster, plus or minus a random Gaussian distributed ΔV comparable to the transverse size of the cluster on the plane of the sky, assuming that clusters have approximately a spherical shape in 3-D. (We assume that the transverse size is 2 deg and 1 deg for Coma and A1367, corresponding to 248 and 124 km s^{-1} respectively.)

Then we parameterize the environment surrounding each galaxy using the 3-D density contrast computed as:

$$\delta_{1,1000} = \frac{\rho - \langle\rho\rangle}{\langle\rho\rangle}$$

where ρ is the local number density and $\langle\rho\rangle$ = 0.05 gal (h^{-1} Mpc)$^{-3}$ represents the mean number density measured in the whole region. The local number density ρ around each galaxy is computed within a cylinder with 1 h^{-1} Mpc radius and 1000 km s^{-1} half-length, which is large enough to comprise the dispersion of small groups and the newly compressed Finger of Gods of Coma and Abell 1367. To take into account boundary effects (the cylinders centered on galaxies near the edges of our sample will partially fall outside the studied volume), for each galaxy we divide ρ by the fraction of the volume of the cylinder that fall inside the survey borders.

We divide the sample in four over-density bins, chosen in order to highlight physically different environments of increasing level of aggregation (see Fig. 2): the UltraLow density bin (UL: $\delta_{1,1000} \leq 0$) describes the underlying cosmic web; the Low density bin (L: $0 < \delta_{1,1000} \leq 4$) comprises the filaments in the Great Wall and the loose groups; the High density bin (H: $4 < \delta_{1,1000} \leq 20$) include the cluster outskirts and the significant groups; the UltraHigh density bin (UH: $\delta_{1,1000} > 20$) corresponds to the cores of the clusters.

We would like to emphasize that the Coma Supercluster is by definition over-dense with respect to the mean Universe. Hogg et al. (2004) find a general density of 0.006 gal (h^{-1} Mpc)$^{-3}$ for $M_i < -19.5$. Our sample has a mean density of 0.05 gal (h^{-1} Mpc)$^{-3}$ for galaxies with $M_i < -17.5$. Adopting $M_i < -19.5$ the mean density in the Coma Supercluster becomes 0.019 gal (h^{-1} Mpc)$^{-3}$, thus we conclude that we are observing a region three times more dense, on average, than the mean density of the Universe. However if from the CS sample we subtract 916 galaxies in the densest bins UH and H, contributed to by the Coma cluster alone, the mean density drops to 0.015 gal/h^{-1} Mpc^3, i.e. 2.5 times over-dense than average.

Figure 2 shows the celestial distribution and the wedge diagram for the 4132 galaxies in the present study, coded according to the 4 over-density bins. Combined with Fig. 1, Fig. 2 indicates that the majority of early-type galaxies belongs to the UH and H bins, while the majority of late-type galaxies are in the L and UL bin.

The parameters of the two clusters and 8 most populated groups identified within the H density bin are listed in Table 1.

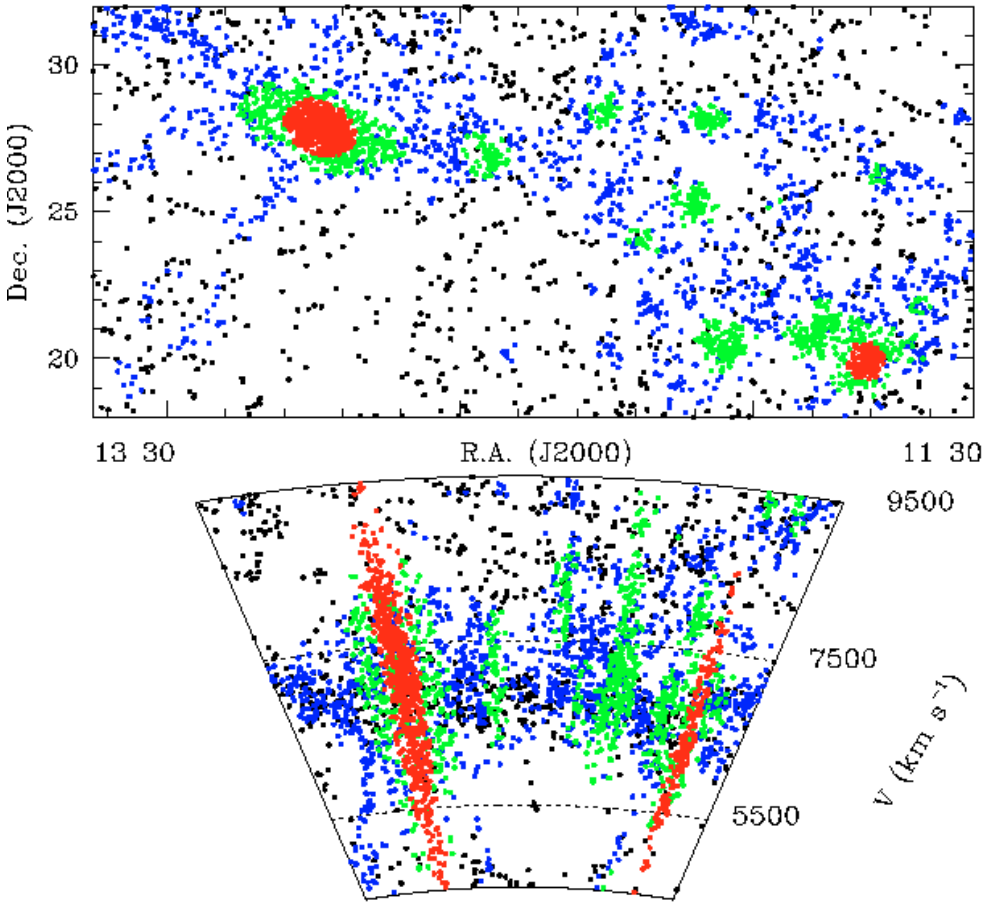

Fig. 2. Same as Fig. 1 except that objects are color coded according to their over-density (see Sect. 3.1) as follows: UH ($\delta_{1,1000} > 20$) are red; H ($4 < \delta_{1,1000} \leq 20$) are green; L ($0 < \delta_{1,1000} \leq 4$) are blue; UL ($\delta_{1,1000} \leq 0$) are black. (This figure is available in color in electronic form.)

Table 1. Mean coordinates, cz, velocity dispersion, density and number of elements of clusters and groups in the H density bin, with $N \geq 20$ members.

	NGC	⟨RA⟩	⟨Dec⟩	$\langle cz \rangle$	σ_v	$\delta^{\max}_{1,1000}$	N
		deg	deg	km s^{-1}	km s^{-1}		
Coma	4889	194.157	27.87	6972	940	60.4	750
A1367	3842	176.243	19.93	6494	762	27.7	220
grp-1	4065	181.069	20.46	7055	401	16.7	155
grp-2	3937	178.039	20.71	6659	294	12.0	83
grp-3	128-34	182.027	25.30	6707	349	9.0	78
grp-4	4555	189.024	26.85	7083	415	7.6	64
grp-5	4104	181.556	28.14	8410	450	8.9	62
grp-6	4295	185.054	28.47	8069	320	6.6	51
grp-7	3910	177.616	21.36	7874	207	11.8	43
grp-8	4213	183.787	24.01	6753	268	4.7	26

Some of these groups are known to contain radiogalaxies with complex morphology, suggestive of ram-pressure bending. The wide angle tail (WAT) radiogalaxy associated with N4061 is in group 1 (NGC 4065) (Jaffe et al. 1986). N4061 was also detected in X-ray by (Doe et al. 1995) implying a central IGM density of 4.9×10^{-4} cm^{-3}. Another WAT radiogalaxy CGCG 128-34 is the brightest member of group 3 (Jaffe & Gavazzi 1986). Mahdavi et al. (2005) report detection of extended X-ray emission from this group. Two among the richest groups identified in the H density bin have gas properties similar to small clusters. All groups have a velocity dispersion in excess of 200 km s^{-1}.

Table 2 gives some information on galaxies in the various density regimes. Red and Blue are above or below $g - i = -0.0585 * (M_i + 16) + 0.78$[3]; Lum and Faint are above or below $M_i = -20.5$ mag.

4. The color–luminosity relation

The $g - i$ color vs. i-band absolute magnitude relation for all galaxies in the CS is given in Fig. 3. Galaxies are coded

[3] The cutting line between blue and red has been arbitrarily set 0.2 mag bluer than $g - i = -0.0585 * (M_i + 16) + 0.98$, i.e. the best linear fit to the early-type galaxies.

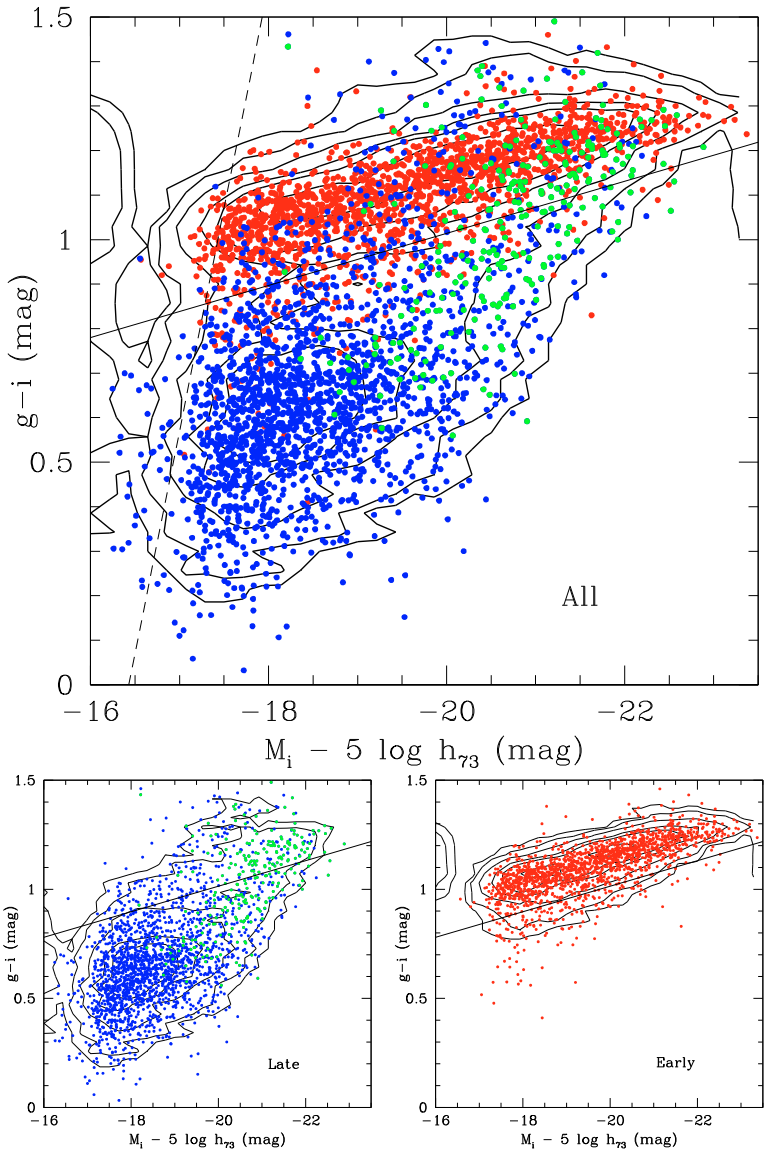

Fig. 3. $g - i$ color versus i-band absolute magnitude relation of all galaxies in the CS coded according to Hubble type: red = early-type galaxies (dE-E-S0-S0a); blue = disk galaxies (Sbc-Im-BCD); green = bulge galaxies (Sa-Sb): all galaxies (*top*); late-type from Sa to Im-BCD (*bottom left*); early type (*bottom right*). Contours of equal density are given. The continuum line $g - i = -0.0585 * (M_i + 16) + 0.78$ represents the empirical separation between the red-sequence and the remaining galaxies (see note 3). The dashed line illustrates the effect of the limiting magnitude $r = 17.77$ of the spectroscopic SDSS database, combined with the color of the faintest E galaxies $g - r \sim 0.70$ mag. (This figure is available in color in electronic form.)

Table 2. Percentage of galaxies in the various density bins (S0a are included among early-type).

	$\delta_{1,1000}$	All	Red	Lum/Faint$_{Red}$	Blue	Early	Late	PSB
		N	%	%	%	%	%	%
UL	≤0	835	22	82	78	18	82	0.5
L	0–4	1476	39	56	61	35	65	0.8
H	4–20	1032	63	47	37	61	39	2.4
UH	>20	789	82	32	18	84	16	7.3
All		4132	50	47	50	47	53	2.6

according to the Hubble type (top panel), with the late-type given alone in the bottom-left panel and the early-type alone in the bottom-right panel. As expected, the cut in morphological type correlates very well with the separation in color. In other words the red-sequence, or the locus of points redder than $g - i = -0.0585 * (M_i + 16) + 0.78$, is mostly populated by early-type galaxies, while the large majority of late-type galaxies form a blue cloud mostly at low luminosity, that steeply becomes redder as the luminosity increases. There are however exceptions, i.e. high luminosity spirals often have redder colors than ellipticals of similar luminosity, as recently emphasized by Lintott et al. (2008) and Bamford et al. (2009). These are large, mostly bulge dominated, sometimes edge-on spirals that are not only reddened by internal absorption, but even when their color is corrected for

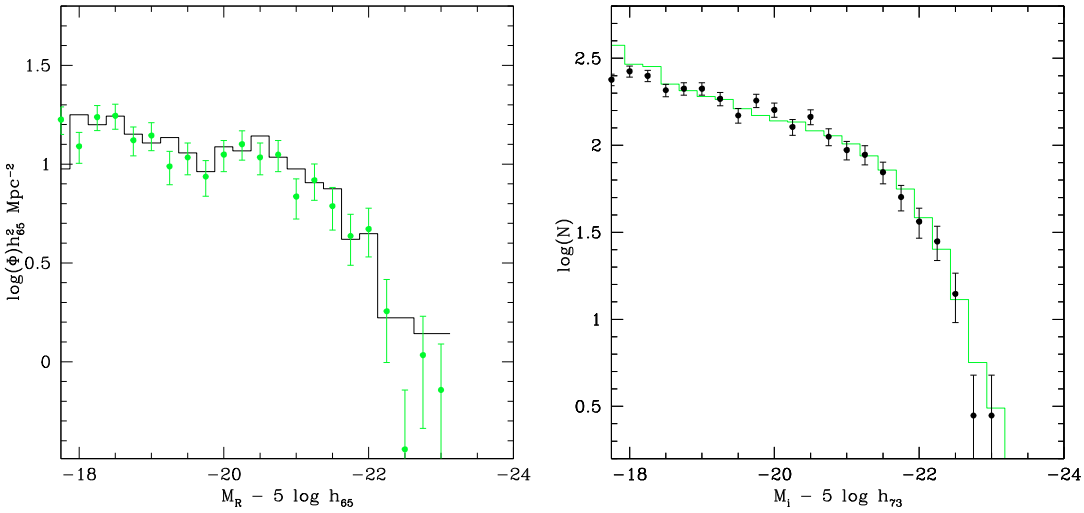

Fig. 4. *Left panel*: the *R*-band luminosity function of the Coma cluster adapted from Mobasher et al. (2003) (green dots) and the distribution of galaxies in the Coma cluster (including H and UH) from this work (black histogram) (converted to *R* and to $H_0 = 65$ km s^{-1} Mpc^{-1}) and normalized according to the areas covered by the two surveys. Error bars are omitted to avoid confusion. *Right panel*: the *i*-band luminosity function as derived from Blanton et al. (2005b) for the general field (green histogram) and the *i*-band luminosity distribution in the CS (including L and UL density) from this work (black dots) (shifted horizontally to account for $H_0 = 100$ km s^{-1} Mpc^{-1} used by Blanton et al. 2005b, and normalized arbitrarily on the vertical axis). (This figure is available in color in electronic form.)

dust absorption (see Fig. 8 of Cortese at al. 2008) they remain redder then lower luminosity spirals, due to the prevalence of their intrinsically red bulges, as concluded by Cortese & Hughes (2009). For example the most luminous spiral galaxy near the center of the Coma cluster, the famous NGC 4921, in spite of being close to face-on (see a plate of this prominent spiral recently taken with the HST by Cook 2006), has $g - i = 1.29$, i.e. comparable to $g - i = 1.27$ and 1.24 of NGC 4874 and NGC 4889 respectively, the two central giant ellipticals of Coma. Spirals would separate better from ellipticals at high luminosity if the NUV-H color index was used instead of $g - i$ (as in Gil de Paz et al. 2007; Cortese et al. 2008; Hughes & Cortese 2009), but unfortunately we don't have access to FIR data necessary to derive the amount of dust obscuration in these galaxies, thus to correct UV magnitudes (see Cortese et al. 2008).

5. Luminosity distributions

For the purpose of checking possible incompleteness in our data, first of all we compute the luminosity distribution obtained from the Sloan *r*-band data for the Coma cluster alone and we compare it, among the plethora of luminosity functions available in the literature, with the *R*-band determination obtained by Mobasher et al. (2003) (after converting our *r*(AB) magnitudes into *R* (Vega) mag and consistently adopting their $H_0 = 65$ km s^{-1} Mpc^{-1}). Our determination is normalized to theirs to account for the different portion of the Coma cluster covered by the two surveys. The two distributions, given in Fig. 4 (left panel), agree in details, including the slight deficit of galaxies near $M_R = -19.5$.

Similarly the *i*-band luminosity distribution of "isolated" galaxies in this work (including the UL and L density bins) is compared in Fig. 4 (right panel) with the luminosity function of the general field of Blanton et al. (2005b) (uncorrected for the effect of surface brightness, shifted horizontally to account for the Blanton et al. 2005b, use of $H_0 = 100$ km s^{-1} Mpc^{-1}, and normalized arbitrarily on the vertical scale). The two determinations are found in good agreement over the whole luminosity interval, supporting the preliminary conclusion that any residual incompleteness of our sample is within few percent. The slight deficit of galaxies for $M_i > -18.5$ should not influence the conclusions of this work. In the next section we study the luminosity distribution of galaxies in the Coma supercluster in bins of local galaxy density and Hubble type. Due to our inability to correct for possible, even though small, residual incompleteness in our data we prefer to give the number counts in (0.5 mag) bins of *i*-band absolute magnitude (without normalizing them to the sampled volume) and to call them *luminosity distributions* instead of *luminosity functions*. The distributions are conservatively plotted for $M_i < -17.75$, corresponding to $i \leq 17.15$ mag, i.e. 0.35 mag brighter than the spectroscopic limit $r = 17.77$ of the SDSS (assuming an average color of $\langle r - i \rangle = 0.25$).

We chose the *i*-band instead of *r*-band because it is a better tracer of the stellar mass in galaxies (Bell et al. 2003).

5.1. Local density

The luminosity distributions obtained in four bins of local galaxy density (see Sect. 3.1) and two of Hubble type are shown in Figs. 5–7. We have fitted the luminosity distributions obtained in this work with Schechter functions, computing the best fit parameters with an IDL code, taking advantage of the MPFIT function, a non linear least squares fitting task based on the Levenberg-Markwardt algorithm (Moré 1978; Markwardt 2009). We have also obtained the covariance matrix of the parameters again from the MPFIT function and we have evaluated the confidence ellipses at 1 and 2σ (as shown in the insets of Figs. 5–7). The fit parameters are given in Table 3.

Figure 5 shows that the distributions obtained mixing together galaxies of all Hubble types are completely insensitive to the environment. From Table 3 it is apparent that α and M_i^* are consistent within the errors in all density bins. This is very much the consequence of a cosmic conspiracy, since the distributions are complementary with respect to the Hubble type, as we will show by separating late-type galaxies from early-types (one can almost obtain Fig. 7 by reversing the symbol-colors in Fig. 6).

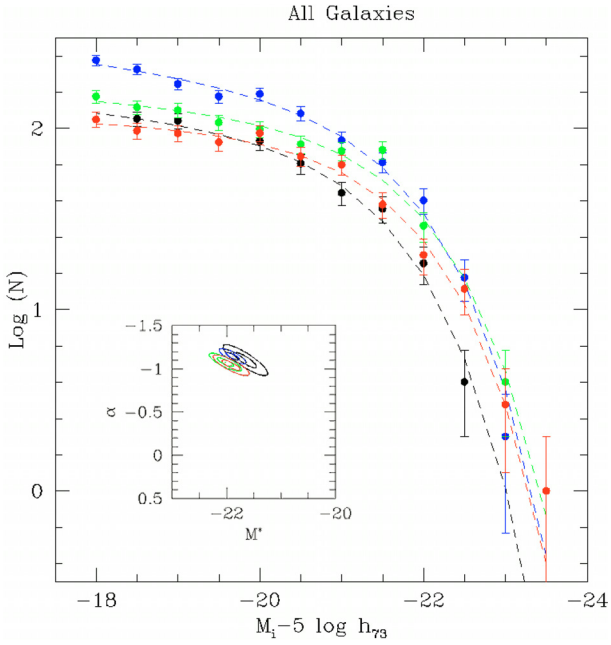

Fig. 5. *i*-band luminosity distribution of galaxies of all Hubble types coded according to bins of $\delta_{1,1000}$ (red = UH, green = H, Blue = L, black = UL). The dashed lines represent Schechter fits to the data whose parameters are given in Table 3. The inset shows the confidence ellipses of the fit parameters. No significant changes are seen in the fit parameters with density. (This figure is available in color in electronic form.)

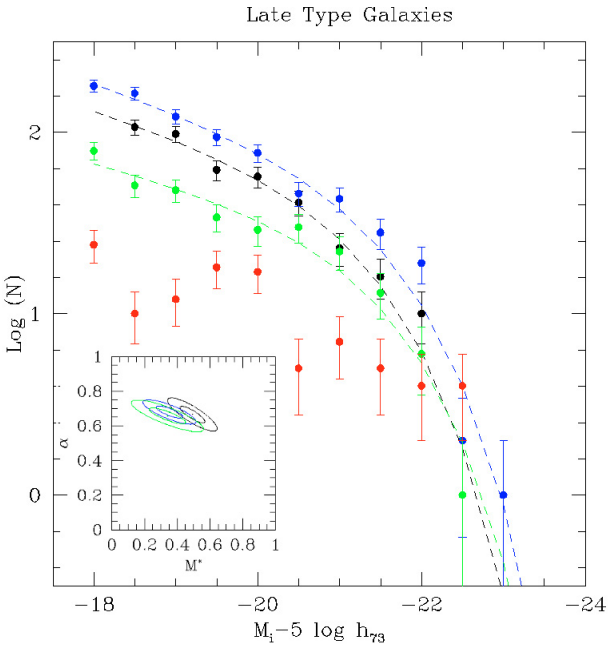

Fig. 6. Same as Fig. 5 for late-type galaxies. No significant changes are seen in the fit parameters with density, except for the UH bin where no reliable fit was obtained. (This figure is available in color in electronic form.)

When we consider the late-type galaxy population alone (Fig. 6) there is an evident decrease in the number of objects with increasing $\delta_{1,1000}$. In the highest density bin (UH) the number of late-type galaxies is so small that it is even insufficient for fitting a Schechter function. The other two fit parameters α and M_i^* are consistent within the errors (in the three lowest density bins we obtain a faint-end slope $\alpha \sim 1.3$ and $M_i^* \sim -21.7$), implying that the shape of the luminosity distribution of the late-type

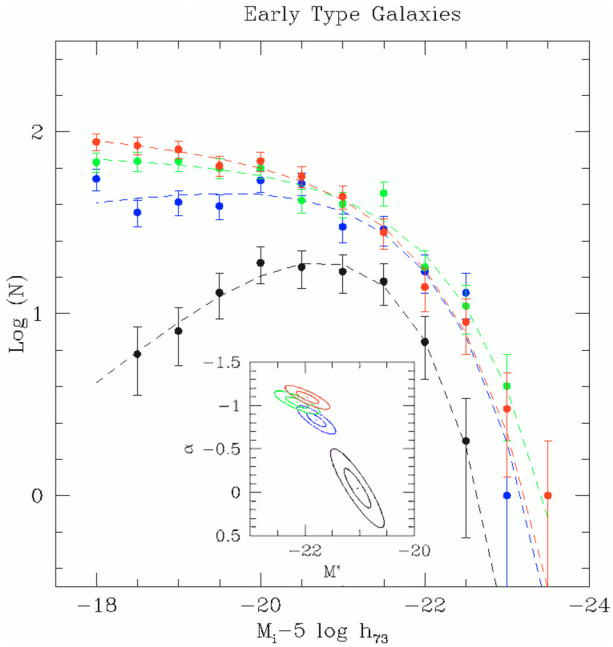

Fig. 7. Same as Fig. 5 for early-type galaxies. There is a significant decrease of α with increasing density. M_i^* stays within one magnitude. (This figure is available in color in electronic form.)

Table 3. Parameters of the Schechter functions fitted to the luminosity distributions.

		Φ	α	M_i^*
all	UH	103 ± 16	-1.04 ± 0.05	-21.91 ± 0.16
	H	120 ± 17	-1.07 ± 0.05	-22.02 ± 0.14
	L	156 ± 20	-1.14 ± 0.04	-21.89 ± 0.12
	UL	100 ± 21	-1.10 ± 0.08	-21.65 ± 0.20
early	UH	72 ± 14	-1.09 ± 0.06	-21.95 ± 0.20
	H	69 ± 13	-1.03 ± 0.06	-22.14 ± 0.20
	L	79 ± 13	-0.83 ± 0.08	-21.79 ± 0.17
	UL	56 ± 7	-0.04 ± 0.22	-21.03 ± 0.24
late	UH	–	–	–
	H	29 ± 10	-1.28 ± 0.10	-21.80 ± 0.30
	L	59 ± 13	-1.37 ± 0.06	-21.84 ± 0.19
	UL	52 ± 17	-1.33 ± 0.10	-21.58 ± 0.27

galaxy population is relatively insensitive to the local galaxy density, except for the highest density environments where late-type galaxies are rare at any luminosity. The luminosity distribution of early-type galaxies is given in Fig. 7 divided in the usual bins of local density. In the three highest density bins (L, H, UH) the luminosity distributions display small but continuous changes: their Schechter fit parameter α increases marginally and M_i^* stays constant within the errors (see Table 3). Highly significant discrepant α is found in the lowest density bin (UL or $\delta_{1,1000} < 0$), but the luminosity distributions of early-type galaxies have negative faint-end slopes in the two lowest density bins. This reflects a genuine lack of low luminosity early-type galaxies (dEs) in the low density cosmic web (UL). At high luminosity instead, even in the lowest density regime it appears that the giant elliptical galaxies are well formed, although M_i^* at UL is probably 0.5–1 mag fainter than at larger densities.

Summarizing, Figs. 5–7 show that the bright end of both the late- and the early-type sequences are consistently formed in all environments (small differences in M^* are due to the small number statistics in the brightest bins). On the opposite the fraction of faint early-type galaxies (dEs) depends on the environment, being significantly higher in dense than in isolated regions. The

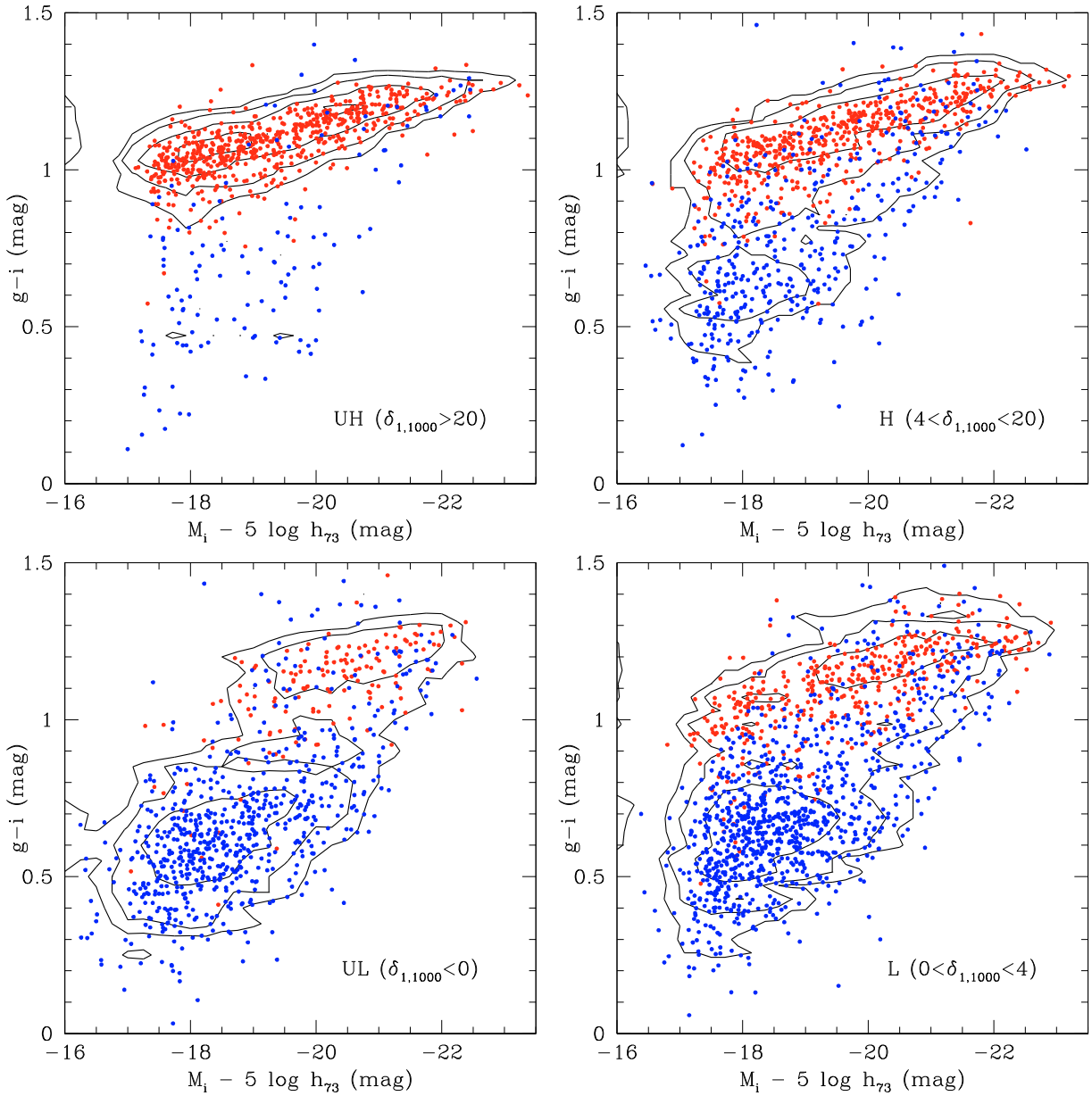

Fig. 8. $g - i$ color versus i-band absolute magnitude relation for galaxies in the CS, from UH to UL clockwise from top left, coded according to galaxy type (blue = late, red = early). Contours of equal density are given. (This figure is available in color in electronic form.)

one of late-types does the opposite, in agreement with Balogh et al. (2004a), Baldry et al. (2006), Martínez & Muriel (2006), Haines et al. (2006, 2007). Among isolated galaxies of low luminosity the missing early types are compensated by the abundant late-types. In dense regions the relative population mix is reversed.

It is remarkable that the luminosity distributions are consistent at the high luminosity end in all environments, suggesting that neither early-type (e.g. Whiley et al. 2008) nor late-type (e.g. Boselli et al. 2006) massive galaxies are currently undergoing major transformations. These have probably been going on at significantly higher redshift (Faber et al. 2007).

6. The environmental dependence of the color–luminosity relation

Among the most relevant achievements of the SDSS there is the discovery that the color (e.g. Blanton et al. 2005c; Haines et al. 2007) and the specific star formation rate (e.g. Kauffmann et al. 2004) of galaxies are strongly influenced by the environment. The Coma supercluster offers a very direct snapshot of these environmental transformations, as illustrated in Fig. 8, showing the 2-Dimensional color-luminosity relations derived in four bins of local galaxy density (UL, L, H, UH). The lowest density bin is composed almost entirely (see Table 2) of blue (78%), late-type (82%), dwarfish galaxies, however even in this bin a hint of red sequence exists (22%) composed of early-type galaxies (18%), but is significantly lacking at low-luminosity ($M_i > -18.5$). As the local density approaches $0 < \delta_{1,1000} < 4$, i.e. the regime traced by small groups and other faint structures in the Great Wall, the blue sequence remains dominating (61%), the red sequence appears well formed in its full luminosity span, but early-type galaxies represent only 35% of all galaxies. By increasing the galaxy density to $4 < \delta_{1,1000} < 20$, dominated by large groups and by the cluster outskirts, the percentage of late type galaxies drops to 39% and that of early-type increases to 61%. At the highest density $\delta_{1,1000} > 20$, i.e. in the core of the rich clusters, galaxies consist of nothing but early-type objects (84%) distributed along the red sequence (82%). We wish to emphasize

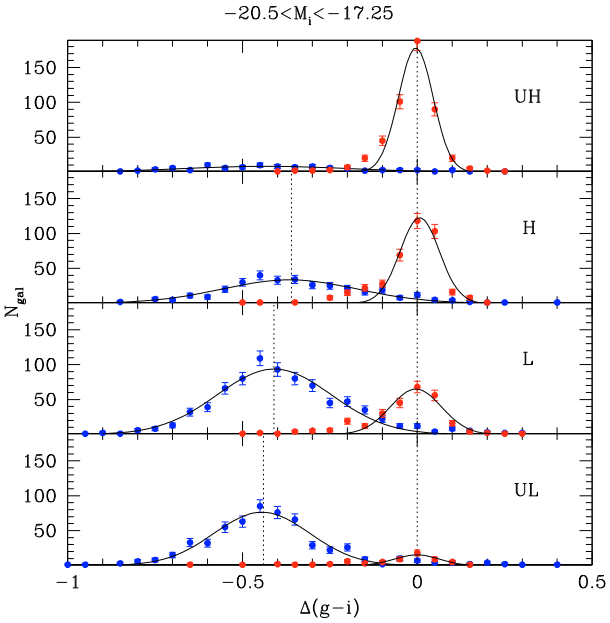

Fig. 9. Histograms and Gaussian fits of $\Delta(g-i)$, representing the difference in color of individual galaxies from the linear fit to the red sequence, for galaxies in four density bins and $M_i > -20.5$. Late-type (blue symbols) are sparated from early-type galaxies (red symbols). (This figure is available in color in electronic form.)

Table 4. Parameters of the Gaussian fitted to the $\Delta(g-i)$ histograms in Fig. 9 for $M_i > -20.5$.

	Late		Early	
Dens	$\langle\Delta(g-i)_L\rangle$	σ_L	$\langle\Delta(g-i)_E\rangle$	σ_E
UH	– –	–	-0.004 ± 0.001	0.049
H	-0.365 ± 0.003	0.193	0.006 ± 0.001	0.056
L	-0.409 ± 0.001	0.162	-0.004 ± 0.001	0.073
UL	-0.444 ± 0.001	0.136	-0.001 ± 0.003	0.063

that some red sequence galaxies exist in all environments but they span the full luminosity range $-17.75 < M_i < -23$ (including dEs) only for densities larger than $\delta_{1,1000} > 0$ and that the mix of morphological type depends on the local galaxy density (see also Fig. 13).

Figure 9 shows histograms of the $\Delta(g-i)$ color, e.g. the difference in color of individual galaxies from the linear fit to the red sequence (see note 3), in other words after removing the slope of the red-sequence from the color-luminosity relation of Fig. 3, in four bins of galaxy density and for $M_i > -20.5$ mag (where the majority of the late-type galaxies are found). The distributions of early and late-type galaxies are fitted with two Gaussians, whose parameters are listed in Table 4. The ratio of late to early objects is strongly density dependent. Moreover the mean color difference of the late-type population with respect to the early-type sequence reddens systematically from UL ($\Delta(g-i) = -0.44$ mag), L ($\Delta(g-i) = -0.41$ mag), H ($\Delta(g-i) = -0.36$ mag) (the contribution of the blue sequence at UH is so marginal that no Gaussian fitting is derived), indicating that galaxies, even though remaining in the blue sequence, migrate to redder colors, i.e. are subject to progressive quenching of the star formation as the environment density progressively increases.

7. Discussion

At the present cosmological epoch there is evidence that dynamical units (clusters) are continuously fed by the infall of clouds predominantly constituted by late-type galaxies occurring along the filamentary structures that compose the cosmic web (Adami et al. 2005; Cortese et al. 2008; Tran et al. 2008), as predicted by simulations of the hierarchical galaxy formation paradigm (e.g. Springel et al. 2005). Direct evidence for infall into the Coma cluster derives from X-ray observations supporting the recent infall of the NGC 4839 group (Neumann et al. 2003) onto the main cluster. More indirect line of evidence for infall of late-type galaxies on the Coma cluster is in our own data, i.e. the velocity distribution of late-type galaxies belonging to the Coma cluster (in the density bin UH and H, corresponding to the core + outskirts) is significantly non Gaussian with $\sigma_V = 1046$ km s^{-1}, exceeding $\sigma_V = 872$ km s^{-1} of early-type members which, instead have isotropic distribution.

The way the color-luminosity plane is populated by ∼4000 galaxies representative of different environments in the local universe around the Coma cluster, as revealed by the Sloan survey, strengthens the following scenario:

1. No strong environmental differences are seen in the galaxy population of the local universe (Fig. 5) unless late-type galaxies (Fig. 6) are counted separately from early-types (Fig. 7): the former decrease in fraction with increasing local density, viceversa the latter.
2. The differences at $z = 0$ involve mostly galaxies of low luminosity (mass) (well below M^*), in agreement with Scarlata et al. (2007). The missing low-luminosity late-type galaxies in dense environments compensate exactly the missing low-luminosity early-type galaxies in loose environments.
3. High luminosity galaxies ($M_i < -20.5$) show little environmental differences in both their early-type and late-type components (see Table 3), i.e. early-type galaxies have $M^* \sim 1$ mag fainter in extreme isolation. This shift shows up even in the global Luminosity Function (all types) as a ∼0.5 mag difference in M^* of UL compared to higher density. A similar shift is found in the zCOSMOS low redshift bin ($0.2 < z < 0.5$) by Tasca et al. (2009) who refers to Bolzonella et al. (2009). Notice however that their study covers a density regime that falls entirely within our UL and L bins and misses high density Coma-like clusters.

Points 1–3 form a coherent evolutionary picture assuming that at recent cosmological epochs strong environmental transformations ("Nurture") of the galaxy population involve low luminosity blue amorphous dwarf galaxies (BCDs) that progressively become dEs in their infall into denser structures, in further agreement with Haines et al. (2008). This major shift consists of a pure color migration from blue to red by about 0.5 mag ($g-i$), causing a major spectroscopical change, accompanied by a minor change in morphology. No significant luminosity growth is seen along this process, as derived from the comparable luminosity of blue systems abundant in isolation and of red dwarfs abundant in denser regions.

High luminosity galaxies appear to be already in place, irrespective of the environment, from previous cosmological epochs, probably as a consequence of the "Nature" process known as downsizing (Cowie et al. 1996; Gavazzi et al. 1996; Gavazzi & Scodeggio 1996; Boselli et al. 2001; Fontanot et al. 2009). Massive ellipticals and massive bulge-dominated spirals are likely to have formed at significant redshift due to major merging (as predicted by merger trees, e.g. De Lucia et al. 2006; and observed by Faber et al. 2007; Scarlata et al. 2007; Bell et al. 2007).

At progressively lower redshift ($z < 1$) no evolution is observed for the massive early-type galaxies (e.g. Whiley et al. 2008; Cool et al. 2008) and the formation of the red sequence

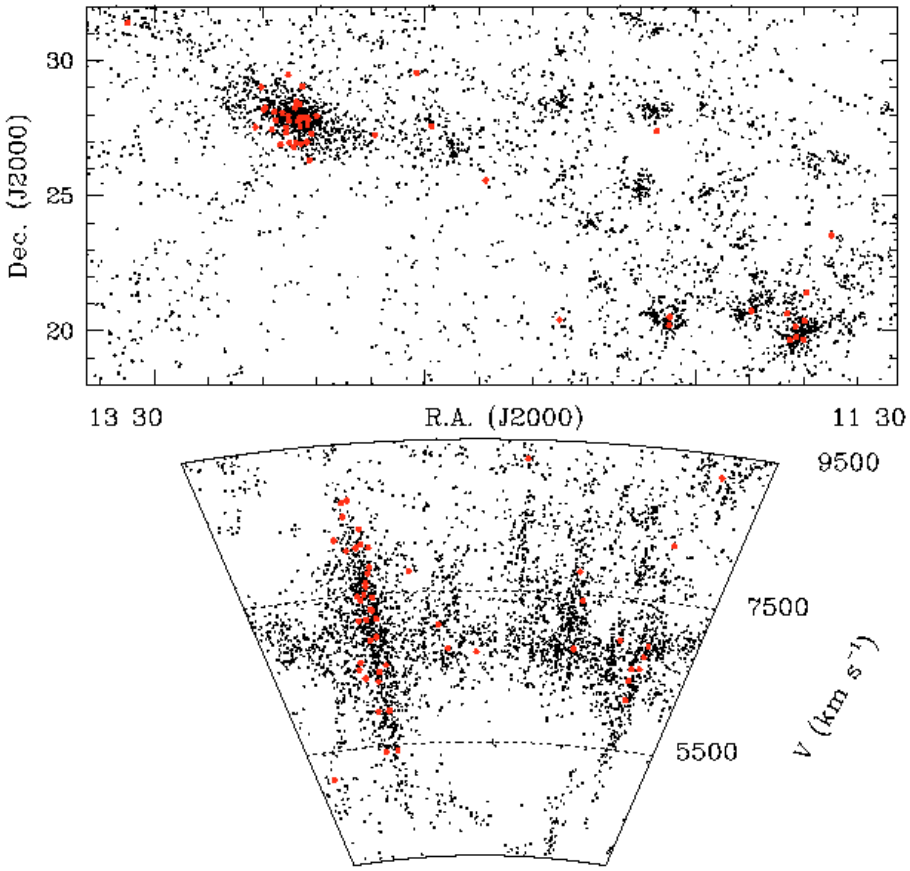

Fig. 10. The projected distribution of the 53 PSB galaxies selected according to Eq. (1) (large red dots) in the Coma Supercluster (small dots). (This figure is available in color in electronic form.)

is shifted to lower luminosities in the environment of over-dense regions (groups and clusters).

The evolutionary scenario emerging from the present investigation of galaxies at $z = 0$ is coherent with the results of De Lucia et al. (2007) who investigated several clusters at high redshift ($0.4 < z < 0.8$). They find that the ratio of luminous to faint galaxies in the red sequence increases with z, and conclude that the low luminosity part of the red sequence was formed only between $z = 0.5$ and $z = 0$[4].

At $z = 0$ our analysis seems to indicate that major merging is not necessarily the relevant environmental process for the build-up of the red sequence at low luminosity. Instead we concur with previous investigations that low mass amorphous blue objects are transformed into dEs by migration across the green valley, due to quenching of the star formation, primarily in galaxies falling into the clusters and to a lesser extent in groups and looser structures. The physical mechanisms that appear most likely to be behind the migration are harassment (Moore et al. 1999), ram-pressure stripping (Gunn & Gott 1972), as proposed by Boselli et al. (2008a,b), confirmed by Hughes & Cortese (2009) for the Virgo cluster, and recently extended to the Perseus cluster by Penny et al. (2010). According to the latest simulations of ram-pressure by Bekki (2009), gas stripping with consequent gradual truncation of the star formation occurs even in small groups, but it proceeds less efficiently than in cluster environments, where low-mass galaxies are likely to truncate their star formation more rapidly.

7.1. Post-star-burst galaxies

In agreement with Boselli et al. (2008a) we propose that post-star-burst (PSB) galaxies represent the current tracer of the above migration. k+a (also named E+A) galaxies, identified by their strong Balmer absorption lines, gained attention after their discovery in distant clusters by Dressler & Gunn (1983) and in the Coma cluster by Caldwell et al. (1993). They were interpreted as Post-Star-Burst galaxies in the seminal work by Couch & Sharples (1987). Nowadays they are known to have rapidly ceased to form stars between 5×10^7 and 1.5×10^9 years prior to observations (see Poggianti et al. 2009, and references therein). Significant downsizing is observed in these systems as their typical luminosity is $M_V \leq -20$ in clusters at $z = 0.5$, compared with $M_V \geq -18.5$ found in the Coma cluster (Poggianti et al. 2004). The youngest (Blue) PSB galaxies are found to correlate with the X-ray structure of the Coma cluster, suggesting that the star formation has been suppressed as a consequence of the hostile environment for those galaxies that have recently accreted (Dressler et al. 1999; Poggianti et al. 1999). Studies at $0.4 < z < 0.8$ confirm that k+a galaxies are preferentially found in dense environments (Poggianti et al. 2009), however this point is controversial (e.g. Zabludoff et al. 1996; Balogh et al. 2005).

We find 53 such galaxies in our survey (meeting the criterion for k+a given in Sect. 2). Their distribution appears significantly clustered. In fact we find only 2 PSBs in the UL bin (0.5%), 6 in the L bin (0.8%), 13 in the H bin (2.4%), predominantly in

[4] By adjusting arbitrarily the limit between luminous and faint galaxies in our survey to $M_i = -20.5$ we obtain that the ratio lum/faint in the red sequence is 0.32 in the UH bin (dominated by the Coma cluster), deliberately matching the value found for the Coma cluster by De Lucia et al. (2007) using V-band observations. This ratio is strongly environment dependent at $z = 0$ as it increases from 0.32 in UH, 0.47 in H, 0.56 in L to 0.82 in UL (see Table 2). This growth with decreasing density mimics remarkably the growth with increasing z found by De Lucia et al. (2007).

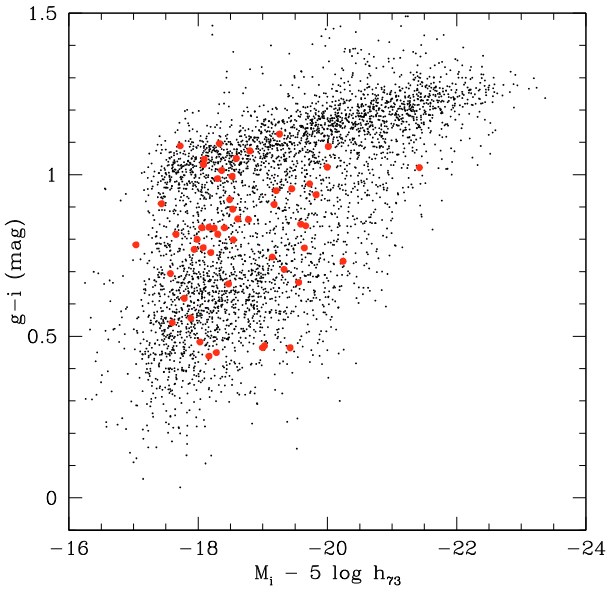

Fig. 11. $g - i$ color versus i-band absolute magnitude relation for all SDSS galaxies (small black dots) and for 90 CGCG galaxies without spectral classification (large black dots). Red dots represent PSB galaxies selected according to Eq. (1). (This figure is available in color in electronic form.)

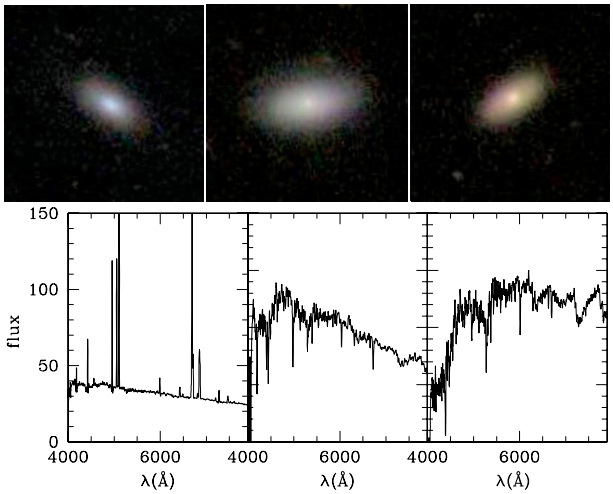

Fig. 12. Images and spectra of (*left to right*) one BCD, one PSB with blue continuum and one dE galaxy from this work. (This figure is available in color in electronic form.)

the outskirt of the Coma cluster, and the remaining 32 belonging to the densest UH bin (7.3%), as illustrated in Fig. 10 and in Table 2[5]. The color of PSB galaxies tend to fill the gap between the red and the blue sequence (green valley), as shown in Fig. 11. In agreement with Poggianti et al. (2004) their distribution is skewed toward low luminosity, (43/53 PSBs have $M_i > -19.5$).

We can exclude that the spectral incompleteness at high luminosity discussed in Sect. 2.2 biases against luminous PSBs since among luminous galaxies ($M_i < -20.5$) we expect to miss only 0.1 ± 0.1 PSB.

PSB galaxies are likely to represent the transition systems between dwarf star forming and quiescent galaxies. They have similarly amorphous morphology, as shown in Fig. 12, where three galaxies with similarly low luminosity ($-18.3 > M_i > -19.7$) are presented, one randomly selected among the plethora of isolated BCDs, one among the blue PSBs and one of the dEs in the Coma cluster. In a black-white picture they would result absolutely indistinguishable. Their distinctive character, represented by the color of their continuum and by the intensity of their lines, resides in their history of star formation, that is currently active in BCDs, has ceased less than 1.5 Gyr ago in PSBs (0.5 Gyr in the blue ones) and is absent among dEs.

Figure 13 gives the fraction of PSBs and of early-type galaxies as a function of the log of the local density (left panels) and of the projected distance from the Coma cluster (right panels). The fraction of PSBs stays constant (approximately at the 1% level) up to $\delta_{1,1000} \sim 10$, and reaches 8% at $\delta_{1,1000} \sim 30$, without further increasing in the cluster core. The radial distribution around the Coma cluster shows a maximum at ∼1–2 Mpc projected radius and does not increase further inward. At this projected distance from the center, the density of the hot gas estimated by Makino (1994) is $n \sim 7 \times 10^{-4}$ cm^{-3}, sufficient to produce significant stripping according to Bekki (2009).

8. Conclusions and summary

If our assumption that PSBs are the carriers of the transformation occurring across the green valley holds true, their strong clustering around the densest structures is in apparent contradiction with the fact that the migration discussed in Sect. 6 involves also much less dense environments. Timescales offer an obvious solution to this riddle. To see the PSB signature in a galaxy spectrum, it is required that the time-scale of the truncation of the star formation should be as short as ∼100 Myr, as concluded by Boselli et al. (2008a) who model a highly efficient ram-pressure event in the Virgo cluster. If gas ablation occurs with longer timescales, the star formation results gradually suppressed, with resultant persistence of residual Balmer lines in emission, thus without PSB signature. Ram pressure stripping in clusters is a fast phenomenon, while the same mechanism in groups (Bekki 2009) and other related mechanisms, such as harassment (Moore et al. 1999) or starvation occur in looser aggregates with longer time scales.

The fact that clusters are fully evolved since $z = 1$ makes them the most favorable environments for the transformations at recent epochs. At larger look back time the action was going on at lower rates in less dense environments, inseminating the red sequence with small amounts of late-type galaxies (see Fig. 8, bottom panels), but since clusters have fully formed, the Nurture effect became more vigorous in their environment, leading to an almost complete draining of blue galaxies (see Fig. 8, top panels).

The main results of the present analysis of ∼4000 galaxies in the Coma Supercluster, carried out using DR7-SDSS data can be summarized as follows:

1. At $z = 0$ there is evidence of little luminosity evolution among high luminosity galaxies ($M_i < -20$).
2. At $z = 0$ there is strong migration of late/blue/star forming into early/red/quiescent systems taking place among dwarf ($M_i > -19$) galaxies, as summarized in Fig. 14.
3. Although the migration takes place also in loose structures it is more efficient in denser environments, such as clusters of galaxies ("Nurture").
4. Quenching of the star formation is induced in clusters by fast gas-ablation mechanism, namely ram-pressure.

[5] The fraction of PSB galaxies in Table 2 has been computed dividing the number of PSBs by the number of galaxies with signal-to-noise ratio >5 in the spectra.

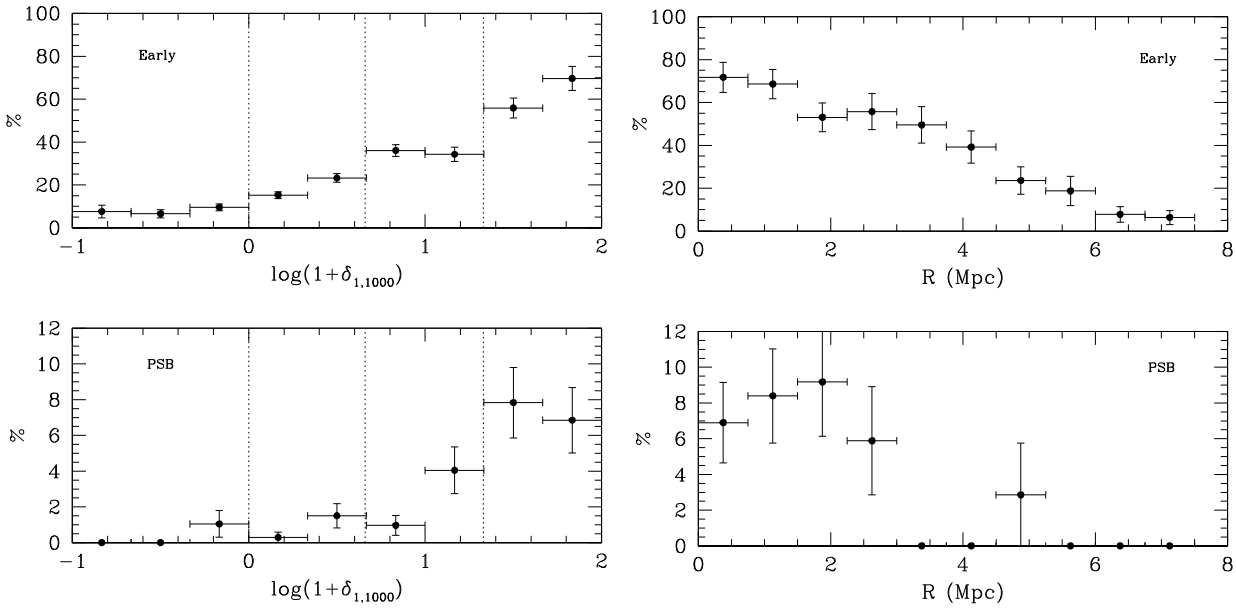

Fig. 13. Fraction of of early-type galaxies (*top*) and of PSB (*bottom*) as a function of the (logarithmic) $\delta_{1,1000}$ (*left*) and of the radial distance from the Coma cluster (*right*). The dashed vertical lines mark the density thresholds adopted in this work.

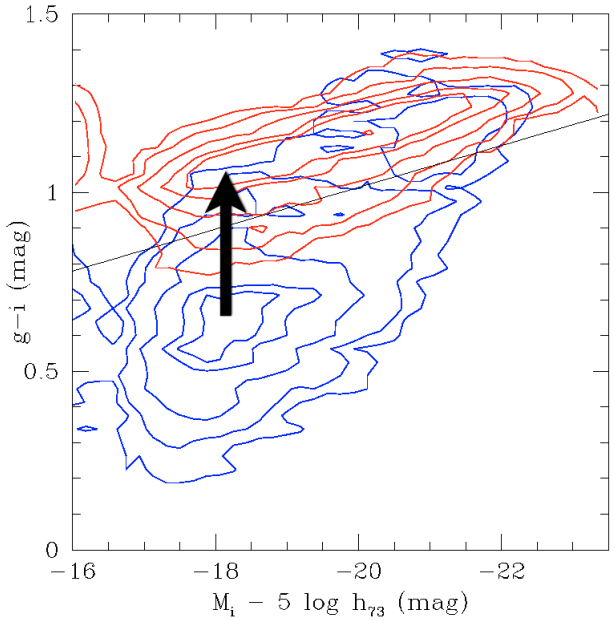

Fig. 14. The $g - i$ color versus i-band absolute magnitude relation for late-type galaxies (blue contours) and for early-type galaxies (red contours). The arrow marks the effect of Nurture at $z = 0$ in dense environments. Low-luminosity blue galaxies have their star formation truncated as a result of gas stripping. (This figure is available in color in electronic form.)

5. Post-star-burst galaxies appear the tracers of the migration taking place in dense environments.

Acknowledgements. We thank Roberto Decarli for help in querying the SDSS archive and Veronique Buat, Gabriella De Lucia, Michele Fumagalli, Bianca Poggianti and Marco Scodeggio for helpful discussions. We are grateful to Paolo Franzetti and Alessandro Donati for their contribution to GOLDMine, the Galaxy On Line Database extensively used in this work (http://goldmine.mib.infn.it). We acknowledge the constructive criticism from an unknown referee. The present study could not be conceived without the DR7 of SDSS. Funding for the Sloan Digital Sky Survey (SDSS) and SDSS-II has been provided by the Alfred P. Sloan Foundation, the Participating Institutions, the National Science Foundation, the US Department of Energy, the National Aeronautics and Space Administration, the Japanese Monbukagakusho, and the Max Planck Society, and the Higher Education Funding Council for England. The SDSS Web site is http://www.sdss.org/. The SDSS is managed by the Astrophysical Research Consortium (ARC) for the Participating Institutions. The Participating Institutions are the American Museum of Natural History, Astrophysical Institute Potsdam, University of Basel, University of Cambridge, Case Western Reserve University, The University of Chicago, Drexel University, Fermilab, the Institute for Advanced Study, the Japan Participation Group, The Johns Hopkins University, the Joint Institute for Nuclear Astrophysics, the Kavli Institute for Particle Astrophysics and Cosmology, the Korean Scientist Group, the Chinese Academy of Sciences (LAMOST), Los Alamos National Laboratory, the Max-Planck-Institute for Astronomy (MPIA), the Max-Planck-Institute for Astrophysics (MPA), New Mexico State University, Ohio State University, University of Pittsburgh, University of Portsmouth, Princeton University, the United States Naval Observatory, and the University of Washington.

References

Adami, C., Biviano, A., Durret, F., & Mazure, A. 2005, A&A, 443, 17
Baldry, I. K., Balogh, M. L., Bower, R. G., et al. 2006, MNRAS, 373, 469
Balogh, M. L., Baldry, I. K., Nichol, R., et al. 2004a, ApJ, 615, L101
Balogh, M., Eke, V., Miller, C., et al. 2004b, MNRAS, 348, 1355
Balogh, M. L., Miller, C., Nichol, R., Zabludoff, A., & Goto, T. 2005, MNRAS, 360, 587
Bamford, S. P., Nichol, R. C., Baldry, I. K., et al. 2009, MNRAS, 393, 1324
Bell, E. F., McIntosh, D. H., Katz, N., & Weinberg, M. D. 2003, ApJS, 149, 289
Bell, E. F., Zheng, X. Z., Papovich, C., et al. 2007, ApJ, 663, 834
Bekki, K. 2009, MNRAS, 399, 2221
Bernardi, M., Sheth, R. K., Tundo, E., & Hyde, J. B. 2007, ApJ, 660, 267
Blanton, M. R., & Berlind, A. A. 2007, ApJ, 664, 791
Blanton, M. R., & Moustakas, J. 2009, ARA&A, 47, 159
Blanton, M. R., Schlegel, D. J., Strauss, M. A., et al. 2005a, AJ, 129, 2562
Blanton, M. R., Lupton, R. H., Schlegel, D. J., et al. 2005b, ApJ, 631, 208
Blanton, M. R., Eisenstein, D., Hogg, D. W., Schlegel, D. J., & Brinkmann, J. 2005c, ApJ, 629, 143
Bolzonella, M., et al. 2009, A&A, submitted, [arXiv:0907.0013v1]
Boselli, A., & Gavazzi, G. 2006, PASP, 118, 517
Boselli, A., Gavazzi, G., Donas, J., & Scodeggio, M. 2001, AJ, 121, 753
Boselli, A., Boissier, S., Cortese, L., et al. 2006, ApJ, 651, 811
Boselli, A., Boissier, S., Cortese, L., & Gavazzi, G. 2008a, ApJ, 674, 742
Boselli, A., Boissier, S., Cortese, L., & Gavazzi, G. 2008b, A&A, 489, 1015
Caldwell, N., Rose, J. A., Sharples, R. M., Ellis, R. S., & Bower, R. G. 1993, AJ, 106, 473
Cassata, P., Guzzo, L., Franceschini, A., et al. 2007, ApJS, 172, 270
Chincarini, G. L., Giovanelli, R., & Haynes, M. P. 1983, ApJ, 269, 13
Cook, K. 2006, HST Proposal, 10842

Cool, R. J., Eisenstein, D. J., Fan, X., et al. 2008, ApJ, 682, 919
Cortese, L., & Hughes, T. M. 2009, MNRAS, 400, 1225
Cortese, L., Gavazzi, G., & Boselli, A. 2008, MNRAS, 390, 1282
Couch, W. J., & Sharples, R. M. 1987, MNRAS, 229, 423
Cowie, L. L., Songaila, A., Hu, E. M., & Cohen, J. G. 1996, AJ, 112, 839
de Lapparent, V., Geller, M. J., & Huchra, J. P. 1986, ApJ, 302, L1
De Lucia, G., Springel, V., White, S. D. M., Croton, D., & Kauffmann, G. 2006, MNRAS, 366, 499
De Lucia, G., Poggianti, B. M., Aragón-Salamanca, A., et al. 2007, MNRAS, 374, 809
Doe, S. M., Ledlow, M. J., Burns, J. O., & White, R. A. 1995, AJ, 110, 46
Dressler, A. 1980, ApJ, 236, 351
Dressler, A., & Gunn, J. E. 1983, ApJ, 270, 7
Dressler, A., Smail, I., Poggianti, B. M., et al. 1999, ApJS, 122, 51
Faber, S. M., Willmer, C. N. A., Wolf, C., et al. 2007, ApJ, 665, 265
Fontana, A., Salimbeni, S., Grazian, A., et al. 2006, A&A, 459, 745
Fontanot, F., De Lucia, G., Monaco, P., Somerville, R. S., & Santini, P. 2009, MNRAS, 397, 1776
Gavazzi, G. 1987, ApJ, 320, 96
Gavazzi, G. 1989, ApJ, 346, 59
Gavazzi, G., & Scodeggio, M. 1996, A&A, 312, L29
Gavazzi, G., Pierini, D., & Boselli, A. 1996, A&A, 312, 397
Gavazzi, G., Carrasco, L., & Galli, R. 1999, A&AS, 136, 227
Gavazzi, G., Boselli, A., Donati, A., Franzetti, P., & Scodeggio, M. 2003, A&A, 400, 451
Gil de Paz, A., Boissier, S., Madore, B. F., et al. 2007, ApJS, 173, 185
Gregory, S. A., & Thompson, L. A. 1978, ApJ, 222, 784
Gunn, J. E., & Gott, J. R. I. 1972, ApJ, 176, 1
Haines, C. P., La Barbera, F., Mercurio, A., Merluzzi, P., & Busarello, G. 2006, ApJ, 647, L21
Haines, C. P., Gargiulo, A., La Barbera, F., et al. 2007, MNRAS, 381, 7
Haines, C. P., Gargiulo, A., & Merluzzi, P. 2008, MNRAS, 385, 1201
Heidt, J., Appenzeller, I., Gabasch, A., et al. 2003, A&A, 398, 49
Hogg, D. W., Blanton, M. R., Brinchmann, J., et al. 2004, ApJ, 601, L29
Hughes, T. M., & Cortese, L. 2009, MNRAS, 396, L41
Jaffe, W., & Gavazzi, G. 1986, AJ, 91, 204
Jaffe, W., Gavazzi, G., & Valentijn, E. 1986, AJ, 91, 199
Kauffmann, G., White, S. D. M., Heckman, T. M., et al. 2004, MNRAS, 353, 713
Lauer, T. R., Tremaine, S., Richstone, D., & Faber, S. M. 2007, ApJ, 670, 249
Lee, J. H., Lee, M. G., Park, C., & Choi, Y.-Y. 2010, MNRAS, 403, 1930
Lintott, C. J., Schawinski, K., Slosar, A., et al. 2008, MNRAS, 389, 1179
Lisker, T., Grebel, E. K., Binggeli, B., & Glatt, K. 2007, ApJ, 660, 1186
Mahdavi, A., Finoguenov, A., Böhringer, H., Geller, M. J., & Henry, J. P. 2005, ApJ, 622, 187
Makino, N. 1994, PASJ, 46, 139
Mandelbaum, R., Hirata, C. M., Seljak, U., et al. 2005, MNRAS, 361, 1287
Markwardt, C. B. 2009, ASP Conf. Ser., 411, 251
Martínez, H. J., & Muriel, H. 2006, MNRAS, 370, 1003
Mobasher, B., Colless, M., Carter, D., et al. 2003, ApJ, 587, 605
Moore, B., Lake, G., Quinn, T., & Stadel, J. 1999, MNRAS, 304, 465
Moré, J. 1978, The Levenberg-Marquardt Algorithm: Implementation and Theory, in Numerical Analysis, ed. G. A. Watson (Berlin: Springer-Verlag), 630, 105
Neumann, D. M., Lumb, D. H., Pratt, G. W., & Briel, U. G. 2003, A&A, 400, 811
Quintero, A. D., Hogg, D. W., Blanton, M. R., et al. 2004, ApJ, 602, 190
Penny, S. J., Conselice, C. J., De Rijcke, S., et al. 2010, MNRAS, submitted, [arXiv:1001.1755]
Poggianti, B. M., Smail, I., Dressler, A., et al. 1999, ApJ, 518, 576
Poggianti, B. M., Bridges, T. J., Komiyama, Y., et al. 2004, ApJ, 601, 197
Poggianti, B. M., Desai, V., Finn, R., et al. 2008, ApJ, 684, 888
Poggianti, B. M., Aragón-Salamanca, A., Zaritsky, D., et al. 2009, ApJ, 693, 112
Ramella, M., Geller, M. J., & Huchra, J. P. 1992, ApJ, 384, 396
Scarlata, C., Carollo, C. M., Lilly, S. J., et al. 2007, ApJS, 172, 494
Scodeggio, M., & Gavazzi, G. 1993, ApJ, 409, 110
Springel, V., White, S. D. M., Jenkins, A., et al. 2005, Nature, 435, 629
Stoughton, C., Lupton, R. H., Bernardi, M., et al. 2002, AJ, 123, 485
Strauss, M. A., Weinberg, D. H., Lupton, R. H., et al. 2002, AJ, 124, 1810
Tasca, L. A. M., Kneib, J.-P., Iovino, A., et al. 2009, A&A, 503, 379
Tran, K.-V. H., Moustakas, J., Gonzalez, A. H., et al. 2008, ApJ, 683, L17
Yasuda, N., Fukugita, M., & Schneider, D. P. 2007, AJ, 134, 698
Whiley, I. M., Aragón-Salamanca, A., De Lucia, G., et al. 2008, MNRAS, 387, 1253
Zabludoff, A. I., Zaritsky, D., Lin, H., et al. 1996, ApJ, 466, 104
Zwicky, F., Herzog, E., & Wild, P. 1961–68, Pasadena: California Institute of Technology (CIT)

Survey: *sdss* Program: *legacy* Target: *GALAXY*
RA=240.67087, Dec=52.24082, Plate=620, Fiber=548, MJD=52375
z=0.04297±0.00001 Class=GALAXY STARFORMING
No warnings.

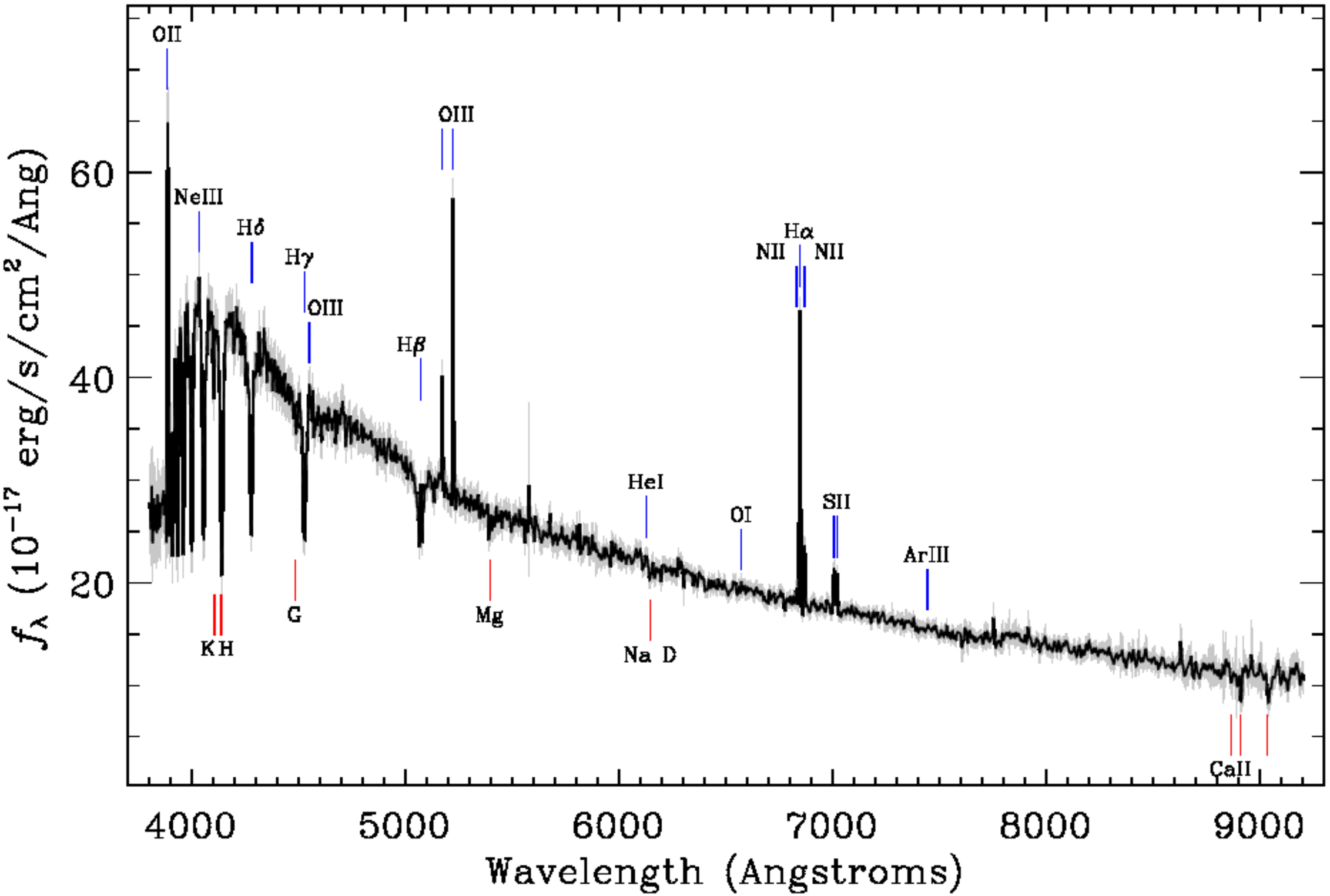

THE ASTROPHYSICAL JOURNAL, 430:121–138, 1994 July 20

MORPHOLOGICAL STUDIES OF THE GALAXY POPULATIONS IN DISTANT "BUTCHER-OEMLER" CLUSTERS WITH *HST*. I. AC 114 AT $z = 0.31$ AND ABELL 370 AT $z = 0.37$[1]

WARRICK J. COUCH
School of Physics, University of New South Wales, P.O. Box 1, Kensington NSW 2033, Australia
AND
RICHARD S. ELLIS, RAY M. SHARPLES, AND IAN SMAIL
Department of Physics, University of Durham, South Road, Durham, DH1 3LE, UK
Received 1993 October 25; accepted 1994 January 21

ABSTRACT

We present the first results of an ongoing program we are undertaking with the Wide Field Camera of the *Hubble Space Telescope* (*HST*) to understand the physical origin of the enhanced star formation seen in moderate-redshift ($z \sim 0.3$–0.4) cluster galaxies. Deep *HST* exposures have been obtained for the central regions of two rich compact "Butcher-Oemler" clusters, AC 114 at $z = 0.31$ and Abell 370 at $z = 0.37$. Both of these clusters have been subject to extensive ground-based spectroscopic and multiband imaging studies with a significant fraction of *confirmed* members being seen in the active or ensuing phases of a starburst. We have used the *HST* images in conjunction with the ground-based data to examine the morphology of individual cluster members, in particular these "starburst" objects. We find that those blue members that display spectral evidence of active or recently completed star formation are predominantly disk-dominated systems whose abundance is greater than that seen in the cores of present-day rich clusters. Furthermore, ~55% of the galaxies in this category in both clusters show convincing evidence of dynamical interactions, in contrast to a 20%–30% rate of occurrence among the red population. While similar conclusions had been drawn from high-quality ground-based data, we demonstrate the unique role *HST* can play in identifying interacting galaxy pairs which have separations less than the current resolution limits of the best ground-based images. There is convincing evidence in these first two clusters we have examined that interactions and mergers play a major role in inciting the star formation activity associated with the Butcher-Oemler effect.

Of equal significance is the morphological nature of the numerous *red* members in our *HST* data set which show various spectroscopic and photometric indications of previous starburst activity, including strong Balmer-line absorption. Most of these galaxies appear to be undisturbed and isolated with a normal E morphology. There is no convincing evidence that these are merger products.

Although larger samples are still required, we conjecture that the Butcher-Oemler effect may involve at least two physical processes arising from the hierarchical growth of clusters: galaxy-galaxy interactions and environmentally induced star formation arising from the hierarchical merging of clusters. Much work remains to be done to understand exactly how the fraction of disk galaxies seen in distant rich clusters declines to its present low value.

Subject headings: galaxies: clusters (AC 114, Abell 370) — galaxies: interactions — galaxies: photometry — galaxies: stellar content

1. INTRODUCTION

A major focus in observational cosmology over the last decade or more has been the mounting evidence for galaxies in the rich cluster environment having undergone significant evolution over the last one-third of a Hubble time. The first to present evidence for such evolution were Butcher & Oemler (1978) whose photometry of two rich concentrated clusters at $z \sim 0.4$ indicated an excess population of blue galaxies in comparison to that seen in present-day clusters. This result—now commonly known as the "Butcher-Oemler" (BO) effect—motivated numerous observational programs which have targeted high-redshift clusters for further broadband photometry (Butcher & Oemler 1984; Couch & Newell 1984), detailed multiband optical and infrared imaging work (Couch et al. 1983; Ellis et al. 1985; MacLaren, Ellis, & Couch 1988; Aragón-Salamanca, Ellis, & Sharples 1991), and spectroscopic investigations (Dressler & Gunn 1982, 1983; Lavery & Henry 1986; Couch & Sharples 1987, hereafter CS). These studies established that the BO effect is both widespread in rich clusters at $z \geq 0.2$ and can be ascribed to a subset of the cluster members either undergoing or having recently completed a vigorous short-lived burst of star formation.

The identification of the BO effect as a starburst-related phenomenon raises the question as to the series of events which triggered such activity at these earlier epochs and yet led to its demise by the present day. The quest for a single mechanism that can explain the diverse observational features discussed above has received much attention (see Oemler 1992 for an excellent review). At the most fundamental level, the observation that local galaxies of a given morphological type show environmental differences in their star formation characteristics and abundances could indicate the transformation of

[1] Based on observations with the NASA/ESA *Hubble Space Telescope*, obtained at the Space Telescope Science Institute, which is operated by the Association of Universities for Research in Astronomy, Inc., under NASA contract NAS 5-26555.

inset). As CS demonstrated, the distant cluster galaxies occupy quite distinct regions of this diagram dependent upon their star formation activity. Objects undergoing a burst of star formation (labeled "starburst" in Fig. 4) are characterized by blue colors and emission-filled Hδ lines and thus reside in the bottom left-hand corner of the diagram. The "post-starburst" (PSG) types are similarly blue but have moderate to strong (EW > 4 Å) Hδ absorption. Galaxies with the spectral characteristics of nearby spirals lie along a sequence of increasing Hδ strength with bluer color as indicated by the cross-hatched region in Figure 4. Within the red galaxy population, CS found a dichotomy in Hδ strength. Those objects with little or no Hδ absorption (EW ≤ 2 Å) resemble the nearby E/S0 galaxy population in terms of their spectra and rest-frame colors. The red galaxies with prominent (EW > 2 Å) Hδ, on the other hand, are interpreted as the products of starbursts occurring in previously dormant galaxies and seen 1–2 Gyr following the completion of the burst. We shall hereafter refer to these latter types as "HDS" galaxies.

Using this spectroscopic classification, for AC 114 we have 11 "active" objects in total (those labeled in Fig. 4), consisting of two starburst galaxies (87 and 111), three PSG galaxies (22, 143, and 146; the latter also shows weak [O II] λ3727 emission, indicating some residual ongoing star formation), one spiral galaxy (74), and five HDS galaxies (4, 40, 89, 187, and 858). The remaining 20 members are in the "inactive" E/S0 class. Spectral classifications for the new objects in the LDSS-1 sample are given in the last column of Table 2. Note that the three red members whose spectral type is denoted by "E/S0:" are cases where the S/N, and hence the precision of the Hδ measurement, is too low to confidently exclude the possibility that they are HDS objects [EW(Hδ) > 2 Å]; as such, they have not been included in Figure 4. The complete set of confirmed members within our WFC field, grouped according to spectral type, is listed in Table 3.

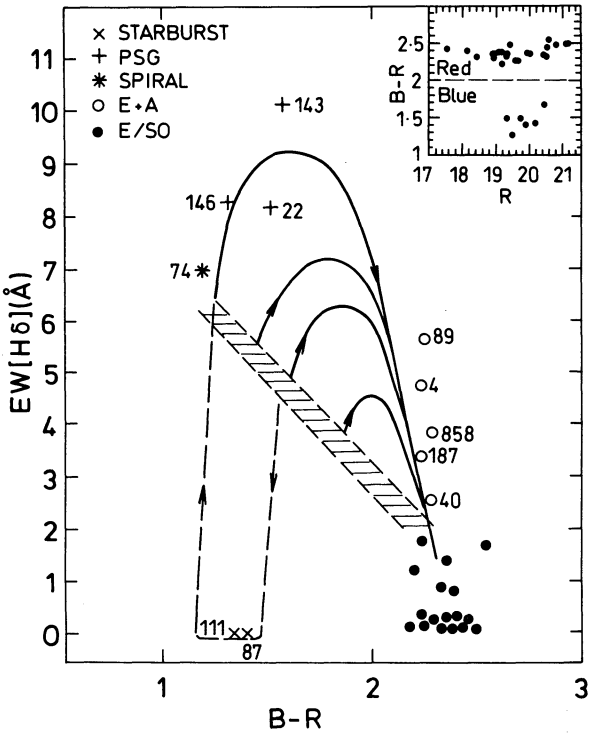

FIG. 4.—Hδ equivalent width vs. $(B-R)_{obs}$ diagram of Couch & Sharples (1987). The points in the diagram represent the spectroscopically confirmed members of AC 114 which lie within our WFC field; their spectroscopic classifications, based on their position in the diagram, are indicated in the legend. The arrowed dashed-solid and solid lines represent evolutionary tracks from the starburst and truncated star formation models, respectively, of Couch & Sharples (1987; see their paper for details). The cross-hatched area represents the region of the diagram occupied by present-day spiral galaxies. *Inset*: distribution of the same AC 114 members in the $[(B-R), R]_{obs}$ color-magnitude plane.

3.2. *Collation of Data for Abell 370*

Spectroscopy for ~90 objects within an ~6′ × 6′ field centered on Abell 370 is available from HL and SMFC. HL's multislit spectroscopy conducted on the CFHT yielded spectra with a resolution of 16 Å and a wavelength coverage of 5100–7000 Å for ~30 blue and red galaxies with $N \leq 20.4$. They have published the redshifts measured from their spectra and, for the 18 objects confirmed as members, measurements of EW(Ca II H + Hε)/EW(Ca II K) and continuum slope, F_ν(5000 Å)/F_ν(4100 Å). Plots of the spectra for nine of the members are also presented. The observations of SMFC, carried out at the CFHT and on the ESO 3.6 m telescope, provide spectra for 84 objects with a resolution of 10–20 Å and a wavelength coverage of either 4500–7200 Å or 4500–6700 Å. The faintest object in their catalog has $N = 20.6$. SMFC present plots of all their spectra together with redshifts and a spectral type based on a comparison with synthetic spectra from Guiderdoni & Rocca-Volmerange (1987). There are 18 galaxies common to both the HL and SMFC studies.

Unfortunately, the S/N of these spectra is often poor, and it is thus not possible to carry out a spectral typing of galaxies according to the quantitative approach of CS. Instead we have classified galaxies qualitatively from the available spectral plots using as a reference representative spectra from CS. To do this we examined each spectrum for the distinctive absorption/emission line features and continuum shape, taking into account the spectral typings given by MacLaren et al. (1988) and SMFC. The results of this procedure for all the Abell 370 members within our WFC field are presented along with other relevant information in Table 4. To aid in the cross-referencing of objects, their numbers under the identity schemes used by Couch & Newell (1984; as also MacLaren et al. 1988), SMFC, and Butcher, Oemler, & Wells (1983) are given in the first three columns, respectively.

Following the practice of CS, we have distinguished galaxies as being either "red" or "blue" and the data in Table 4 are listed accordingly. The basis for this distinction is the distribution of objects within the color-magnitude plane, constructed using the $N, J-N$ photographic photometry of Butcher et al. (presented here in cols. [5] and [6] of Table 4) and shown as Figure 5. This figure reveals a clear division of the data into a "red" E/S0 color-magnitude sequence and a population of "blue" objects below it. Formally, we take a value of $J-N = 2.3$ as the dividing line between the two populations.

Although the spectral data for Abell 370 are of lesser quality, there is more complete ground-based photometry. Specifically, from the studies of MacLaren et al. (1988) and Aragón-Salamanca et al. (1991), we can examine those red galaxies with photometric excesses (UVX and IRX) that may indicate recent star formation. The red galaxies are therefore subgrouped to distinguish these particular types (as well as the spectroscopically identified HDS galaxies) from the ordinary E/S0 class. Although some of the UVX and IRX galaxies were not

PROCEEDINGS OF SCIENCE

Evolution of galaxies in clusters

Bianca Poggianti[*†]
INAF-Padova Astron. Observatory, Italy
E-mail: poggianti@pd.astro.it

I summarize what is know about the evolution of galaxies in clusters from the observational point of view presenting results at high ($z \sim 1$), intermediate (~ 0.5) and low ($z \sim 0$) redshifts. I comment on the comparison between observations and predictions of CDM models, highlighting the observational landmarks more relevant for this comparison, such as the establishment and evolution of the morphology-density relation, the Butcher-Oemler effect, the evolution of red galaxies/ellipticals, the star formation histories of galaxies in clusters, the downsizing effect and the history of mass assembly.

Baryons in Dark Matter Halos
5-9 October 2004
Novigrad, Croatia

[*]Speaker.

[†]The author wishes to thank the organizers of this School+meeting for their kind invitation and generous support, and for unlimited patience in waiting for this written contribution.

Published by SISSA http://pos.sissa.it/

1. Introduction

The goal of this lecture is to give an overview of the state-of-the-art in the field of galaxy evolution in clusters and to point out the main observational milestones that a model of galaxy formation and evolution should attempt to reproduce and explain, trying to underline where the current models succeed and where they most struggle.

Understanding the role of *environmental conditions* in determing how galaxies are and evolve is *especially important in the context of a hierarchical cosmological scenario.* As structures grow, galaxies can join more and more massive structures and experience different environmental conditions during their history. Separating galaxy evolution into "field" and "cluster" evolution hardly makes sense in this scenario, since a cluster galaxy today may have been a group or field galaxy during the earlier phases of its evolution.

The physical mechanisms that are usually considered when trying to assess the influence of the environment on galaxy evolution can be grouped in four main families:

1. Mergers and strong galaxy-galaxy interactions (Toomre & Toomre 1972, Hernquist & Barnes 1991, see Mihos 2004 for a review). They are most efficient when the relative velocities between the galaxies are low, thus are expected to be especially efficient in galaxy groups.

2. Tidal forces due to the cumulative effect of many weaker encounters (also known as "harassment") (Richstone 1976, Moore et al. 1998). They are expected to be especially important in clusters, and particularly on smaller / lower mass galaxies.

3. Gas stripping - Interactions between the galaxy and the inter-galactic medium (IGM) (Gunn & Gott 1972, Quilis et al. 2000). The interstellar medium of a galaxy can be stripped via various mechanisms, including viscous stripping, thermal evaporation and – the most famous member of this family – ram pressure stripping. Ram pressure can be efficient when the IGM gas density is high and the relative velocity between the galaxy and the IGM is high. These conditions are expected to be met especially in the very central regions of cluster cores.

4. Strangulation (also known as starvation, or suffocation) (Larson, Tinsley & Caldwell 1980, Bower & Balogh 2004). Assuming galaxies possess an envelope of hot gas that can cool and feed the disk with fuel for star formation, the removal of such reservoir of gas is destined to inhibit further activity once the disk gas is exhausted. In semi-analytic models, for example, the gas halo is assumed to be removed when a galaxy enters as satellite in a more massive dark matter halo.

Note that while stripping gas from the disk induces a truncation of the star formation activity on a short timescale ($\sim 10^7$ yrs), strangulation is expected to affect a galaxy star formation history on a long timescale (> 1 Gyr) provoking a slowly declining activity which consumes the disk gas after the supply of cooling gas has been removed.

Some of these processes have en empirical motivation (e.g. ram pressure stripping and mergers can be observed at work), while others have a more "theoretical ground" (e.g. strangulation and harassment).

The former two of these families of processes affect the galaxy structure, thus morphology, in a direct way: the merger of two spirals can produce an elliptical galaxy, and repeated tidal encounters can change a late–type into an early-type galaxy. The latter two families, instead, act on the gas content of galaxies, hence their star formation activity, and can modify their morphologies in an indirect way: once star formation is halted in a disk, this can fade significantly, the bulge-to-disk relative importance can change and the galaxy appearance and morphology can appear significantly modified.

2. Evolution with redshift

2.1 Galaxy morphologies and star formation activity

At the time of this School, high–quality data of distant clusters have been obtained with the Advanced Camera for Surveys by several groups, and results should appear soon (Postman et al. 2005, Desai et al. in prep.). Here I summarize the published results, which are all based on Wide Field and Planetary Camera 2 data.

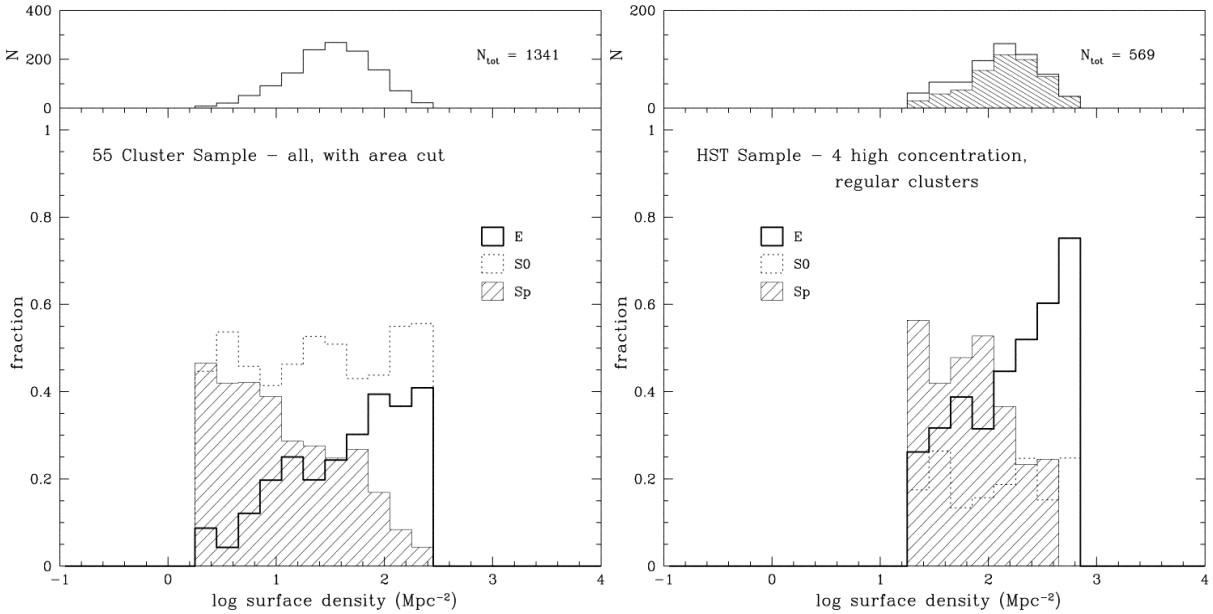

Figure 1: From Dressler et al. (1997). *Left.* Morphology-density relation for 55 clusters at low redshift (Dressler 1980). *Right.* Morphology-density relation for 4 regular clusters at $z \sim 0.45$ (Dressler et al. 1997).

The HST images have revealed the presence of large numbers of spiral galaxies in all distant clusters observed, in proportions that are much higher than in nearby clusters of similar richness (Dressler et al. 1994, Couch et al. 1994, Dressler et al. 1997). This is reflected also in the evolution of the Morphology-Density (MD) relation. The MD relation is the observed correlation between

the frequency of the various Hubble types and the local galaxy density, normally defined as the projected number density of galaxies within an area including its closest neighbours. In clusters in the local Universe, the existence of this relation has been known for a long time: ellipticals are frequent in high density regions, while the fraction of spirals is high in low density regions (Oemler 1974, Dressler et al. 1980). At $z = 0.4 - 0.5$, an MD relation is already present, but it is *quantitatively* different from the relation at $z = 0$: the fraction of S0 galaxies at $z = 0.5$ is much lower, at all densities, than in clusters at $z = 0$ (Fig. 1, Dressler et al. 1997). The fraction of S0s in clusters appears to increase towards lower redshifts, while the proportion of spirals correspondingly decreases (Fig. 2, Dressler et al. 1997, Fasano et al. 2000). Interestingly, ellipticals are already as abundant at $z = 0.5$ as at $z = 0$. These findings strongly suggest that a significat fraction of the S0 galaxies in clusters today have evolved from spirals at relatively recent epochs. Adopting a more conservative distinction between "early-type" (Es+S0s) and late-type (spirals) galaxies, a similar evolution is found, with the early-type fraction decreasing at higher redshifts (van Dokkum et al. 2000, Lubin et al. 2002). First results at $z \sim 0.7 - 1.3$ seem to indicate that between $z = 0.5$ and $z = 1$ what changes in the MD relation is only the occurrence of early-type galaxies in the very highest density regions (Smith et al. 2004).

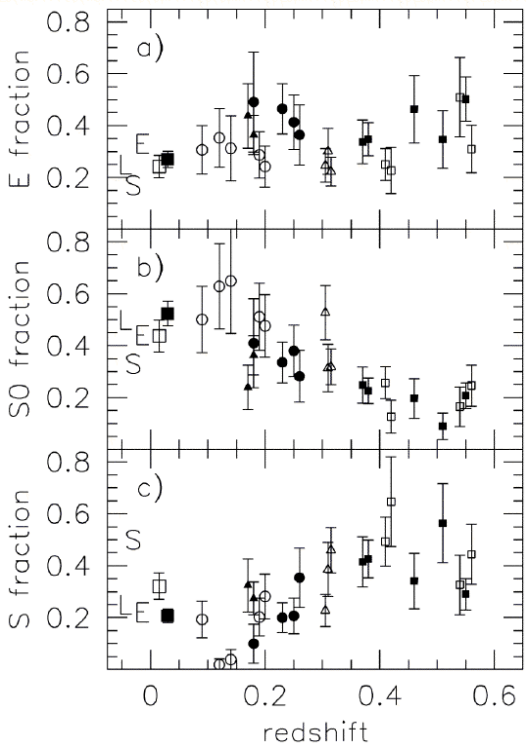

Figure 2: From Fasano et al. (2000). Evolution of the morphological mix in clusters. The fraction of ellipticals, S0 and spiral galaxies is shown for clusters between $z = 0.55$ and $z = 0$.

Interestingly, "an" MD relation, originally found in the cluster cores, has been shown to be present across a wide range of environments, in all types of clusters, rich and poor, concentrated and irregular, with low and high L_X (Dressler 1980, Balogh et al. 2002a), in groups (Postman & Geller 1984) and at large cluster radii (Treu et al. 2003), though the relation seems to vary from

rich to less rich clusters (Dressler 1980, Balogh et al. 2002).

Comparing HST morphologies and spectroscopy, it has been shown that galaxies with active star formation in distant clusters are for the great majority spirals (Dressler et al. 1999), but that the viceversa is not always true: several of the cluster spirals, in fact, do not display any emission line in their spectra, and both their spectra and their colors indicate a lack of current star formation activity (Poggianti et al. 1999, Couch et al. 2001, Goto et al. 2003). These "passive spirals" might be an intermediate stage when star–forming spirals are being transformed into passive S0 galaxies.

Historically, the first evidence for a higher incidence of star-forming galaxies in distant clusters compared to nearby clusters came from photometric studies that identified large numbers of *blue* galaxies (Butcher & Oemler 1978, 1984, Ellingson et al. 2001, Kodama & Bower 2001). Those galaxies in distant clusters that are *red* and already lie on the color-magnitude sequence have instead very old stellar populations formed at $z > 2-3$ that have evolved passively after that (Ellis et al. 1997, Kodama et al. 1998, Barger et al. 1998, van Dokkum et al. 1999,2000,2001). They are only a subset of the galaxies that lie on the red sequence today (van Dokkum & Franx 2001) but they are easily recognizable as signposts of high density regions out to very high redshifts (e.g. Stanford et al. 2002, Blakeslee et al. 2003, De Lucia et al. 2004). As we will see in Sec. 2.2, the fraction of galaxies involved in the evolution from blue to red doesn't depend only on redshift, but strongly also on galaxy mass.

Compared to colors, spectroscopy is a more direct way to identify galaxies with ongoing star formation. For distant galaxies, the Hα line is redshifted at optical wavelengths that are severely affected by sky or is observed in the near-IR, thus the feature most commonly used is the [OII]λ3727 line.

In the MORPHS sample of 10 clusters at $z \sim 0.4-0.5$, the fraction of emission–line galaxies is $\sim 30\%$ for galaxies brighter than $M_V = -19 + 5\log h^{-1}$ (Dressler et al. 1999, Poggianti et al. 1999). In the CNOC cluster sample, at an average redshift $z \sim 0.3$, this fraction is about 25% (Balogh et al. 1999). This incidence is much higher than it is observed in similarly rich clusters at $z = 0$ (Dressler, Thompson & Shectman 1988). Significant numbers of emission-line galaxies have been reported in virtually all spectroscopic surveys of distant clusters (e.g. Couch & Sharples 1987, Fisher et al. 1998, Postman et al. 1998, 2001).

The increasing importance of the [OII] emission with redshift can also be assessed from cluster composite spectra, that are obtained summing up the light from all galaxies in a given cluster to produce a sort of "cluster integrated spectrum" (Fig. 3, Dressler et al. 2004). As expected, the strength of [OII] in these composite spectra displays a large cluster–to–cluster variation at any redshift, but there is a tendency for the $z = 0.5$ clusters to have on average a stronger composite EW([OII]) than the clusters at $z = 0$.

If numerous observations indicate that emission–line galaxies were more prominent in clusters in the past than today, and if these results are unsurprising given the evolution with z of the star formation activity in the general "field", *quantifying* this evolution in clusters has proved to be very hard. The fact that the emission–line incidence varies strongly from a cluster to another at all redshifts, and the relatively small samples of clusters studied in detail at different redshifts, have so far hindered our progress in measuring how the fraction of emission–line galaxies evolves with redshift as a function of the cluster properties.

Discriminating between cosmic evolution and cluster–to–cluster variance is a problem also for

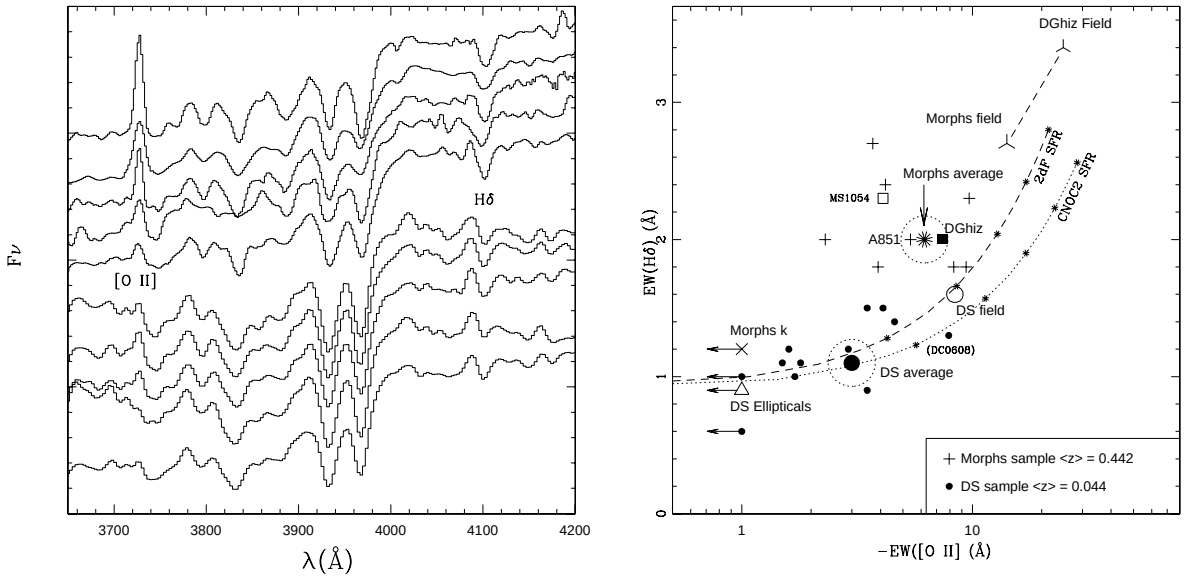

Figure 3: From Dressler et al. (2004). *Left.* Composite spectra of five clusters at $z \sim 0.5$ (top five) and five clusters at $z \sim 0$ (bottom five). The [OII] line is generally more prominent in the high-z spectra. *Right.* Equivalent widths of [OII] versus Hδ as measured from composite spectra of clusters at $z \sim 0.4 - 0.5$ (crosses) and clusters at $z \sim 0$ (filled dots).

Hα cluster–wide studies. Using narrow–band imaging or multiplex multislit capabilities, a handful of clusters have been studied to date at $z \geq 0.2$ (Couch et al. 2001, Balogh et al. 2002b, Finn et al. 2004, and submitted, Kodama et al. 2004, Umeda et al. 2004). These studies have confirmed that the fraction of emission–line (Hα–detected, in this case) galaxies is lower in clusters than in the field at similar redshifts, and have shown that the bright end of the Hα luminosity function does not seem to depend strongly on environment. As shown in Fig. 4, the number of clusters studied is still insufficient to pin down the star formation rate (SFR) per unit of cluster mass as a function of redshift AND of global cluster properties such as the cluster velocity dispersion.

A word of caution is compulsory when using emission–lines and assuming they provide an unbiased view of the evolution of the star formation activity in cluster galaxies. There are several indications that dust extinction is in fact important and strongly distorts our view of the star formation activity in at least some cluster galaxies. Evidence for dust arises from optical spectroscopy itself, which finds many dusty starbursting or star–forming galaxies with relatively weak emission–lines both in distant clusters and in the field at similar redshifts (Poggianti et al. 1999, Shioya et al. 2000, Poggianti et al. 2001a, Bekki et al. 2001). The radio–continuum detection of galaxies with no optical emission lines (Smail et al. 1999, Miller & Owen 2002) and mid-IR estimates of the star formation rate (Duc et al. 2002, Biviano et al. 2004, Coia et al. 2005a,b) indicate that even the majority or all of the star formation activity of some cluster galaxies can be obscured at optical wavelengths. Whether taking into account dust obscuration changes significantly the evolutionary picture inferred from emission lines is still a critical open question that Spitzer is likely to answer.

Precious informations about the star formation histories of cluster galaxies can also be obtained from absorption–line spectra. In distant clusters, the presence of galaxies with strong Balmer lines

The Astrophysical Journal, 671:1503–1522, 2007 December 20

A WIDE-FIELD SURVEY OF TWO $z \sim 0.5$ GALAXY CLUSTERS: IDENTIFYING THE PHYSICAL PROCESSES RESPONSIBLE FOR THE OBSERVED TRANSFORMATION OF SPIRALS INTO S0s

Sean M. Moran,[1] Richard S. Ellis,[1] Tommaso Treu,[2,3] Graham P. Smith,[4] R. Michael Rich,[5] and Ian Smail[6]

Received 2007 June 29; accepted 2007 July 26

ABSTRACT

We present new results from our comparative survey of two massive, intermediate-redshift galaxy clusters, Cl 0024+17 ($z = 0.39$) and MS 0451−03 ($z = 0.54$). Combining optical and UV imaging with spectroscopy of member galaxies, we identify and study several key classes of "transition objects" whose stellar populations or dynamical states indicate a recent change in morphology and star formation rate. For the first time, we have been able to conclusively identify spiral galaxies in the process of transforming into S0 galaxies. This has been accomplished by locating both spirals whose star formation is being quenched and their eventual successors, the recently created S0s. Differences between the two clusters in both the timescales and spatial location of this conversion process allow us to evaluate the relative importance of several proposed physical mechanisms that could be responsible for the transformation. Combined with other diagnostics that are sensitive to either ICM-driven galaxy evolution or galaxy-galaxy interactions, we describe a self-consistent picture of galaxy evolution in clusters. We find that spiral galaxies within infalling groups have already begun a slow process of conversion into S0s, likely via gentle galaxy-galaxy interactions. The fates of spirals upon reaching the core of the cluster depend heavily on the cluster ICM, with rapid conversion of all remaining spirals into S0s via ram pressure stripping in clusters where the ICM is dense. In the presence of a less dense ICM, the conversion continues at a slower pace, with other mechanisms continuing to play a role. We conclude that the buildup of the local S0 population through the transformation of spiral galaxies is a heterogeneous process that nevertheless proceeds robustly across a variety of different environments.

Subject headings: galaxies: clusters: individual (Cl 0024+1654, MS 0451−0305) — galaxies: elliptical and lenticular, cD — galaxies: evolution — galaxies: spiral — galaxies: stellar content — ultraviolet: galaxies

Online material: color figures, machine-readable tables

1. INTRODUCTION

It is well known that environmental processes play a significant role in shaping the evolution of galaxies as they assemble onto clusters. With the aid of *Hubble Space Telescope* (*HST*) imaging and deep optical spectroscopy, recent studies have quantified this evolution in galaxy properties, painting a picture where the fraction of early-type (elliptical and S0) galaxies and the fraction of passive non–star-forming galaxies both grow with time, and at a rate that seems to depend sensitively on the local density of galaxies (Dressler et al. 1997; Poggianti et al. 1999; Smith et al. 2005a; Postman et al. 2005).

Yet there are a wide variety of physical processes that may be responsible for these evolutionary trends, including galaxy mergers, galaxy-galaxy harassment, gas stripping by the ICM, or tidal processes (Moore et al. 1999; Fujita 1998; Bekki et al. 2002). Observationally, it has so far been impossible to fully separate the effects of the various physical processes, in large part due to the overlapping regimes of influence for each of the proposed mechanisms (see Treu et al. 2003, hereafter Paper I). Further complicating the picture, the large-scale assembly states of clusters show considerable variety (Smith et al. 2005b), such that the dominant forces acting on galaxies are likely to vary from cluster to cluster, or over the course of an individual cluster's assembly history. But gaining an understanding of the complex interplay between a variable ICM, the properties of assembling galaxies, and the overall cluster dynamical state is crucial if we are to have a complete picture of the growth and evolution of galaxies in a hierarchical universe.

In this paper we combine optical (*HST*) and UV (*GALEX*) imaging of two $z \sim 0.5$ galaxy clusters with ground-based spectroscopy of member galaxies, in an attempt to trace directly the buildup of passive early-type galaxies via a detailed "case study" of the galaxy population across each cluster. The two studied clusters, Cl 0024+17 ($z = 0.40$) and MS 0451 ($z = 0.54$), are part of a long-term campaign to trace the evolution of galaxies in wide fields ($\sim$10 Mpc diameter) centered on both clusters, using a variety of methods. By undertaking an in-depth, wide-field comparative study of two prominent clusters, we hope to provide a complement to other observational (e.g., Cooper et al. 2007; Poggianti et al. 2006) and theoretical investigations (e.g., de Lucia et al. 2006) that trace with a broad brush the evolution in star formation rate (SFR) and the buildup of structure in the universe.

The first paper in our series, Paper I, introduced our panoramic *HST* imaging of Cl 0024 and began our ongoing discussion of the physical processes that may be acting on galaxies within clusters. In several subsequent papers, whose results are summarized in § 2, we have added extensive optical spectroscopy to the program, allowing targeted investigations of galaxy stellar populations and SFRs as a function of clustercentric radius, local density, and morphology. Our goal for this paper is to bring our complete survey data set to bear on the question of how galaxies are affected by their environment, as a function of both the overall cluster properties and the local environment within each cluster. For maximum clarity and deductive power, we focus our investigation on

[1] Department of Astronomy, California Institute of Technology, MS 105-24, Pasadena, CA 91125; smm@astro.caltech.edu, rse@astro.caltech.edu.
[2] Department of Physics, University of California, Santa Barbara, CA 93106; tt@physics.ucsb.edu.
[3] Alfred P. Sloan Research Fellow.
[4] School of Physics and Astronomy, University of Birmingham, Edgbaston, Birmingham B15 2TT, UK.
[5] Department of Physics and Astronomy, UCLA, Los Angeles, CA 90095.
[6] Institute for Computational Cosmology, Durham University, Durham DH1 3LE, UK.

TABLE 1
Basic Properties of the Clusters

Name	R.A. (deg)	Decl. (deg)	R_{vir} (Mpc)	M_{200} ($M_\odot$)	z	L_X ($L_\odot$)	T_X (keV)
Cl 0024	6.65125	17.162778	1.7[a]	8.7×10^{14}[b]	0.395	7.6×10^{10}[c]	3.5[c]
MS 0451	73.545417	−3.018611	2.6	1.4×10^{15}[d]	0.540	5.3×10^{11}[d]	10.0[d]

[a] Paper I.
[b] Paper II.
[c] Zhang et al. (2005).
[d] Donahue et al. (2003).

several key populations of "transition galaxies" in the clusters, galaxies whose stellar populations or dynamical states indicate a recent or ongoing change in morphology or SFR.

In evaluating cluster galaxies for signs of evolution, we have adopted a strategy to make maximal use of our *HST*-based morphologies by characterizing signs of recent evolution in spirals and early types separately. This approach is similar to using the color-magnitude relation to divide our sample into "red sequence" and "blue cloud" galaxies, but it provides additional leverage to identify galaxies in transition. Early-type galaxies that have been either newly transformed or prodded back into an active phase or spiral galaxies where star formation is being suppressed or enhanced will all stand out in our sample. At the same time, their morphologies reveal important information about their formation histories prior to their current transition state, information that colors alone do not provide. Our strategy also has the benefit of allowing us to directly investigate the hypothesis that many cluster spirals transform into S0s between $z \sim 0.5$ and today (Dressler et al. 1997), an investigation that will form the basis of this paper.

In the next section we outline our rationale for selecting Cl 0024 and MS 0451, describe the large-scale properties of each cluster, and give a summary of what we have concluded so far in our study of galaxy evolution in both clusters. In § 3 we describe new data not covered in previous papers in our series. In § 4 we investigate the properties of "passive spirals" across the two clusters, suggesting that they are in the process of transforming into S0 galaxies. We confirm in § 5 that this is the case, via identification of newly created S0s that we believe reflect the distinct passive spiral populations found in each cluster. In § 6 we consider the environments of these galaxies in transition and begin to investigate the physical mechanisms that may be responsible for these transformations. In § 7 we outline a model of how galaxy evolution proceeds in each cluster. We consider the fundamental plane (FP) as a way to further constrain the physical mechanisms at work and derive similar constraints from the populations of compact emission-line galaxies in both clusters. Finally, in § 8 we summarize our conclusions about the transformation of spirals into S0s at $z \sim 0.5$. In this paper we adopt a standard ΛCDM cosmology with $H_0 = 70\ \mathrm{km\ s^{-1}\ Mpc^{-1}}$, $\Omega_m = 0.3$, and $\Omega_\Lambda = 0.7$.

2. A COMPARATIVE SURVEY OF TWO $z \sim 0.5$ CLUSTERS

Cl 0024 and MS 0451 were chosen for study primarily because of their comparable total masses, similar galaxy richness, and strong-lensing features, while exhibiting X-ray properties that are quite distinct (see Table 1). While MS 0451 is one of the most X-ray–luminous clusters known (Donahue et al. 2003), Cl 0024 is somewhat underluminous in the X-ray, with a mass inferred from *XMM-Newton* observations that significantly underestimates the mass derived from other methods (Zhang et al. 2005). MS 0451 has X-ray luminosity 7 times larger than Cl 0024, with a corresponding gas temperature nearly 3 times as high. This implies a large difference in the density and radial extent of the intracluster medium (ICM) between the two clusters. As a result, ICM-related physical processes are naively expected to be more important in the evolution of currently infalling MS 0451 galaxies than in Cl 0024.

In the schematic diagram shown in Figure 1, we apply simple scaling relations to estimate the regimes of influence for several key physical processes that could be acting on infalling galaxies, following the procedure described in Paper I. ICM-related processes, such as gas starvation (Larson et al. 1980; Bekki et al. 2002) and ram pressure stripping (Gunn & Gott 1972), begin to affect galaxies at much larger radius in MS 0451. As in Paper I, we expect that other ICM-related processes such as thermal evaporation (Cowie & Songaila 1977) or viscous stripping (Nulsen

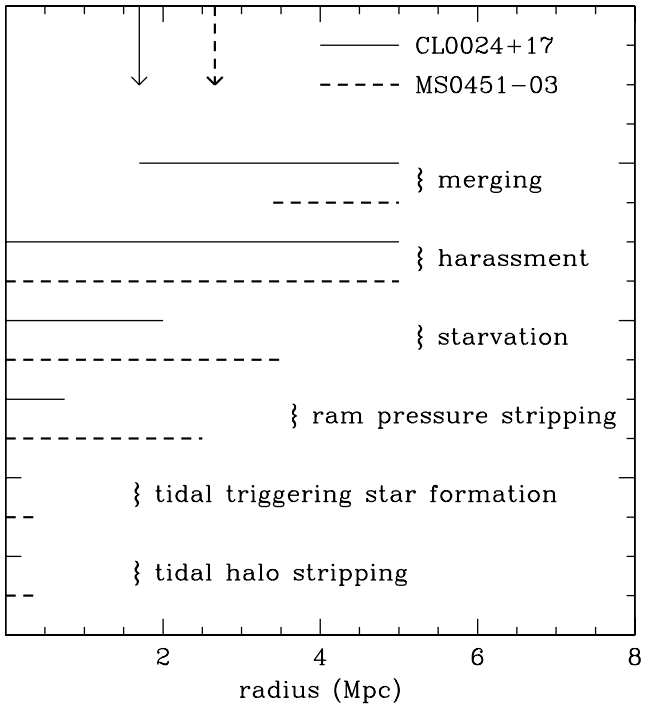

Fig. 1.—Schematic diagram indicating the clustercentric radius over which each of several listed physical mechanisms may be effective at fully halting star formation or transforming the visual morphology of a radially infalling galaxy. Each physical mechanism listed can act effectively over the radial range indicated by the solid (Cl 0024) or dashed line (MS 0451). Arrows indicate the virial radius for each cluster. Note that tidal processes here refer to interactions with the cluster potential, while tidal forces during galaxy-galaxy interactions are a component of the harassment mechanism. Each regime of influence was calculated according to the simple models described in Paper I for Cl 0024, using the global cluster properties given in Table 1.

Astronomy & Astrophysics manuscript no. 25599final
April 16, 2015

CLASH-VLT: Substructure in the galaxy cluster MACS J1206.2-0847 from kinematics of galaxy populations ⋆,⋆⋆

M. Girardi[1,2], A. Mercurio[3], I. Balestra[2], M. Nonino[2], A. Biviano[2], C. Grillo[4], P. Rosati[5], M. Annunziatella[1,2], R. Demarco[6], A. Fritz[7], R. Gobat[8], D. Lemze[9], V. Presotto[1], M. Scodeggio[7], P. Tozzi[10], G. Bartosch Caminha[5], M. Brescia[3], D. Coe[11], D. Kelson[12], A. Koekemoer[11], M. Lombardi[13], E. Medezinski[9], M. Postman[11], B. Sartoris[1,2], K. Umetsu[14], A. Zitrin[15,16], W. Boschin[17,18,19], O. Czoske[20], G. De Lucia[2], U. Kuchner[20], C. Maier[20], M. Meneghetti[21,22,23], P. Monaco[1,2], A. Monna[24], E. Munari[1,2], S. Seitz[24,25], M. Verdugo[20], and B. Ziegler[20]

(Affiliations can be found after the references)

Received / Accepted

ABSTRACT

Aims. In the effort to understand the link between the structure of galaxy clusters and their galaxy populations, we focus on MACS J1206.2-0847 at $z \sim 0.44$ and probe its substructure in the projected phase space through the spectrophotometric properties of a large number of galaxies from the CLASH-VLT survey.

Methods. Our analysis is mainly based on an extensive spectroscopic dataset of 445 member galaxies, mostly acquired with VIMOS@VLT as part of our ESO Large Programme, sampling the cluster out to a radius $\sim 2R_{200}$ ($4\ h_{70}^{-1}$ Mpc). We classify 412 galaxies as passive, with strong Hδ absorption (red and blue galaxies), and with emission lines from weak to very strong. A number of tests for substructure detection are applied to analyze the galaxy distribution in the velocity space, in 2D space, and in 3D projected phase-space.

Results. Studied in its entirety, the cluster appears as a large-scale relaxed system with a few secondary, minor overdensities in 2D distribution. We detect no velocity gradients or evidence of deviations in local mean velocities. The main feature is the WNW-ESE elongation. The analysis of galaxy populations per spectral class highlights a more complex scenario. The passive galaxies and red strong Hδ galaxies trace the cluster center and the WNW-ESE elongated structure. The red strong Hδ galaxies also mark a secondary, dense peak $\sim 2\ h_{70}^{-1}$ Mpc at ESE. The emission line galaxies cluster in several loose structures, mostly outside R_{200}. Two of these structures are also detected through our 3D analysis. The observational scenario agrees with MACS J1206.2-0847 having WNW-ESE as the direction of the main cluster accretion, traced by passive galaxies and red strong Hδ galaxies. The red strong Hδ galaxies, interpreted as poststarburst galaxies, date a likely important event 1-2 Gyr before the epoch of observation. The emission line galaxies trace a secondary, ongoing infall where groups are accreted along several directions.

Key words. galaxies: clusters: individual: MACS J1206.2-0847 – galaxies: clusters: general – galaxies: kinematics and dynamics – galaxies: evolution – cosmology: observations

1. Introduction

In the hierarchical scenario for large-scale structure formation, clusters of galaxies are not relaxed structures. Numerical simulations show that clusters form preferentially through anisotropic accretion of subclusters along the large-scale structure (LSS) filaments (Colberg et al. 1998, 1999 and references therein). From the observational point of view, it is well known that a large fraction of clusters (30%-70%) contain substructures, as shown by studies based on optical (e.g., Baier & Ziener 1977; Geller & Beers 1982; Girardi et al. 1997; Ramella et al. 2007; Wen & Han 2013), on X-ray data (e.g., Jones & Forman 1999; Buote 2002; Jeltema et al. 2005; Zhang et al. 2009, Böhringer et al. 2010), and on gravitational lensing techniques (e.g., Athreya et al. 2002; Dahle et al. 2002; Smith et al. 2005: Grillo et al. 2014a), indicating that past signatures of cluster accretion are quite common. Much progress has been made in the study of cluster accretion phenomena (see Feretti et al. 2002 for a general review) and recent, dedicated studies have often focused on a few major, ongoing cluster mergers, for instance in the context of Dynamical Analysis Radio Clusters project (DARC, e.g., Girardi et al. 2011) and MUlti-Wavelength Sample of Interacting Clusters project (MUSIC, Maurogordato et al. 2011). Other dedicated studies have focused on larger scales, i.e., on cluster accretion through filaments (e.g., Fadda et al. 2008; Dietrich et al. 2012). On-going cluster formation is also evident in distant clusters as pioneering studies have shown that most clusters identified at $z \geq 0.8$ are elongated, clumpy, or with a filamentary structure (e.g., Donahue et al. 1998; Gioia et al. 1999; Demarco et al. 2007; Fassbender et al. 2011).

It is well established that the properties of cluster galaxies differ from those of field galaxies and that clusters are characterized by radial gradients. Galaxies in denser, central regions are usually of earlier morphological type, redder color, and lower star formation rate (hereafter SFR; e.g., Gerken et al. 2004). However, the precise details of the connection between galaxy evolution and cluster environment are still unknown. Several

Send offprint requests to: M. Girardi, e-mail: girardi@oats.inaf.it

⋆ Based in large part on data acquired at the ESO VLT (prog.ID 186.A-0798).

⋆⋆ Full Table 2 is only available in electronic form at the CDS via anonymous ftp to cdsarc.u-strasbg.fr (130.79.128.5) or via http://cdsweb.u-strasbg.fr/cgi-bin/qcat?J/A+A/

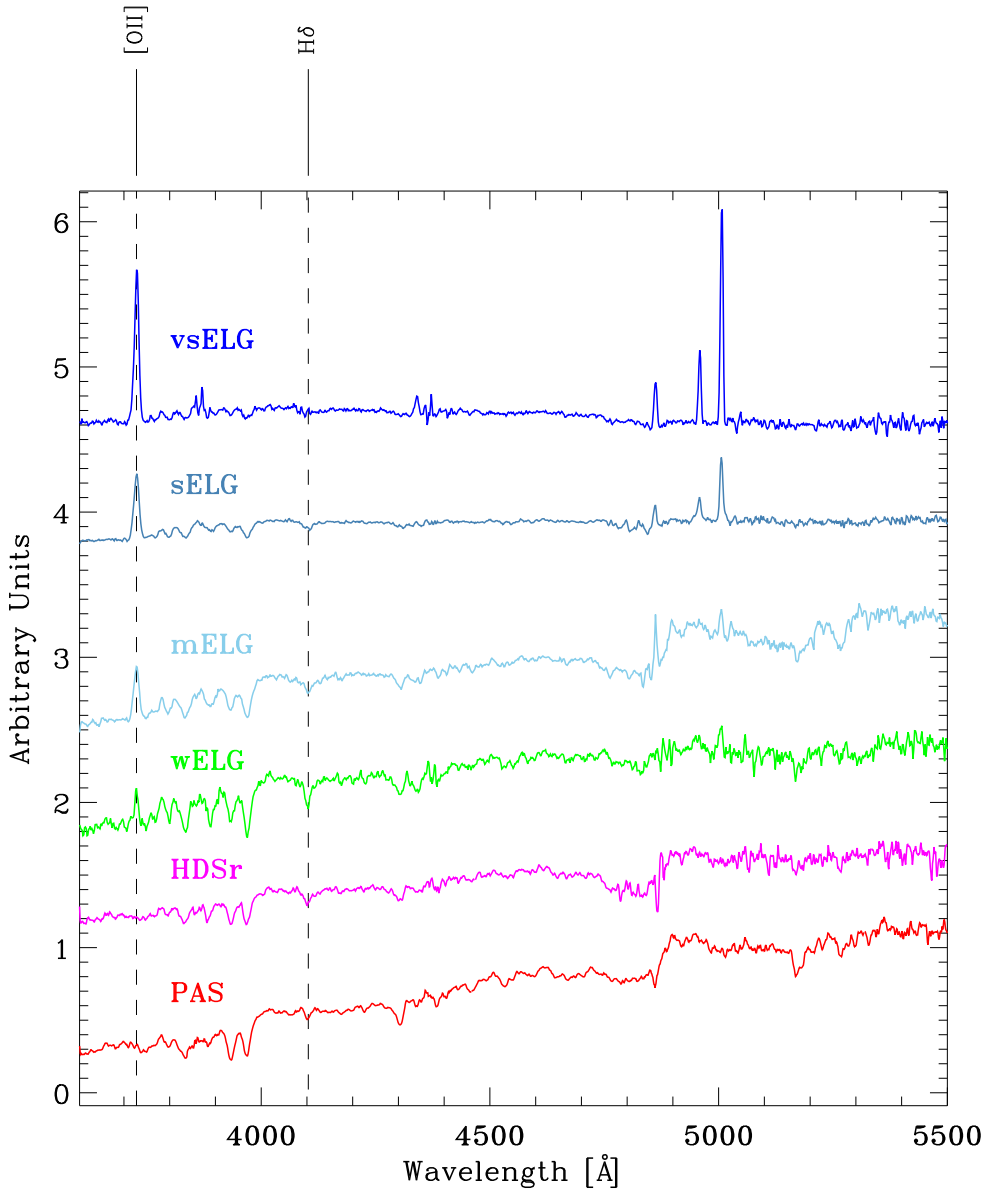
[OII]
Hδ
vsELG
sELG
mELG
wELG
HDSr
PAS
Arbitrary Units
Wavelength [Å]
0
1
2
3
4
5
6
4000
4500
5000
5500

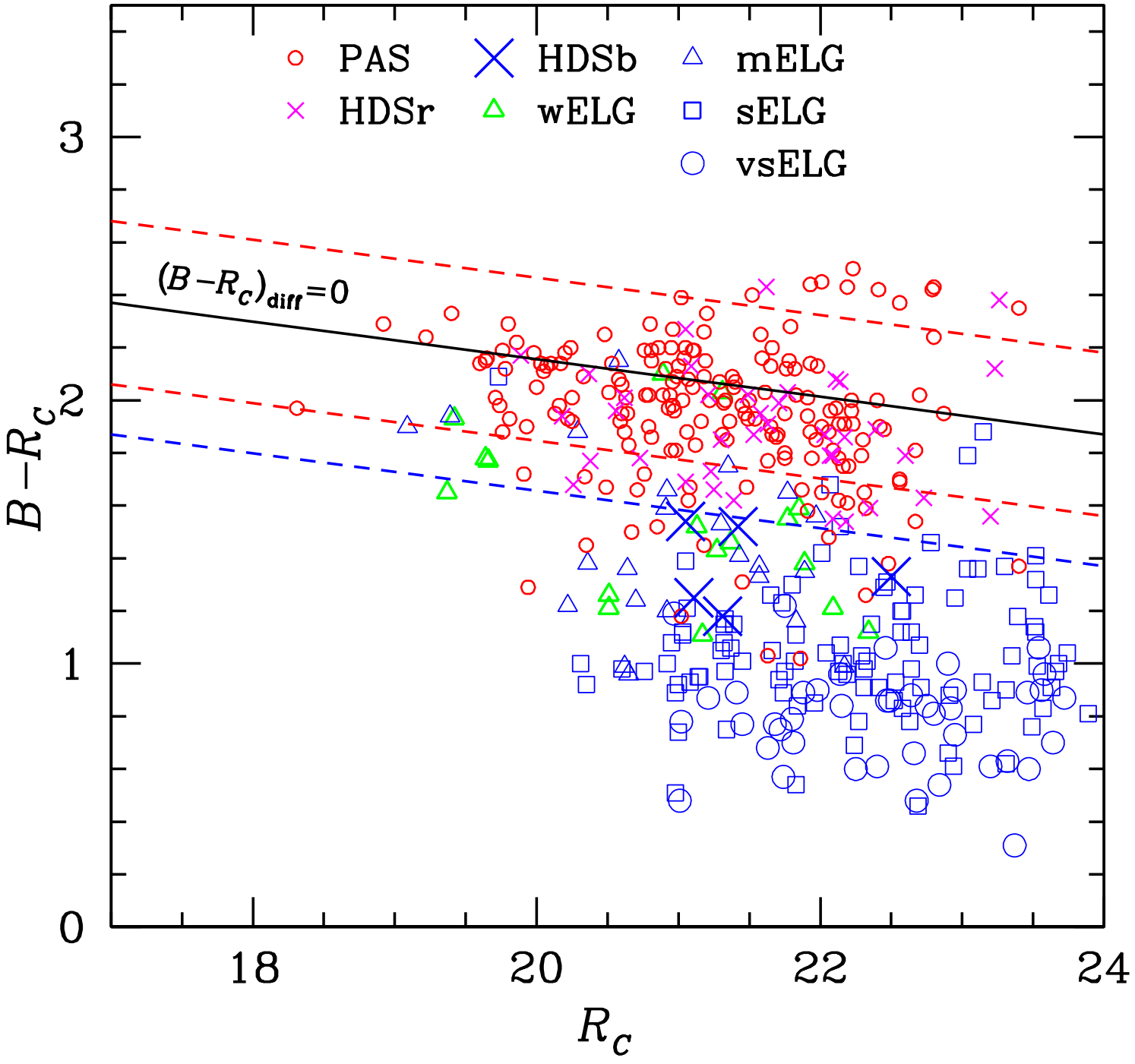
PAS
HDSb
mELG
HDSr
wELG
sELG
vsELG
$(B-R_c)_{diff}=0$
$B-R_c$
R_c
0
1
2
3
18
20
22
24

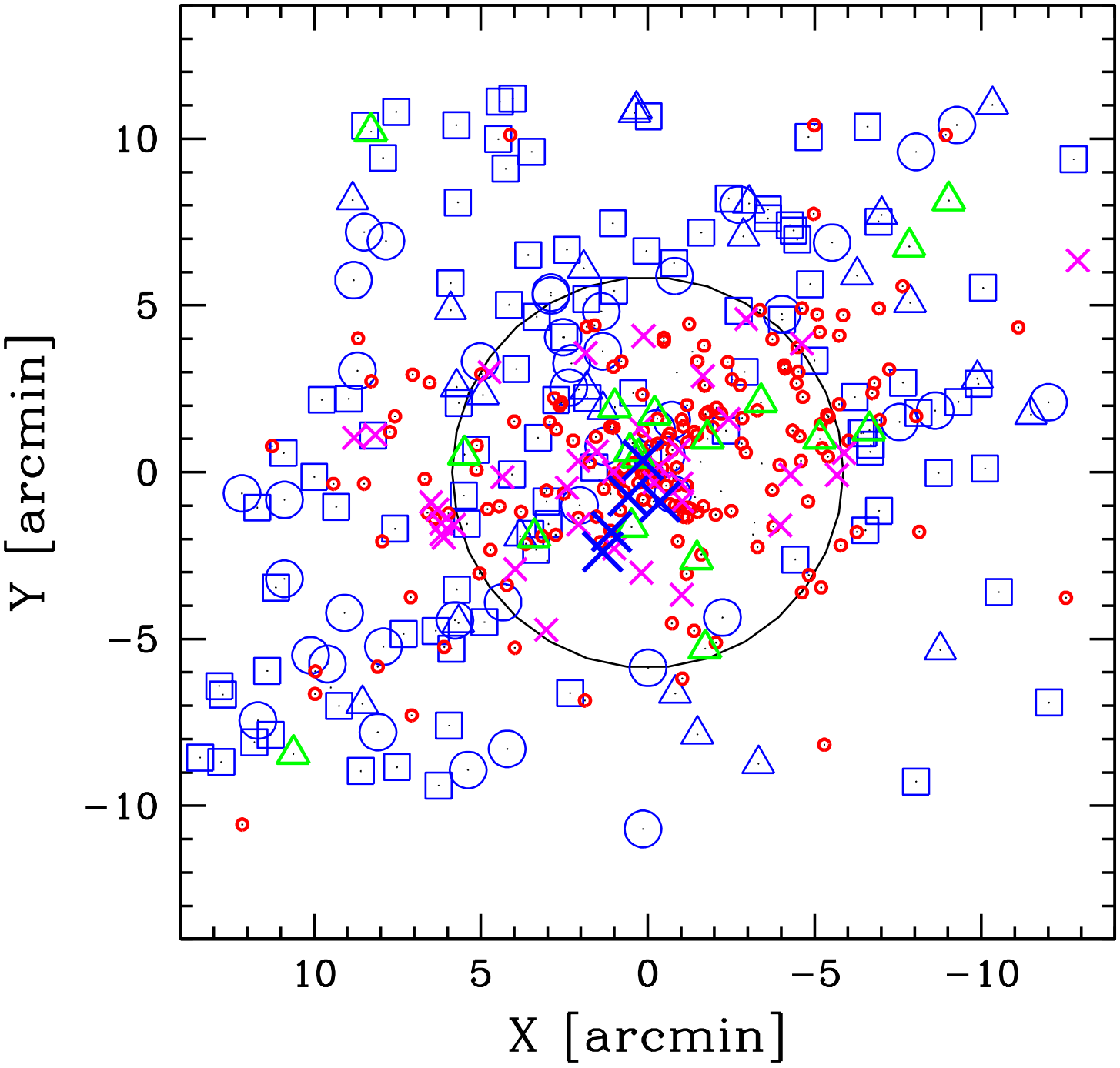
10
5
0
−5
−10
Y [arcmin]
10
5
0
−5
−10
X [arcmin]

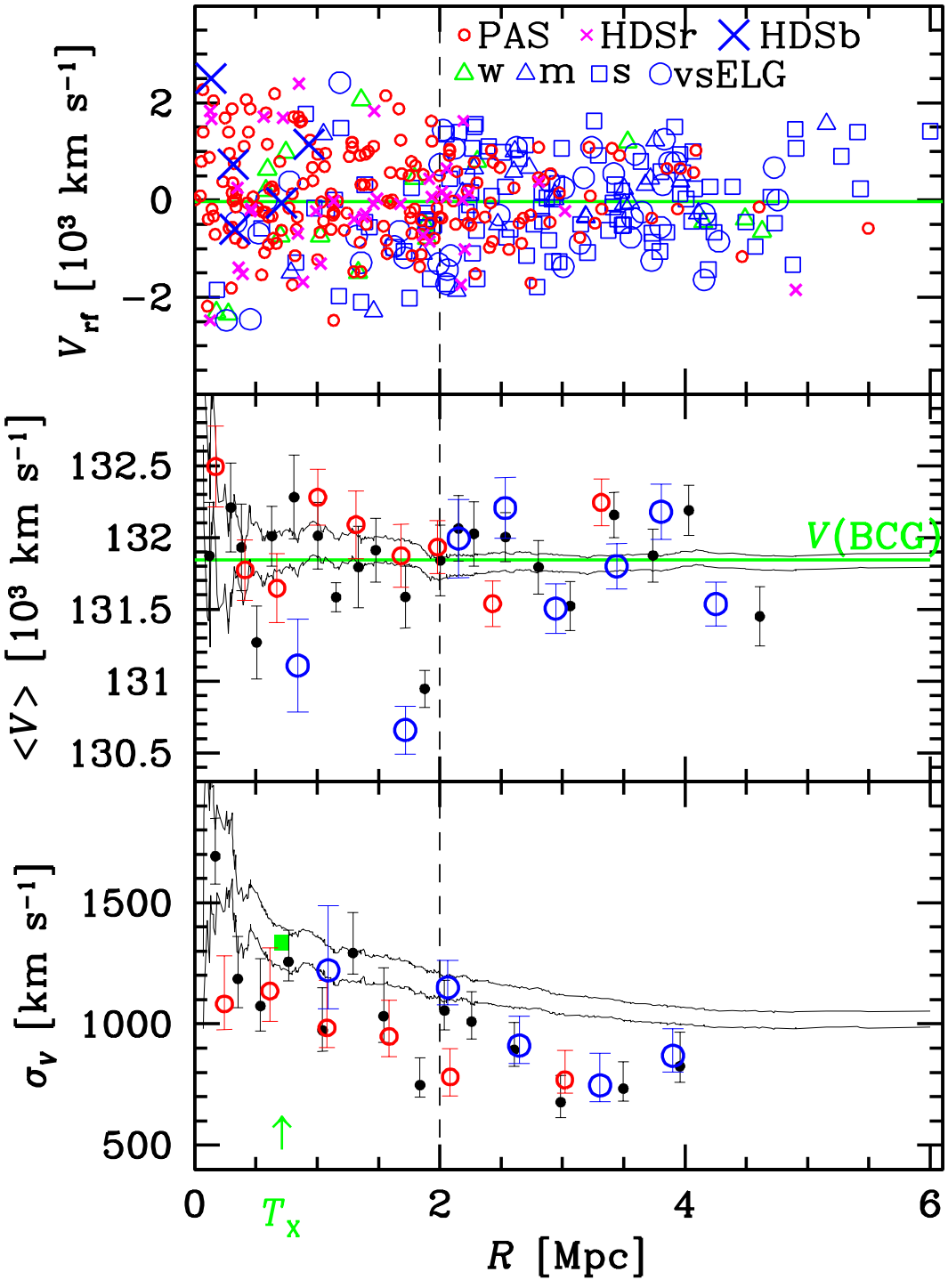
PAS
HDSr
HDSb
w
m
s
vsELG
V_{rf} [10^3 km s^{-1}]
2
0
−2
<V> [10^3 km s^{-1}]
132.5
132
131.5
131
130.5
V(BCG)
σ_v [km s^{-1}]
1500
1000
500
0
T_X
2
4
6
R [Mpc]

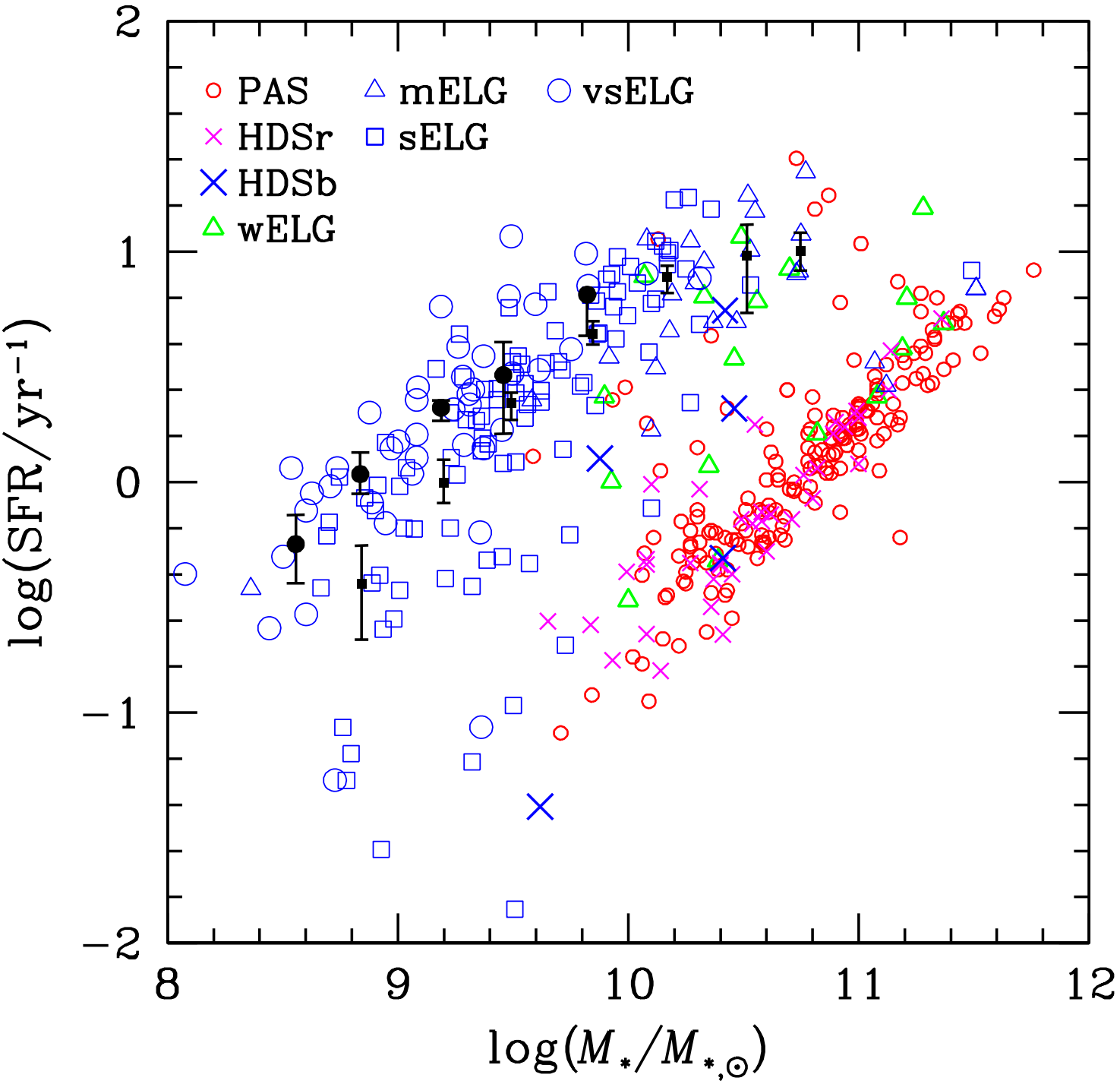
PAS
mELG
vsELG
HDSr
sELG
HDSb
wELG
2
1
0
−1
−2
8
9
10
11
12
log(SFR/yr⁻¹)
log(M*/M*,⊙)

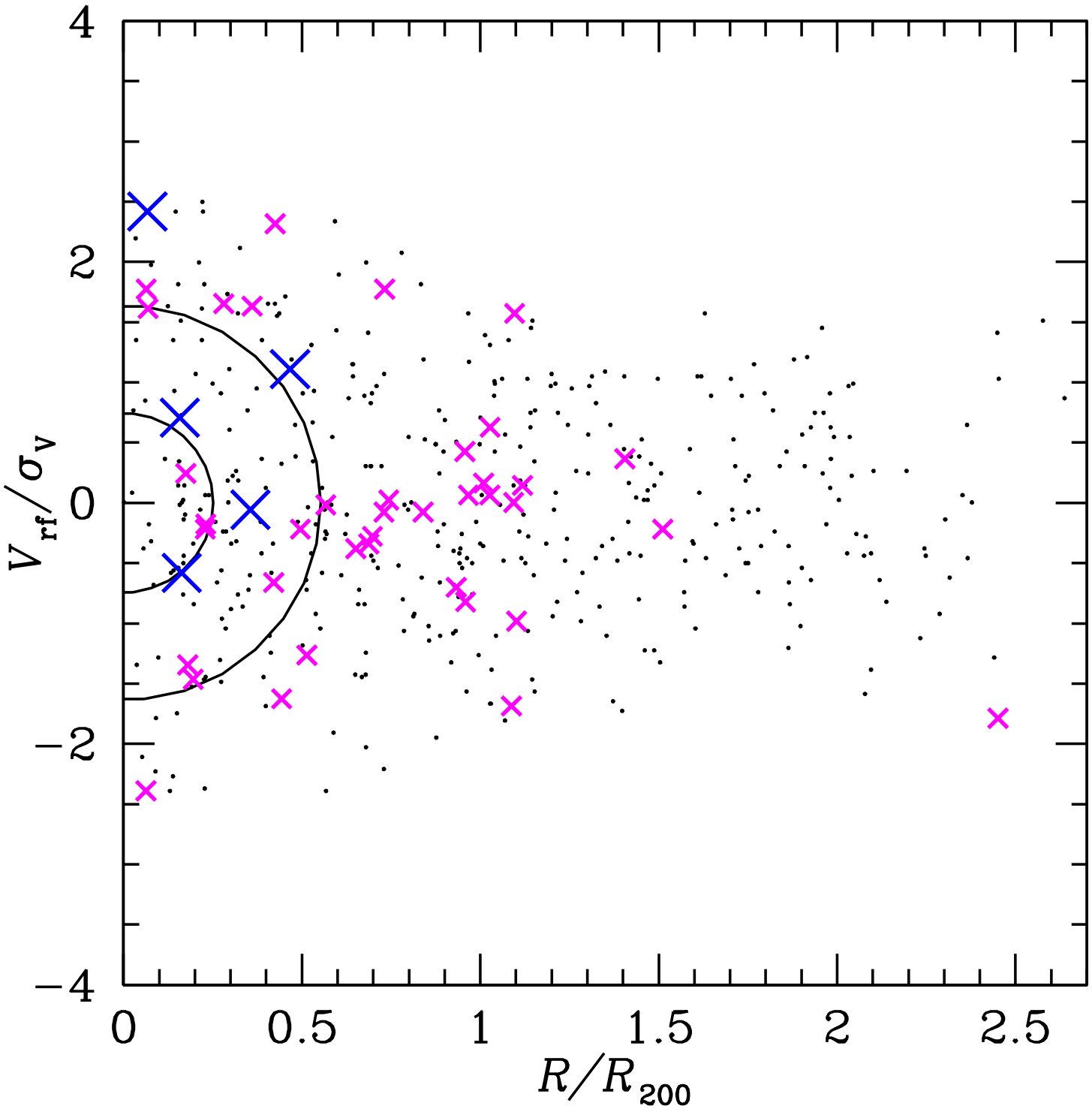
4
2
0
−2
−4
0
0.5
1
1.5
2
2.5
V_{rf}/σ_v
R/R_{200}

Astronomy & Astrophysics manuscript no. mannunziatella
September 4, 2014

CLASH-VLT: The stellar mass function and stellar mass density profile of the z=0.44 cluster of galaxies MACS J1206.2-0847 ⋆

M. Annunziatella[1,2], A. Biviano[2], A. Mercurio[3], M. Nonino[2], P. Rosati[4], I. Balestra[2], V. Presotto[1,2], M. Girardi[1,2], R. Gobat[5], C. Grillo[6], D. Kelson[7], E. Medezinski[8], M. Postman[9], M. Scodeggio[10], M. Brescia[3], R. Demarco[11], A. Fritz[10], A. Koekemoer[9], D. Lemze[8], M. Lombardi[12], B. Sartoris[1,2,13], K. Umetsu[14], E. Vanzella[14], L. Bradley[9], D. Coe[9], M. Donahue[15], L. Infante[16], U. Kuchner[17], C. Maier[17], E. Regős[18], M. Verdugo[17], and B. Ziegler[17]

(Affiliations can be found after the references)

ABSTRACT

Context. The study of the galaxy stellar mass function (SMF) in relation to the galaxy environment and the stellar mass density profile, $\rho_\star$(r),is a powerful tool to constrain models of galaxy evolution.

Aims. We determine the SMF of the z=0.44 cluster of galaxies MACS J1206.2-0847 separately for passive and star-forming (SF) galaxies, in different regions of the cluster, from the center out to approximately 2 virial radii. We also determine $\rho_\star$(r) to compare it to the number density and total mass density profiles.

Methods. We use the dataset from the CLASH-VLT survey. Stellar masses are obtained by spectral energy distribution fitting with the `MAGPHYS` technique on 5-band photometric data obtained at the Subaru telescope. We identify 1363 cluster members down to a stellar mass of $10^{9.5}M_\odot$, selected on the basis of their spectroscopic ($\sim 1/3$ of the total) and photometric redshifts. We correct our sample for incompleteness and contamination by non members. Cluster member environments are defined using either the clustercentric radius or the local galaxy number density.

Results. The whole cluster SMF is well fitted by a double Schechter function, which is the sum of the two Schechter functions that provide good fits to the SMFs of, separately, the passive and SF cluster populations. The SMF of SF galaxies is significantly steeper than the SMF of passive galaxies at the faint end. The SMF of the SF cluster galaxies does not depend on the environment. The SMF of the passive cluster galaxies has a significantly smaller slope (in absolute value) in the innermost ($\leq$ 0.50 Mpc, i.e., $\sim$ 0.25 virial radii), and in the highest density cluster region than in more external, lower density regions. The number ratio of giant/subgiant galaxies is maximum in this innermost region and minimum in the adjacent region, but then gently increases again toward the cluster outskirts. This is also reflected in a decreasing radial trend of the average stellar mass per cluster galaxy. On the other hand, the stellar mass fraction, i.e., the ratio of stellar to total cluster mass, does not show any significant radial trend.

Conclusions. Our results appear consistent with a scenario in which SF galaxies evolve into passive galaxies due to density-dependent environmental processes, and eventually get destroyed very near the cluster center to become part of a diffuse intracluster medium. Dynamical friction, on the other hand, does not seem to play an important role. Future investigations of other clusters of the CLASH-VLT sample will allow us to confirm our interpretation.

Key words. Galaxies: luminosity function, mass function; Galaxies: clusters: individual: MACS J1206.2-0847; Galaxies: stellar content; Galaxies: evolution

1. Introduction

Many galaxy properties, such as colors, luminosities, morphologies, star formation rates, and stellar masses, follow a bimodal distribution (e.g., Baldry et al. 2004; Kauffmann et al. 2003). Galaxies can therefore be classified in two broad classes, red, bulge-dominated, high-mass, passively-evolving galaxies, and blue, disk-dominated, low-mass, star-forming galaxies. The relative number fraction of these two populations changes with redshift (z) and with the local galaxy number density, blue galaxies dominating at higher z and in lower density environments (see Silk & Mamon 2012 for a recent review on galaxy formation and evolution). This suggests that the redshift evolution of these two populations is somehow shaped by physical processes related to the environment in which they reside, such as major and minor mergers, tidal interactions among galaxies or between a galaxy and a cluster gravitational field, and ram-pressure stripping (see, e.g., Biviano 2008 and references therein). All these processes use or remove gas from galaxies, leading to a drop in star-formation due to lack of fuel and to an aging of the stellar population, and consequent reddening of the galaxy light with time. Some of these processes also lead to morphological transformations. These quenching mechanisms have been implemented in both N-body simulations and semi-analytical models with the aim of reproducing the phenomenology of galaxy evolution, and in particular the changing fraction of red and blue galaxies with time. However, there are still many discrepancies between observations and theoretical predictions, such as, e.g., the evolution of galaxy colors, luminosities, and stellar masses (e.g., Cucciati et al. 2012; De Lucia et al. 2012; Silk & Mamon 2012 and references therein).

The distributions of galaxy luminosities and stellar masses ($M_\star$ hereafter), namely, the galaxy luminosity and stellar mass functions (SMF hereafter), are key observables for testing galaxy evolutionary models (e.g., Macciò et al. 2010; Menci et al.

Send offprint requests to: M. Annunziatella, annunziatella@oats.inaf.it

⋆ Based in large part on data collected at the ESO VLT (prog.ID 186.A-0798), at the NASA HST, and at the NASJ Subaru telescope

Gyr. However, an upper limit for this value is provided by the age of the universe at the considered redshift.

For each galaxy model MAGPHYS produces both the dust free and the attenuated spectrum. The attenuated spectra are obtained using the dust model of Charlot & Fall (2000). The main parameter of this model is the total effective V-band absorption optical depth of the dust as seen by young stars inside birth clouds, $\widehat{\tau_V}$. This parameter is distributed according to a probability density function which is approximately uniform over the interval from 0 to 4 and drops exponentially to zero at $\widehat{\tau_V} \sim 6$.

As an output of the SED fitting procedure, MAGPHYS provides both the parameters of the best-fit model and the marginalized probability distribution of each parameter. We adopt the median value of the probability distribution as our fiducial estimate of a given parameter, with lower and upper limits provided by the 16% and 84% percentiles of the same distribution. Using these limits we find that the typical 1 σ error on the $M_\star$ estimates is ~ 0.15 dex.

We translate our completeness limit in magnitude, $R_C = 24$, to a completeness limit in mass, $10^{9.5}\,M_\odot$, based on the relation between these two quantities shown in Fig. 2. The completeness mass limit we choose is that for the passive galaxies population, which guarantees our sample is also complete for the population of SF galaxies since they are intrinsically less massive than passive galaxies at a given magnitude.

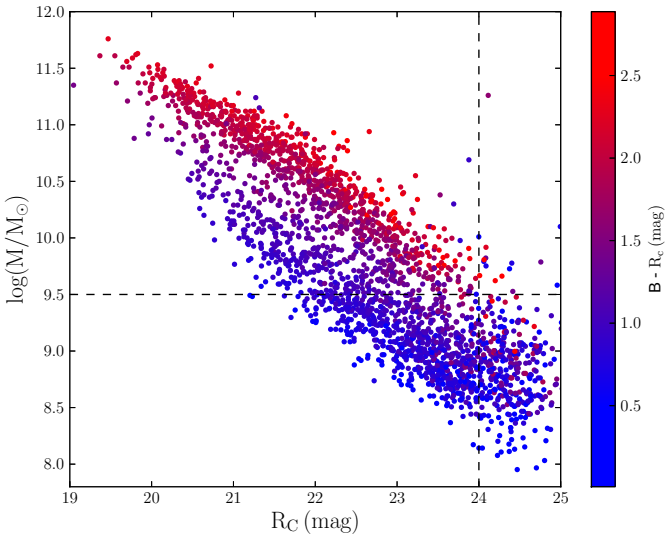

Fig. 2. Galaxy stellar mass as function of R_C magnitude for cluster members. The points are color coded according to their $B - R_C$ color. The vertical dashed line represents the completeness magnitude of our sample, and the horizontal dashed line represents the corresponding completeness mass.

In addition to $M_\star$, among all the parameters provided by the MAGPHYS procedure, we also consider the specific star formation rate (i.e., star formation rate per unit mass, sSFR $\equiv$ SFR/$M_\star$). The sSFR values are used to distinguish between SF and passive galaxies. Even if we do not expect the sSFR estimates from optical SED fitting to be very accurate, they are sufficiently good to allow identification of the well-known bimodality in the galaxy distribution (see Sect. 1). This can be better appreciated by looking at the sSFR distribution of cluster galaxies, shown in Fig. 3. This distribution is clearly bimodal. Following Lara-López et al. (2010, and references therein) we use the value sSFR= 10^{-10} yr^{-1} to separate the populations of SF and passive galaxies. This value also corresponds to a local minimum in the sSFR distribution.

In the public MAGPHYS library, there are many more dusty and SF models than passive models (E. da Cunha, priv. comm.). Whenever an optical SED can be equally well fitted by a passive model and by a dusty SF model, the median solution is biased in favor of dusty SF models, since they occupy a larger area of the parameter space than passive models. It is therefore possible that some truly passive galaxies are classified as dusty SF galaxies. To estimate how serious this misclassification might be, we fit the sSFR distribution with two Gaussian distributions (see Fig. 3). We make the hypothesis that misclassified passive galaxies lie in the high-sSFR tail of the Gaussian centered at low sSFR. The fraction of the area occupied by this Gaussian at sSFR> 10^{-10} yr^{-1} is 0.5%, and this is our estimate of the fraction of passive galaxies misclassified as SF. Similarly, one can estimate that the fraction of SF galaxies incorrectly classified as passive is 4%. Given that these fractions are small, we consider our sSFR estimates sufficiently good to separate our sample into the two populations of passive and SF galaxies.

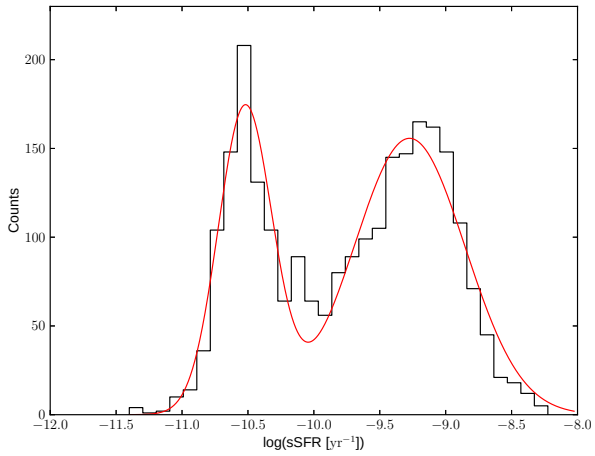

Fig. 3. Distribution of the sSFR for the total sample of cluster galaxies. The red curve represents the best-fit to this distribution with two Gaussians.

In order to check the reliability of our $M_\star$ estimates, we make use of the data from the UltraVista survey[2] (McCracken et al. 2013) which is an ultra-deep, near-infrared survey with the VISTA survey telescope of the European Southern Observatory. From the UltraVista public catalog we select only 'USE = 1' objects, i.e., objects classified as galaxies, with a K magnitude above the detection limit of 23.9, and with uncontaminated and accurate photometry (Muzzin et al. 2013b). We select only galaxies with masses larger than our completeness limit ($10^{9.5}\,M_\odot$), and in the same photometric redshift range $0.38 \leq z_{phot} \leq 0.50$ used for our cluster membership selection – UltraVista z_{phot} have been obtained with the EAZY code of Brammer et al. (2008). To separate the UltraVista sample into the passive and SF populations we use the separations provided by Muzzin et al. (2013a) in the UVJ diagram.

We compare the masses provided in the UltraVista database (and obtained using the FAST SED-fitting code of Kriek et al. 2009) with those we obtained applying MAGPHYS on the UltraVista photometric catalog, using all of the

[2] http://home.strw.leidenuniv.nl/ ultravista/

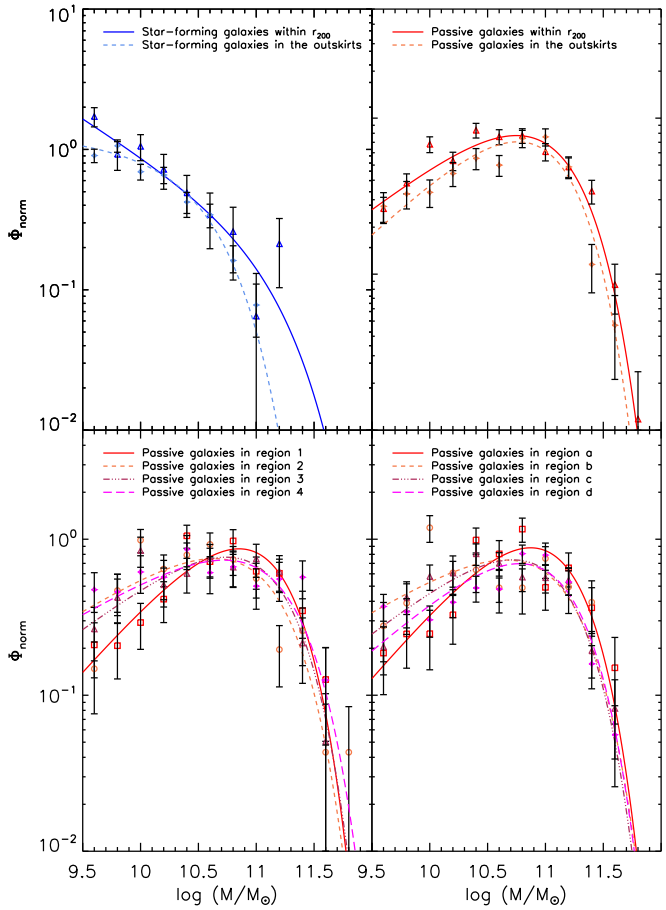

Fig. 8. SMFs of SF and passive galaxies in different cluster regions and in the field. Upper left (resp. right) panel: SMFs of SF (resp. passive) cluster galaxies beyond and within r_{200}. Bottom left panel: SMFs of passive cluster galaxies in four different regions, defined by their distances from the cluster center (see text). Bottom right panel: SMFs of passive cluster galaxies in four different regions, defined by their local number densities. SMFs are normalized to the total number of galaxies contained in the respective samples.

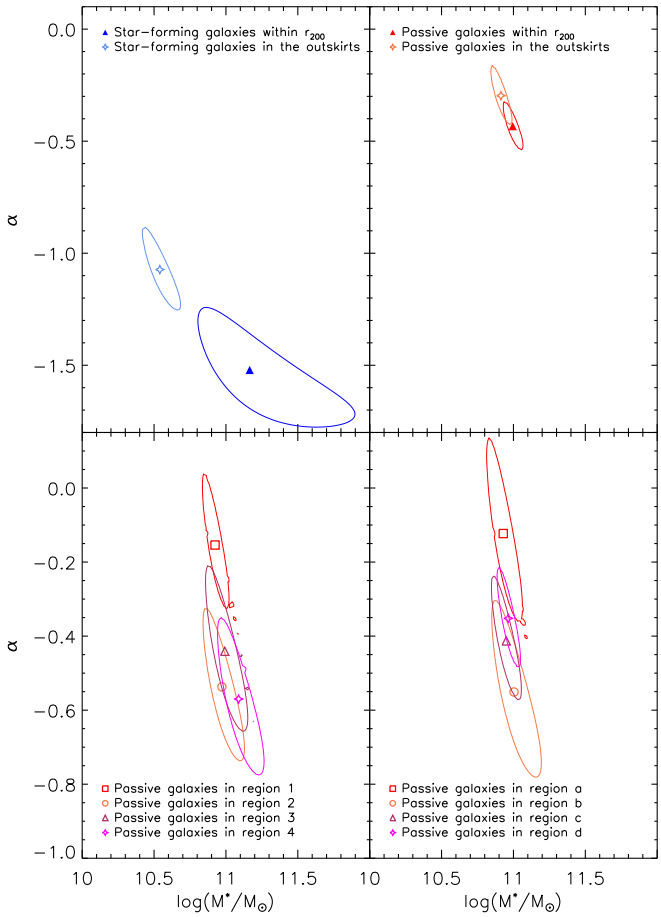

Fig. 9. Best-fit Schechter parameters M^* and α and 1 σ likelihood contours, after marginalizing over the Φ^* parameter for the SMFs of SF and passive galaxies in different cluster regions and in the field. The panels correspond one-to-one to those of Fig. 8.

To highlight a possible radial dependence of the cluster SMF we compare the $M_\star$ distributions of cluster members in adjacent regions, using the K-S test, separately for SF and passive galaxies, whenever there are at least ten galaxies in each of the subsamples. The $M_\star$ distributions of the SF cluster galaxies in the different regions are not statistically different (see Table 4). On the other hand, the K-S tests indicate a significant difference of the $M_\star$ distributions of passive cluster members in Region 1 (the innermost one) and the adjacent Region 2. For no other adjacent regions does the K-S test highlight a significant difference from the SMFs of passive galaxies.

From Fig. 9 (bottom left panel) and Table 3 one can see that the difference of the SMFs in Regions 1 and 2 is reflected in a difference in the values of the best-fit Schechter parameter α. From Fig. 8 (bottom left panel) we can indeed see that the SMF of passive galaxies in Region 1 is characterized by a low-mass end drop that is more rapid than for the SMFs in other Regions.

From Fig. 9, one can notice that the SMFs of passive galaxies in Region 1 intersects those of passive galaxies in the other regions at $\log(M_\star/M_\odot) \sim 10.5$. Since these SMFs are normalized by the total number of galaxies in their respective samples, this does not mean that in Region 1 there are more galaxies with $\log(M_\star/M_\odot) \sim 10.5$ than in other regions. This mass value only indicates where the relative ratio of the number of galaxies more massive and less massive than a given value is maximally different for the SMF in Region 1 and in the other regions. We therefore use this value to separate 'giant' from 'subgiant' galaxies and plot the giant/subgiant number ratio (GSNR hereafter) as a function of radial distance from the cluster center in Fig. 11. Note that we use the correction factors defined in Sect. 2.2 as weights to compute the GSNR. The GSNR of passive galaxies decreases rapidly from the center (Region 1) to R ~ 0.8 Mpc, then gently increases again toward the cluster outskirts (R > 3.5 Mpc) but without reaching the central value again. The GSNR of SF galaxies does not seem to depend on radius and is systematically below that of passive galaxies at all radii.

3.2.2. Density dependence

As an alternative definition of 'environment', we consider here the local number density of cluster members. This density is defined by smoothing the projected distribution of galaxies with a two-dimensional Gaussian filter in an iterative way. Initial estimates of the densities are obtained by using a fixed 'optimal' (in the sense of Silverman 1986) characteristic width for the Gaus-

Astronomy & Astrophysics manuscript no. ICL_Presotto14_accepted
March 21, 2014

Intra Cluster Light properties in the CLASH-VLT cluster MACS J1206.2-0847 ⋆

V. Presotto[1,2], M. Girardi[1,2], M. Nonino[2], A. Mercurio[3], C. Grillo[4], P. Rosati[5], A. Biviano[2], M. Annunziatella[1,2], I. Balestra[3,2], W. Cui[1,2,6], B. Sartoris[1,27], D. Lemze[8], B. Ascaso[9], J. Moustakas[10], H. Ford[8], A. Fritz[11], O. Czoske[12], S. Ettori[13,14], U. Kuchner[12], M. Lombardi[15], C. Maier[12], E. Medezinski[16], A. Molino[9], M. Scodeggio[11], V. Strazzullo[17], P. Tozzi[18], B. Ziegler[12], M. Bartelmann[19], N. Benitez[9], L. Bradley[20], M. Brescia[3], T. Broadhurst[21], D. Coe[20], M. Donahue[22], R. Gobat[23], G. Graves[24,25], D. Kelson[26], A. Koekemoer[20], P. Melchior[27], M. Meneghetti[13,14], J. Merten[28], L. Moustakas[28], E. Munari[1,2], M. Postman[20], E. Regős[29], S. Seitz[30,31], K. Umetsu[32], W. Zheng[8], and A. Zitrin[33,34]

(Affiliations can be found after the references)

ABSTRACT

Aims. We aim at constraining the assembly history of clusters by studying the intra cluster light (ICL) properties, estimating its contribution to the fraction of baryons in stars, f_*, and understanding possible systematics/bias using different ICL detection techniques.
Methods. We developed an automated method, *GALtoICL*, based on the software GALAPAGOS to obtain a refined version of typical BCG+ICL maps. We applied this method to our test case MACS J1206.2-0847, a massive cluster located at z∼0.44, that is part of the CLASH sample. Using deep multi-band SUBARU images, we extracted the surface brightness (SB) profile of the BCG+ICL and we studied the ICL morphology, color, and contribution to f_* out to R_{500}. We repeated the same analysis using a different definition of the ICL, *SBlimit* method, i.e., a SB cut-off level, to compare the results.
Results. The most peculiar feature of the ICL in MACS1206 is its asymmetric radial distribution, with an excess in the SE direction and extending towards the 2^{nd} brightest cluster galaxy which is a Post Starburst galaxy. This suggests an interaction between the BCG and this galaxy that dates back to $\tau \leq 1.5$Gyr. The BCG+ICL stellar content is $\sim 8\%$ of $M_{*,500}$ and the (de-) projected baryon fraction in stars is $f_* = 0.0177(0.0116)$, in excellent agreement with recent results. The *SBlimit* method provides systematically higher ICL fractions and this effect is larger at lower SB limits. This is due to the light from the outer envelopes of member galaxies that contaminate the ICL. Though more time consuming, the *GALtoICL* method provides safer ICL detections that are almost free of this contamination. This is one of the few ICL study at redshift $z > 0.3$. At completion, the CLASH/VLT program will allow us to extend this analysis to a statistically significant cluster sample spanning a wide redshift range: $0.2 \lesssim z \lesssim 0.6$.

Key words. Galaxies: clusters: individual: MACS J1206.2-0847; Cosmology: observations

1. Introduction

Since its first discovery by Zwicky (1951) to the most recent works (Guennou et al. 2012; Burke et al. 2012; Adami et al. 2012) the intra cluster light (ICL) has gained increasing interest because it can help us understanding both the assembly history of galaxy clusters and its contribution to the baryonic budget. The ICL consists of stars which are bound to the cluster potential after being stripped from member galaxies as they interacted and merged with either the brightest cluster galaxy (BCG) or the other member galaxies (Murante et al. 2004; Sommer-Larsen et al. 2005; Monaco et al. 2006; Murante et al. 2007; Conroy et al. 2007; Puchwein et al. 2010; Rudick et al. 2011; Cui et al. 2013; Contini et al. 2013). The ICL signature can be seen in the surface brightness (SB) profile of the BCG as an excess of light with respect to the typical $r^{1/4}$ law (de Vaucouleurs 1953). Gonzalez et al. (2005) showed that a double $r^{1/4}$ model provides a better fit to the BCG+ICL SB profile and that the ICL has a more concentrated profile than that of the total cluster light (see also Zibetti et al. 2005).

The origin of the ICL strictly connects it to the evolutionary history of the clusters, thus, we can recall the assembly history of the clusters by studying the ICL properties. The ICL colors can provide us information on the timescales involved in ICL formation and on its progenitors when compared to BCG colors. Some works found that ICL colors are consistent with those of the BCG (e.g., Zibetti et al. 2005; Krick & Bernstein 2007; Pierini et al. 2008; Rudick et al. 2010), suggesting that the ICL has been originated by ongoing interactions among cluster members and the BCG. The merging cluster in the sample of Pierini et al. (2008) and some compact groups (Da Rocha & Mendes de Oliveira 2005) represent an exception showing bluer colors for the ICL, hinting to either *in-situ* star formation or blue dwarf disruption after interaction.

Usually the ICL is found to be strongly aligned with the position angle (PA) of the BCG (Gonzalez et al. 2005; Zibetti et al. 2005), but there are cases of misalignment and/or prominent features/plumes (Mihos et al. 2005; Krick & Bernstein 2007). Studying the connections between the ICL spatial distribution and the presence of cluster substructures can shed a light on the origin of the ICL and its connection to the assembly history of the cluster. ICL plume-like structures bridging together the BCG and other galaxies, arcs and tidal streams of ICL have been found by many works (e.g., Gregg & West 1998; Calcáneo-Roldán et al. 2000; Feldmeier et al. 2004; Krick et al. 2006; Da Rocha et al. 2008). According to simulations these features trace recent

⋆ Based on data collected at the NASJ Subaru telescope, at the ESO VLT (prog.ID 186.A-0798), and the NASA HST.

Table 3. Best fit parameters for different profiles, where 'deVauc' and 'Sérs' refer to the de Vaucouleurs and Sérsic profile respectively.

Profile type	Mag_{tot} (AB mag)	r_e (h_{70}^{-1} kpc)	n	q	PA (deg)	$\tilde{\chi}^2$
single deVauc	18.35±0.01	28.4±0.3	4	0.47±0.01	-73.42±0.19	19.3
single Sérs	18.48±0.00	22.4±0.1	3.16±0.01	0.48±0.01	-74.24±0.02	34.9
single Sérs ($4 < n < 8$)	17.83±0.01	77.1±1.1	6.78±0.04	0.43±0.01	-72.74±0.02	2.6
deVauc+deVauc	18.72±0.07 19.41±0.18	26.3±1.4 37.1±10.1	4 4	0.51±0.06 0.44±0.06	-79.5±12.0 -71.4±4.6	9.6
deVauc+Sérs	19.09±0.01 18.13±0.01	32.2±0.07 138.1±0.04	4 6.72±0.04	0.42±0.01 0.43±0.01	-72.33±0.06 -74.42±0.07	2.5
deVauc+Sérs ($n \leq 3.99$)	19.03±0.01 18.07±0.01	15.4±0.07 174.7±1.6	4 3.35±0.01	0.41±0.01 0.41±0.02	-76.35±0.12 -70.11±0.08	3.0

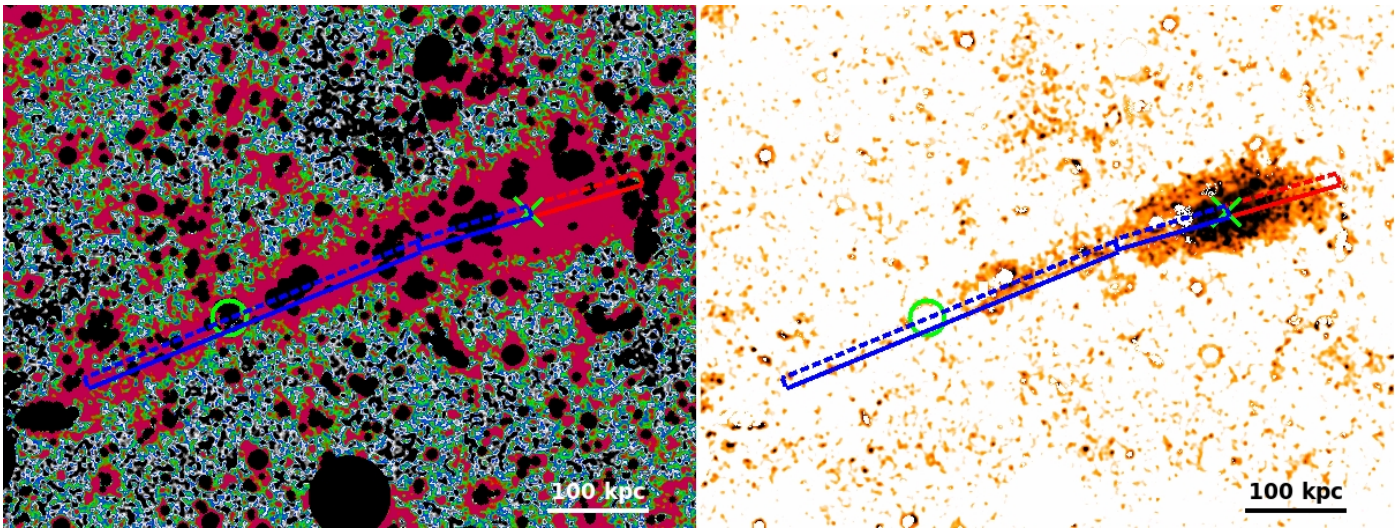

Fig. 6. *Left panel:* Zoom of the Rc-band BCG+ICL map of MACS1206 smoothed with a Gaussian kernel of 3x3 pixels. We overlaid the slits along the SE (blue) and NW (red) direction from which we extract the SB profiles. The green cross and circle correspond to the location of the BCG and the second brightest galaxy respectively. *Right panel:* (B-Rc) color map of BCG+ICL. Slits are overlaid as in the *left panel*.

h_{70}^{-1} kpc the SB profile in the NW direction blurs into the sky regime, while in the SE direction there is still signal. We also detect signal from the extra slit even if it is at sky level.

Both SB profiles show an excess with respect to the single de Vaucouleurs best fit model, so we tried different models to describe the light profiles: 1) a generic Sérsic profile either constraining or not the allowed range for the Sérsic index (Oemler 1976; Carter 1977; Schombert 1986; Stott et al. 2011), 2) a double de Vaucouleurs model (Gonzalez et al. 2005), and 3) a composite de Vaucouleurs plus generic Sérsic profile with either free n or within a constrained range of allowed values. In the top left panel of Fig. 7 the dot-dot-dot-dashed, long-dashed, dot-dashed, short-dashed, and solid lines refer to the generic Sérsic (gs), generic Sérsic with high index (gshn), double de Vaucouleurs (dd), de Vaucouleurs plus generic Sérsic (ds), and de Vaucouleurs plus generic Sérsic with low index (dsln) best fit models respectively. The generic Sérsic best fit profile (n = 3.16) gives even worse results than the single de Vaucouleurs one, especially in the outer region where the ICL contribution becomes important. The double de Vaucouleurs profile improves the fit even though there is still an excess of light that can not be fit in the outer region. This light excess can be better appreciated in the zoomed version of the SB profile in the right panel of Fig. 7. Color code and line types are the same as in the left panel, but we show only the SB profile at $20 \leq R \leq 100$ h_{70}^{-1} kpc . On the contrary, both the composite de Vaucouleurs plus generic Sérsic profiles and the single generic Sérsic profile with $4 < n < 8$ manage to fit also the light excess at large distances. The de Vaucouleurs plus generic Sérsic with high index profiles provides the best $\tilde{\chi}^2$. The bottom panels show the residulas of single component fitted profiles (left) and composite fitted profiles (right).

In Tab. 3 we list the best fit parameters for each profile. We notice that both the PA and the ellipticity, $\epsilon = 1 - q$, show a small range of values among all the adopted profiles: $-70° \lesssim PA \lesssim -80°$ and $0.59 \lesssim \epsilon \lesssim 0.49$ respectively. This also suggests that in case of a two component profile the BCG and the ICL show a good alignment irrespective of the model choice in agreement with the findings of Gonzalez et al. (2005); Zibetti et al. (2005). In case of a single component fit the effective radius ranges between ~ 20 h_{70}^{-1} kpc and ~ 80 h_{70}^{-1} kpc , while when we adopt a composite profile, the component associated with the BCG has $15 \lesssim r_{e,BCG} \lesssim 32$ h_{70}^{-1} kpc whereas the ICL one is less concentrated and it has larger effective radius: $37 \lesssim r_{e,ICL} \lesssim 175$ h_{70}^{-1} kpc .

As mentioned above we chose to use the Rc band global best fit model as the benchmark model to be adapted for the B-band,

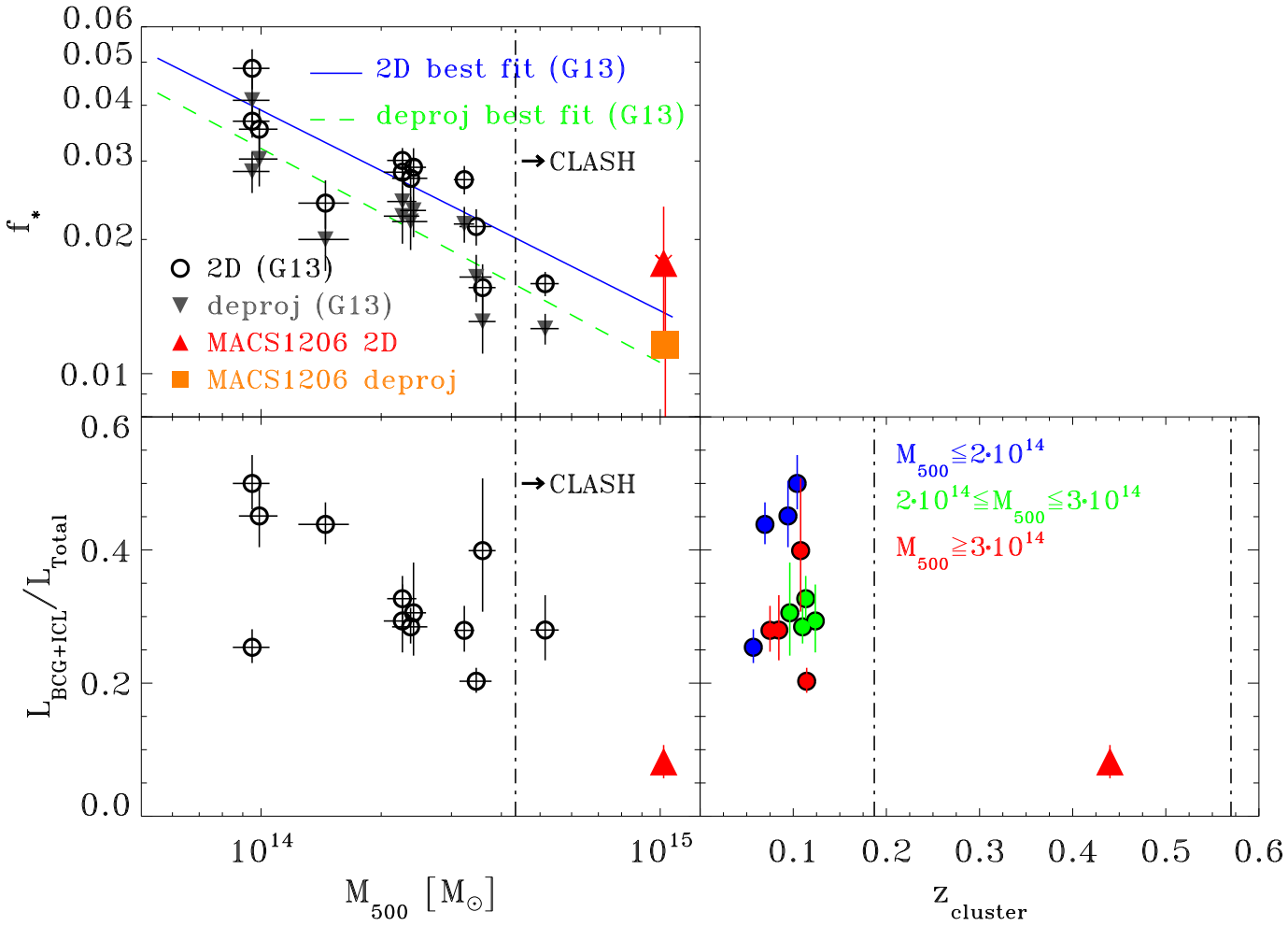

Fig. 13. *Top panel:* Stellar baryon fraction as a function of M_{500} for both MACS1206 and the cluster sample of Gonzalez et al. (2013, G13 hereafter). (Orange square) Red triangle refers to the (de-)projected f_* for MACS1206, while (upside-down grey triangles) open circles refer to the (de-)projected G13 sample. The (green dashed) blue solid line correspond to the (de-)projected best fit relation from G13 while the dot-dashed line indicates the predicted cluster mass M_{500} lower limit for the CLASH sample (see text for details). *Bottom left panel:* BCG+ICL fraction of light/mass within R_{500} as function of cluster mass for both MACS1206 and the G13 cluster sample, symbols/lines as above . *Bottom right panel:* BCG+ICL fraction of light/mass within R_{500} as function of cluster redshift. G13 sample is color coded according to their M_{500}. Blue, green, red circles correspond to $M_{500} \leq 2 \times 10^{14} M_{\odot}$, $2 \times 10^{14} \leq M_{500} \leq 3 \times 10^{14} M_{\odot}$, and $M_{500} \geq 4 \times 10^{14} M_{\odot}$ respectively.

the ICL. As a consequence, the ICL contribution on small scales is very important, though on larger scales it becomes less significative. This is clearly shown in the right panel of Fig. 10 once we adopt a SB threshold on our BCG+ICL maps, i.e., red points, on the contrary applying the same SB limit to the original image shows a plateau of the ICL fraction at large radii. This highlights the systematic error in the ICL contribution estimate depending on the adopted method: light from the outer envelopes of member galaxies can significantly affect the ICL fraction when using the SB limit method. This effect is larger at lower SB limits, but even at the higher SB limit the estimated ICL fraction is twice that obtained with the *GALtoICL* method. Once again we stress the importance of removing all the light from galaxy members that can affect the real ICL contribution. Unfortunately the *SBlimit* method is the best way to compare results among observational works and simulations. We find good agreement between our ICL fractions at Rc-band SB levels corresponding to $\mu_V(z = 0) \geq 26.5$ mag/arcsec^2 and those expected from simulations. For a cluster with the same M_{500} as MACS1206, Cui et al. (2013) estimates ICL fraction at R_{500} of 10-20% and 5-10% for $\mu_V(z = 0) = 26.5$ and 27.5 respectively depending on the adopted simulation, i.e., with either gas cooling, star forming, and supernova feedback or including AGN feedback, thus showing good agreement with our results. Rudick et al. (2011) simulated clusters with a smaller mass range, still if we consider their most massive cluster B65, M_{200}=6.5 × 10^{14} $M_{\odot}$, the ICL fraction for $\mu_V(z = 0) = 26.5$ is nearly 12% within $1.5 \times R_{200}$, see left panel of their Fig. 3. Given that they claim only a smaller increase in the ICL fraction within R_{500}, these values are in good agreement with our results. A direct comparison with observational works is less trivial due to different ICL enclosing radius or lack of cluster total mass information. For instance Feldmeier et al. (2004) finds ICL fraction of ∼10 (2)% above $\mu_V(z = 0) = 26.5(27.5)$ mag/arcsec^2 for a set of clusters located at z∼0.17. These values are in good agreement with our ICL fraction of ∼12 (4)% at Rc-band SB levels corresponding to $\mu_V(z = 0) \geq 26.5(27.5)$ mag/arcsec^2, thus suggesting a lack of evolution in the ICL fraction with cosmic time. This result agrees with the absence of strong variation in the amount of ICL between z=0 and z=0.8 reported by Guennou et al. (2012) and other authors (Krick & Bernstein 2007). However we should remind that this comparison is regardless of the cluster total mass and/or ICL enclos-

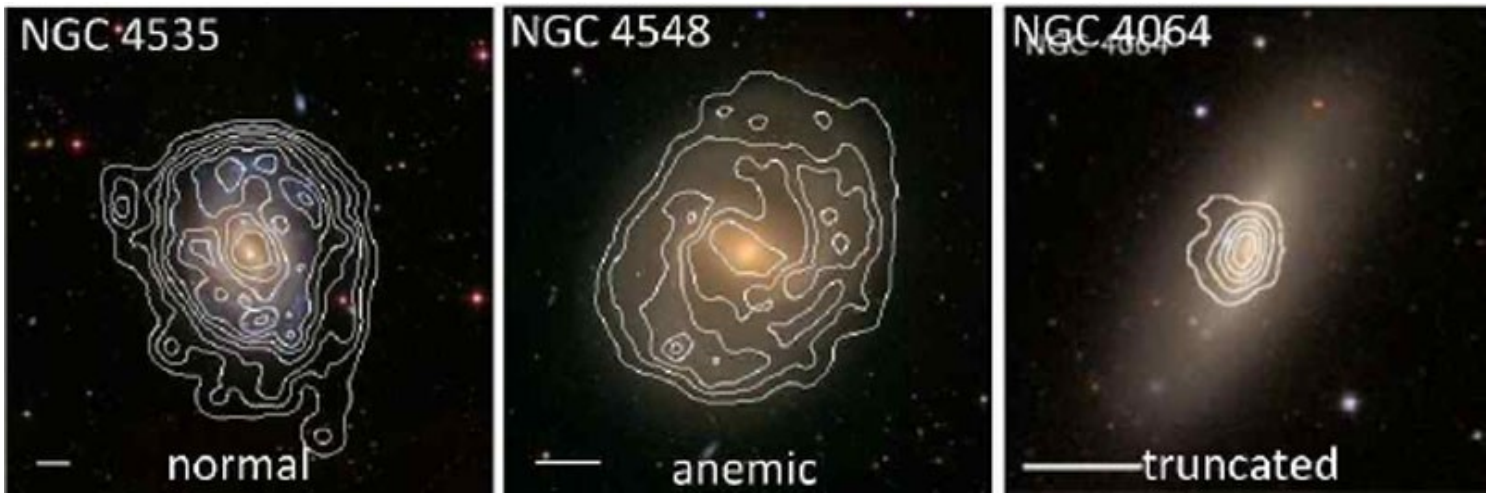

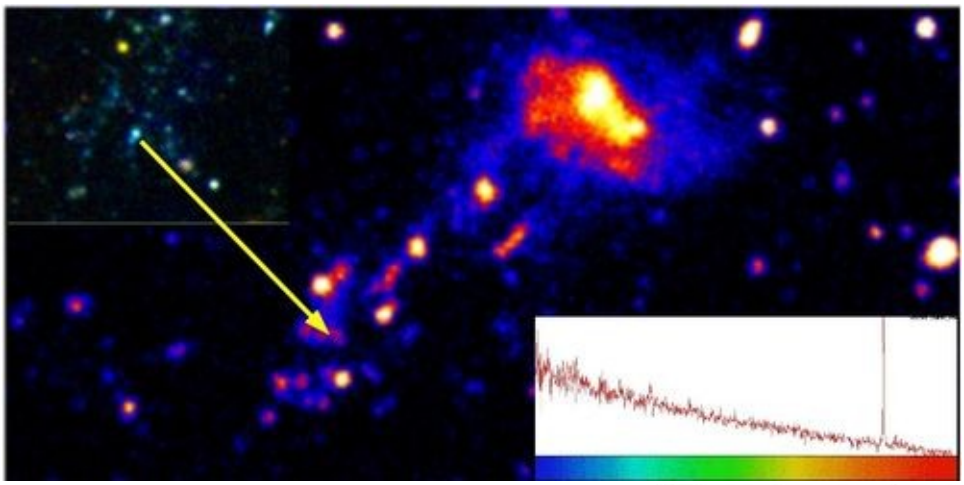

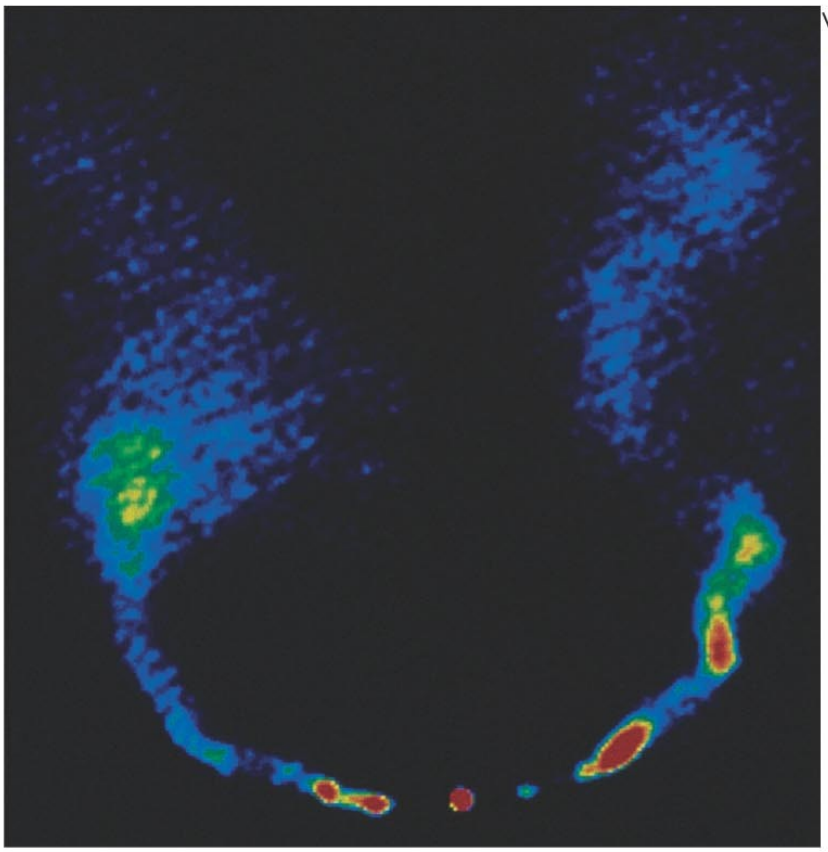

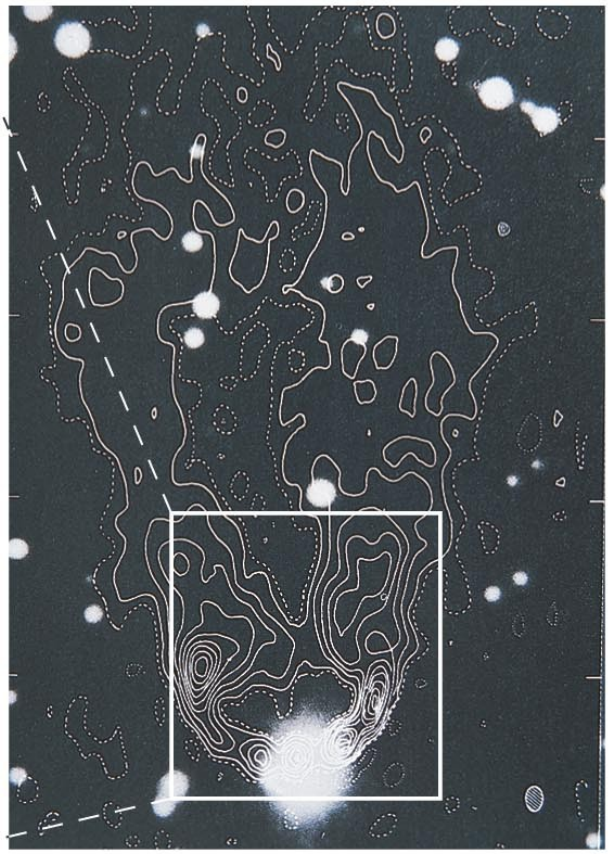

(a)

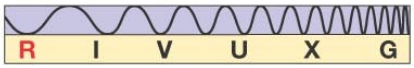

(b)

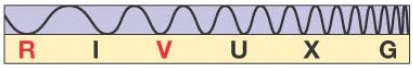

Astronomy & Astrophysics manuscript no. group
August 8, 2014

The stripping of a galaxy group diving into the massive cluster A2142

D. Eckert[1,2], S. Molendi[2], M. Owers[3], M. Gaspari[4,5], T. Venturi[6], L. Rudnick[7], S. Ettori[5,8], S. Paltani[1], F. Gastaldello[2,9], and M. Rossetti[10,2]

[1] Department of Astronomy, University of Geneva, ch. d'Ecogia 16, 1290 Versoix, Switzerland
e-mail: Dominique.Eckert@unige.ch
[2] INAF - IASF-Milano, Via E. Bassini 15, 20133 Milano, Italy
[3] Australian Astronomical Observatory, PO Box 915, North Ryde, NSW 1670, Australia
[4] Max Planck Institute for Astrophysics, Karl-Schwarzschild-Strasse 1, 85741 Garching, Germany
[5] INAF - Osservatorio Astronomico di Bologna, Via Ranzani 1, 40127 Bologna, Italy
[6] INAF - Istituto di Radioastronomia, via Gobetti 101, 40129, Bologna, Italy
[7] Minnesota Institute for Astrophysics, School of Physics and Astronomy, University of Minnesota, 116 Church Street SE, Minneapolis, MN 55455, USA
[8] INFN, Sezione di Bologna, viale Berti Pichat 6/2, 40127 Bologna, Italy
[9] Department of Physics and Astronomy, University of California at Irvine, 4129 Frederick Reines Hall, Irvine, CA 92697-4575, USA
[10] Università degli studi di Milano, Dip. di Fisica, via Celoria 16, 20133 Milano, Italy

Preprint online version: August 8, 2014

ABSTRACT

Structure formation in the current Universe operates through the accretion of group-scale systems onto massive clusters. The detection and study of such accreting systems is crucial to understand the build-up of the most massive virialized structures we see today. We report the discovery with *XMM-Newton* of an irregular X-ray substructure in the outskirts of the massive galaxy cluster Abell 2142. The tip of the X-ray emission coincides with a concentration of galaxies. The bulk of the X-ray emission of this substructure appears to be lagging behind the galaxies and extends over a projected scale of at least 800 kpc. The temperature of the gas in this region is 1.4 keV, which is a factor of ~ 4 lower than the surrounding medium and is typical of the virialized plasma of a galaxy group with a mass of a few $10^{13} M_{\odot}$. For this reason, we interpret this structure as a galaxy group in the process of being accreted onto the main dark-matter halo. The X-ray structure trailing behind the group is due to gas stripped from its original dark-matter halo as it moves through the intracluster medium (ICM). This is the longest X-ray trail reported to date. For an infall velocity of $\sim$1,200 km s^{-1} we estimate that the stripped gas has been surviving in the presence of the hot ICM for at least 600 Myr, which exceeds the Spitzer conduction timescale in the medium by a factor of $\gtrsim 400$. Such a strong suppression of conductivity is likely related to a tangled magnetic field with small coherence length and to plasma microinstabilities. The long survival time of the low-entropy intragroup medium suggests that the infalling material can eventually settle within the core of the main cluster.

Key words. X-rays: galaxies: clusters - Galaxies: clusters: general - Galaxies: groups: general - Galaxies: clusters: intracluster medium - cosmology: large-scale structure

1. Introduction

Galaxy clusters are thought to have grown through the continuous accretion and merging of smaller halos across cosmic time (e.g. Springel et al. 2006). These processes are expected to be still active in the outer regions of massive local clusters, through the accretion of galaxies and groups of galaxies onto the main dark-matter halo. Accreting substructures in the form of infalling galaxies and galaxy groups contribute significantly to the growth of galaxy clusters in mass, member galaxies and hot gas (e.g. Berrier et al. 2009; Genel et al. 2010; De Lucia et al. 2012). Therefore, such events provide us with excellent laboratories for the study of the processes leading to the assembly of galaxy clusters.

There are many examples of substructures observed in the optical (e.g. Girardi & Biviano 2002, and references therein), indicating that the majority of clusters are still dynamically active. The dynamics of small structures is however complicated to infer directly from optical data because of the small number of members, and their association with an underlying dark-matter halo is difficult to assess (Lemze et al. 2013). Weak-lensing studies (e.g. LoCuSS, Okabe et al. 2010) are effective at detecting massive halos, but are insufficiently sensitive to minor mergers (i.e. mergers with mass ratio $\sim$1/100 or lower). The detection of extended X-ray emission provides a cleaner way of assessing the presence of low-mass infalling halos, since hot gas is an unambiguous signature of a virialized halo.

While X-ray observatories like *Chandra* have provided spectacular examples of merging clusters (Markevitch & Vikhlinin 2007; Owers et al. 2009, and references therein), the accretion of smaller halos onto massive clusters has proven more elusive. During infall,

the ram pressure applied by the ambient ICM is responsible for stripping the gas from its original halo and heating it up (Gunn & Gott 1972; Vollmer et al. 2001; Heinz et al. 2003; Roediger & Brüggen 2008), leading to the virialization of the gas in the main dark-matter halo. This process has been observed in a handful of interacting galaxies in the nearest clusters like Virgo (e.g. Machacek et al. 2004; Randall et al. 2008), A3627 (Sun et al. 2007; Zhang et al. 2013), Pavo (Machacek et al. 2005) and A1367 (Sun & Vikhlinin 2005).

In the local Universe, groups with a gravitational mass in the range of a few $10^{13} M_{\odot}$ are the largest reservoir of cosmic gas and total matter (Fukugita et al. 1998). Thus, at the present epoch the continuous infall of such groups is the major process by which clusters grow in the current favored scenario of hierarchical structure formation in a cold dark matter dominated Universe. The ΛCDM paradigm predicts that there should be approximately ∼1 such accreting group per massive cluster and per Gyr (Dolag et al. 2009). There are a few examples of accreting groups directly observed in X-rays such as NGC 4839 in Coma (Briel et al. 1992; Neumann et al. 2001) and the southern group in A85 (Kempner et al. 2002; Durret et al. 2005). However in both instances, the bulk of the X-ray emission is localized around the dominant elliptical galaxy of the group.

Abell 2142 is a massive ($M_{200} = 1.3 \times 10^{15} M_{\odot}$, Munari et al. 2013), X-ray luminous galaxy cluster at a redshift of 0.09 (Owers et al. 2011). This cluster is known to be dynamically active, as highlighted by its X-ray morphology elongated in the NW-SE direction (Buote & Tsai 1996), the presence of prominent cold fronts (Markevitch et al. 2000; Rossetti et al. 2013), and of Mpc-scale radio emission (Farnsworth et al. 2013). A dynamical analysis of ∼1,000 member galaxies indicates the presence of several small subgroups (Owers et al. 2011).

We obtained an *XMM-Newton* mosaic of this cluster covering the entire azimuth out to the virial radius. In this paper, we report the discovery in this program of an accreting galaxy group in the outskirts of A2142. The paper is organized as follows. In Sect. 2, we introduce the available data and the analysis procedure. In Sect. 3 we present our results and the existing multiwavelength information (optical and radio). The implications of our findings are discussed in Sect. 4.

Throughout the paper, we assume a ΛCDM cosmology with $H_o = 70$ km s^{-1}, $\Omega_m = 0.3$ and $\Omega_\Lambda = 0.7$. At the redshift of A2142 ($z = 0.09$), this corresponds to $1'' = 1.7$ kpc. For an average cluster temperature of 9.0 keV (De Grandi & Molendi 2002) and using the scaling relations of Arnaud et al. (2005), we estimate $R_{500} = 1450$ kpc $= 14.4$ arcmin[1] and $R_{200} = 2200$ kpc $= 21.6$ arcmin. All the quoted error bars are at the 1σ level.

2. Data analysis

2.1. Imaging

Abell 2142 was mapped by *XMM-Newton* in 2011 and 2012 through a central 50 ks pointing (OBSID 067456, see Rossetti et al. 2013) and four 25 ks offset pointings (OBSID 069444), which allowed us to obtain a coverage of the entire azimuth of the cluster out to R_{200}. The data were processed using the *XMM-Newton* Scientific Analysis System (XMMSAS) v13.0. We extracted raw images in the [0.7-1.2] keV band for all three EPIC detectors (MOS1, MOS2 and pn) using the Extended Source Analysis Software package (ESAS, Snowden et al. 2008). The choice of the [0.7-1.2] keV energy band is motivated by the fact that this band maximizes the source-to-background ratio (Ettori & Molendi 2011) and avoids the bright Al and Si background emission lines, whilst maintaining a large effective area since the collecting power of the *XMM-Newton* telescopes peaks at 1 keV. Exposure maps for each instrument were created, taking into account the variations of the vignetting across the field of view. A model image of the non X-ray background (NXB) was computed using a collection of closed-filter observations and was adjusted to each individual observation by comparing the count rates in the unexposed corners of the EPIC detectors. Point sources were detected down to a fixed flux threshold and excluded using the ESAS task `cheese`.

We computed surface-brightness images by subtracting the NXB from the raw images and dividing them by the exposure maps. To maximize the signal-to-noise ratio, we then combined the surface-brightness images of the three EPIC detectors by weighing each detector by its relative effective area, and created a combined mosaic image of the cluster using all 5 observations. The total *XMM-Newton*/EPIC image of A2142 is shown in Fig. 1. The dashed circles indicate the approximate locations of R_{500} and R_{200}. An intriguing diffuse, irregular structure is observed at $\sim R_{500}$ northeast (NE) of the cluster core, highlighted by the red square in Fig. 1. For the remainder of the paper, we focus on this

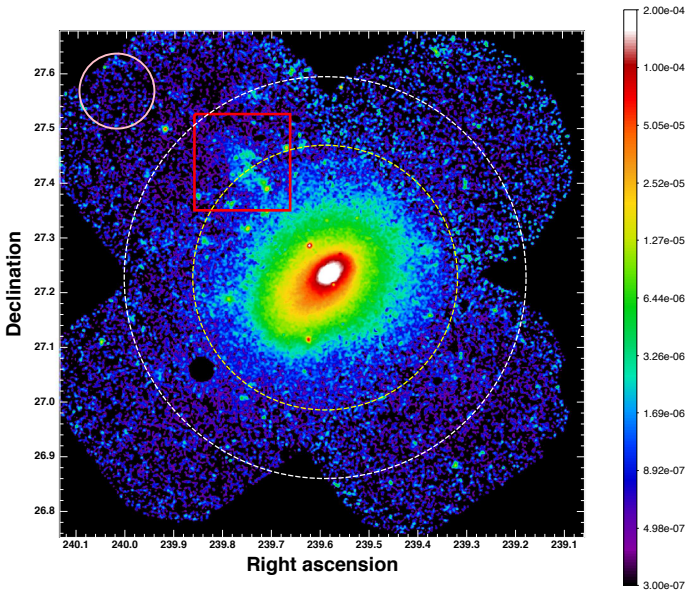

Fig. 1. Exposure-corrected, NXB-subtracted combined *XMM-Newton*/EPIC mosaic image of A2142 in the [0.7-1.2] keV band, smoothed with a Gaussian of width 15 arcsec. The units for the color bar are MOS counts s^{-1}. The dashed circles show the approximate locations of R_{500} and R_{200}, while the red square indicates the position of a newly-discovered X-ray substructure in this cluster. The pink circle in the top-left corner shows the region used to estimate the local background components.

[1] For a given overdensity Δ, R_Δ is the radius for which $M_\Delta/(4/3\pi R_\Delta^3) = \Delta\rho_c$

particular structure; the global mosaic will be the subject of a forthcoming paper.

2.2. Spectral analysis

We performed a spectral analysis of this structure using our 25 ks observation of the NE region in A2142. Spectra and response files for each region considered were extracted using the ESAS tasks `mos-spectra` and `pn-spectra` and were fit in XSPEC v12.7.1. The spectra were grouped to ensure a minimum of 20 counts per spectral channel. Since the surface brightness of the emission in the NE excess region barely exceeds the background level, a detailed modeling of all the various background components is necessary to obtain reliable measurements of the relevant parameters. We adopted the following approach to model the different spectral components:

- *The source:* We modeled the diffuse emission in each region using the thin-plasma emission code APEC (Smith et al. 2001), leaving the temperature, metal abundance and normalization as free parameters. This component is absorbed by the Galactic hydrogen column density along the line of sight, which we fix to the 21cm value ($N_H = 3.8 \times 10^{20}$ cm^{-2}, Kalberla et al. 2005).
- *The non X-ray background (NXB):* We used closed-filter observations to estimate the spectrum of the NXB component in each region, following the procedure described in Snowden et al. (2008). Instead of subtracting the NXB component, we approximated it by a phenomenological model, which we then included as an additive component in the spectral modeling (Leccardi & Molendi 2008b). This method has the advantage of retaining the statistical properties of the original spectrum, which allows the use of C-statistic (Cash 1979). We left the normalization of the NXB component free to vary during the fitting procedure, which allows for possible systematic variations of the NXB level. The normalization of the prominent background lines is also left free. Since the observation was very weakly contaminated by soft proton flares (IN over OUT ratio of 1.05, Leccardi & Molendi 2008b), we do not need to include a component to model the residual soft protons.
- *The sky background components:* We used an offset region located ~ 31 arcmin away from the cluster core (see the pink circle in Fig. 1), where no cluster emission is detected, to measure the sky background components in the region of A2142. We complemented these data with the *ROSAT* all-sky survey spectrum of the same region (Snowden et al. 1997), and fitted the *XMM-Newton* and *ROSAT* data jointly. We modeled the sky background using a three-component model: *i)* a power law with photon index fixed to 1.46 to model the cosmic X-ray background (CXB, De Luca & Molendi 2004); *ii)* a thermal component at a temperature of 0.22 keV to estimate the Galactic halo emission (McCammon et al. 2002); *iii)* an unabsorbed thermal component at 0.11 keV for the local hot bubble (McCammon et al. 2002). The best-fit spectrum for the offset region is shown in Fig. 2, and the corresponding normalizations for the various components are provided in Table 1. The best-fit CXB component has a flux of $(2.07 \pm 0.15) \times 10^{-11}$ ergs cm^{-2} s^{-1} deg^{-2} in the 2-10 keV band, which agrees with the value of De Luca & Molendi (2004). To model the sky background in a different region, the normalization of each component was rescaled by the ratio of the corresponding areas, accounting for CCD gaps and bad pixels. The CXB component was left free to vary by $\pm 15\%$ to allow for cosmic variance (Moretti et al. 2003).

Table 1. Best-fit parameters for the sky background components from Fig. 2.

Component	Norm arcmin^{-2}
Local Bubble	$(8.1 \pm 0.5) \times 10^{-7}$
Galactic Halo	$(1.15 \pm 0.08) \times 10^{-6}$
CXB	$(9.7 \pm 0.7) \times 10^{-7}$

Column description: 1: Background component (see Sect. 2.2). 2: Normalization of the model per arcmin^2. For APEC (local bubble and galactic halo), this corresponds to $10^{-14}/(4\pi d_A^2 (1+z)^2) \int n_e n_H \, dV$; for a power law (CXB) this is in units of photons keV^{-1} cm^{-2} s^{-1} at 1 keV.

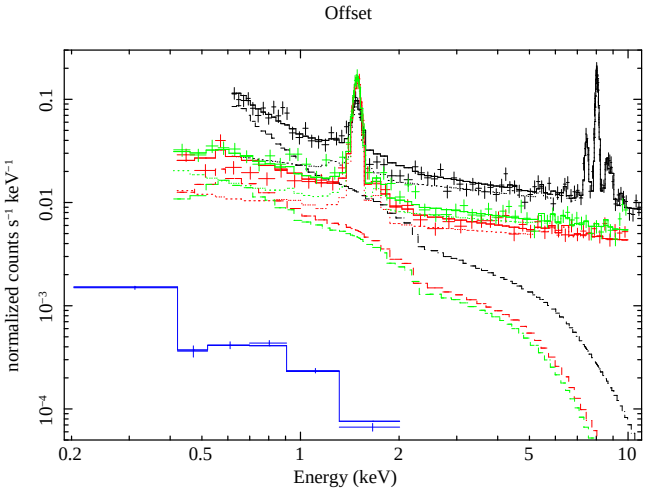

Fig. 2. Spectrum of an offset region located ~ 32 arcmin north of the cluster core to measure the sky background components, from EPIC pn (black), MOS1 (green), and MOS2 (red), and from *ROSAT*/PSPC (blue). The dotted lines show the model NXB for each instrument, while the dashed lines show the best-fit three-component sky background model.

3. Results

3.1. Morphology of the NE feature

We studied the morphology of the newly-discovered NE feature using the method described in Sect. 2.1. To highlight the presence of features in the X-ray image, we created a residual image by subtracting the azimuthally-averaged cluster emission from the EPIC [0.7-1.2] keV mosaic image shown in Fig. 1. For this purpose, we extracted the surface-brightness profile of the cluster centered on the surface-brightness peak, using the method described in Eckert et al. (2011). We then subtracted the cluster emission from each pixel and masked the detected sources. Finally, the resulting image was adaptively smoothed using the SAS task `asmooth`.

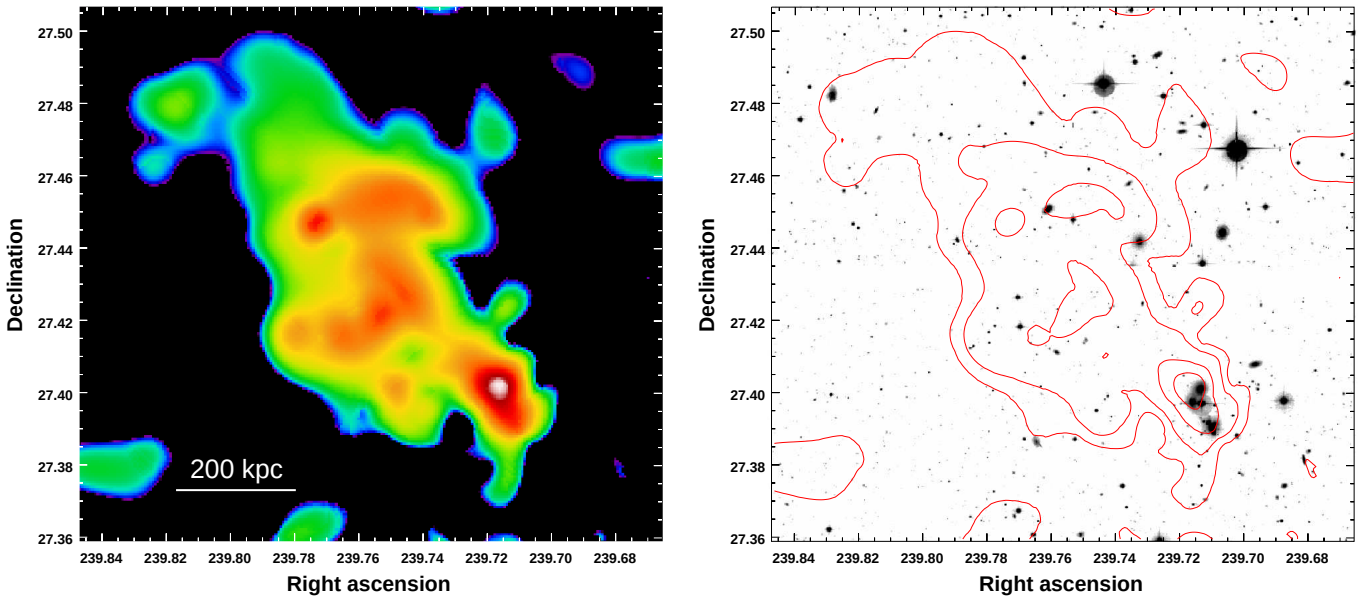

Fig. 3. *Left:* Adaptively-smoothed residual image of the NE feature highlighted by the red square in Fig. 1. *Right:* CFHT/MegaCam g-band image of the same region, with X-ray contours overlayed in red.

In the left panel of Fig. 3 we show the resulting residual image zoomed on the NE feature. The feature has an irregular morphology elongated in the northeast-southwest (SW) direction, which ends in a bright "tip" at its SW pointing towards the cluster center. The tip hosts an X-ray point source (which has been masked in Fig. 3) surrounded by a region of diffuse emission. In the right panel of Fig. 3 we show an archival CFHT/MegaCam g-band image of the same region with X-ray contours overlayed. The tip corresponds with a concentration of at least 5 galaxies; this suggests a possible association of the X-ray feature with these galaxies. Apart from this structure, no particular optical substructure is seen in this region of the cluster (see Fig. 12 of Owers et al. 2011), and no background concentration of galaxies is seen.

Starting from the tip, the X-ray substructure extends in the NE direction over a scale of ~ 8 arcmin and a width of $2-3$ arcmin. At the redshift of the cluster this corresponds to a projected linear scale of about 800 kpc. We extracted a surface-brightness profile starting from the tip to study the distribution of X-ray brightness. We used elliptical annuli in the sector with position angles 105-165° to follow the morphology of the feature as closely as possible. The NXB was subtracted using the modeling described in Sect. 2.1. We used the offset region defined in Fig. 1 (see also Fig. 2) to estimate the local sky background contribution and subtract it from the surface-brightness profile. The resulting profile is shown in Fig. 4. The surface brightness of the feature is flat out to ~ 500 kpc, decreasing only by a factor of ~ 3 compared to the maximum, then decreases more steeply out to 800 kpc, which is the maximum radius at which we are detecting the feature.

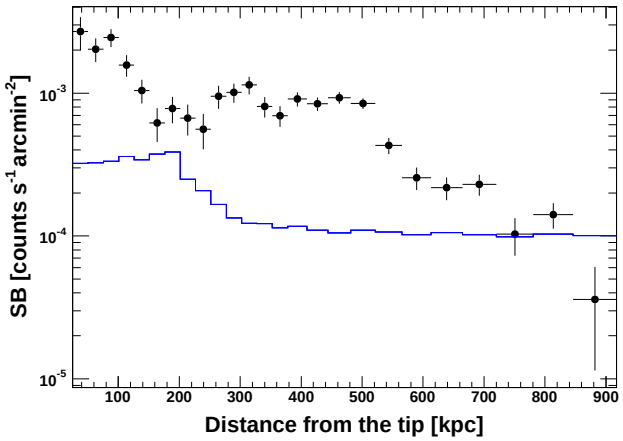

Fig. 4. Background-subtracted EPIC surface-brightness profile in elliptical annuli starting from the tip in the NE direction (position angles 105-165). The sky background intensity was estimated in the pink circle in Fig. 1. The NXB level is shown by the blue line.

3.2. Spectral properties

To study the thermodynamical properties of the structure, we extracted the spectrum of the source in 5 sectors along the NE feature. The regions used for the spectral analysis are shown in Fig. 5. The "tip" region was defined excluding the X-ray point source observed there. The following sectors were chosen to trace the morphology of the feature as closely as possible. The spectra and best-fit models for the regions defined in Fig. 5 are shown in Fig. 6. Only the pn spectra are displayed here for clarity, however the fit was performed jointly on the 3 EPIC detectors. In each case, the color lines highlight the various background components (NXB, CXB, Galactic halo and local hot bubble). The best-fit parameters are given in Table 2. We note that beyond the tip of the substructure the surrounding ICM emission is significantly below the observed emission (by at least an order of magnitude) and the background components; adding such a component in the spectra does not affect the best-fit parameters provided here.

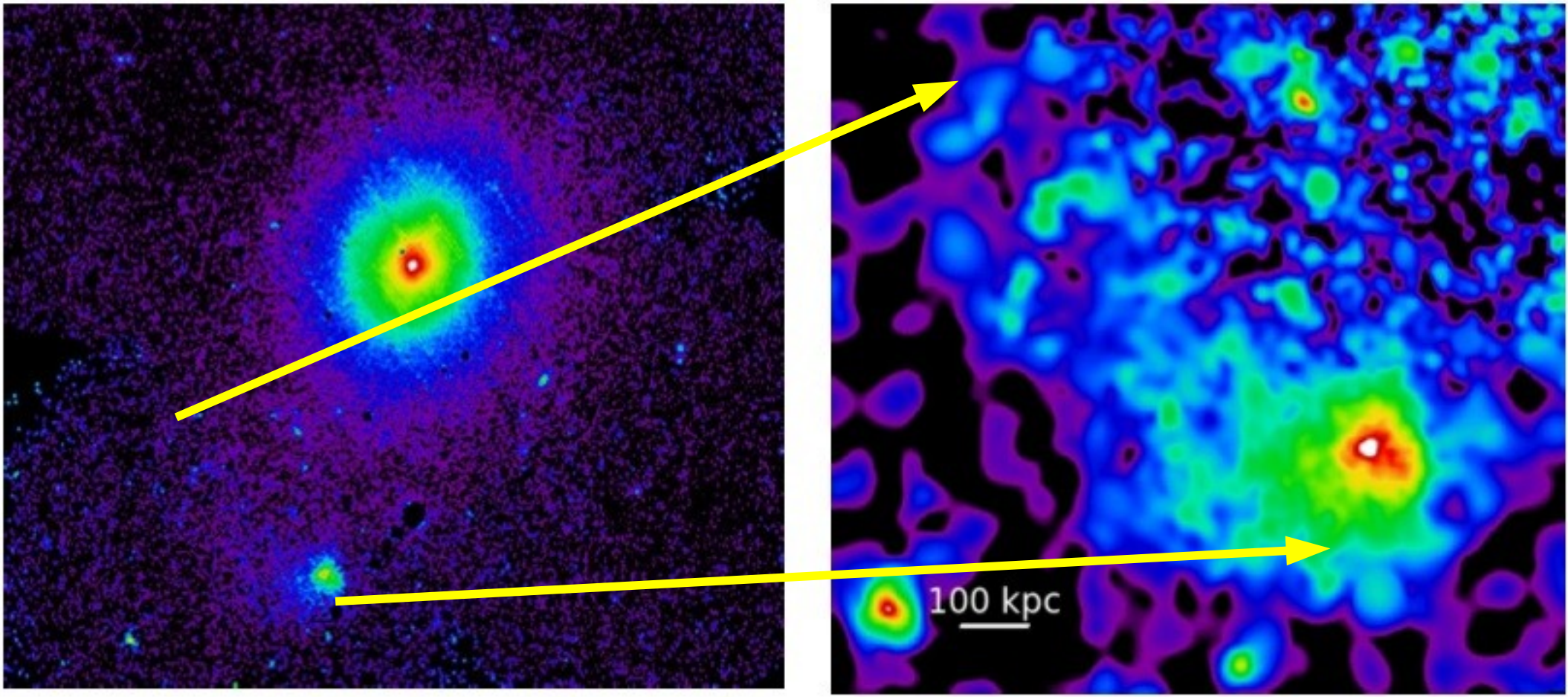
100 kpc